Stony Brook University

Substrate Recognition by Bacterial Enoyl Reductases from *Escherichia coli* and *Mycobacterium tuberculosis*

A Dissertation Presented

by

Xujie Zhang

to

The Graduate School

in Partial Fulfillment of the Requirements

for the Degree of

Doctor of Philosophy

in

Chemistry

Stony Brook University

August 2008

Stony Brook University

The Graduate School

Xujie Zhang

We, the dissertation committee for the above candidate for the **Doctor of Philosophy**

degree, hereby recommend acceptance of this dissertation

Peter J. Tonge PhD. Advisor
Professor
Department of Chemistry

Dale G. Drueckhammer PhD. Chairman of Defense
Professor
Department of Chemistry

Erwin London PhD.
Professor
Department of Biochemistry and Cell Biology

Todd Miller PhD.
Professor
Department of Physiology and Biophysics

This dissertation is accepted by the Graduate School

Lawrence Martin

Dean of the Graduate School

Abstract of the Dissertation

Substrate Recognition by Bacterial Enoyl Reductases from *Escherichia coli* and *Mycobacterium tuberculosis*

By

Xujie Zhang

Doctor of Philosophy

in

Chemistry

Stony Brook University

2008

Tuberculosis (TB) kills over two million people every year, and one third of the world's population is infected with *Mycobacterium tuberculosis* (*Mtb*), the organism that causes TB. Fatty acids are key components of cell membranes. Bacterial fatty acid biosynthesis (FAS II) has been repeatedly validated as a drug target due to its lack of similarity to the mammalian fatty acid synthase system (FAS I). Acyl carrier protein (ACP) is a necessary cofactor in fatty acid biosynthesis and other acyl transfer

reactions, since all fatty acyl intermediates are covalently attached to it. Despite considerable effort, there are no reported crystal structures of FAS II enzyme-ACP complexes.

The structure of the *E. coli* enoyl-ACP reductase, FabI, in complex with ACP has been determined using X-ray crystallography and molecular dynamics simulation. In order to further investigate the role of specific FabI residues involved in ACP recognition, site-directed mutagenesis was used on selected FabI residues which were predicted to be at the FabI-ACP protein-protein interface based on the crystal structure. In agreement with the proposed model, steady state kinetics analysis of these mutants resulted in a dramatic effect on the reduction of ACP substrate but not CoA substrate. Fluorescence titration experiments were also used to investigate the interaction of ACP and FabI.

InhA, the homolog of FabI in *M. tb*, is a key regulator of fatty acid biosynthesis. InhA is a validated target for drug discovery and we are investigating the interaction of InhA with inhibitors as well as with the natural acyl carrier protein substrate (AcpM). The expression and purification of AcpM (a 13 kDa protein) is challenging given that there are 3 forms of the protein in cells (apo, holo and acyl). A significant amount of effort was devoted to developing the ability to purify Apo-AcpM which was then used for the synthesis of the appropriate enoyl-AcpM substrate using Holo-ACP synthase. Based on studies with the *E. coli* homolog, it was hypothesized

that three basic residues close to the substrate binding loop in InhA, R195, R225, and K233, interact with acidic residues in the AcpM recognition helix. Site-directed mutagenesis together with enzyme kinetics were used to evaluate the importance of the residues for AcpM recognition. These residues were extended to include R45, R49, and R53 in helix α2 and Q214, Q224, and E220 at the proposed interface. Based on the studies, it was concluded that AcpM interacts with InhA in a fundamental different way than FabI-ACP interaction site.

While most of the FASII components have been characterized, the enzyme responsible for catalyzing the dehydration of (3R)-hydroxyacyl-AcpM still remain to be identical. Based on sequence analysis, it was proposed the *Rv0636* encoded the FASII (3R)-hydroxyacyl-AcpM dehydratase. This protein was cloned and expressed. However, while activity was observed when CoA substrate, no activity was detected using AcpM substrate.

Table of Contents

List of Figures

List of Tables

List of Abbreviations and Symbols

Aas	acyl-ACP synthase
AccABCD	acetyl-CoA carboxylase
ACP	acyl carrier protein
AcpM	acyl carrier protein from *M. tuberculosis*
AcpS	holo-ACP synthase
ADP	adenosine diphosphate
Ala	alanine
Arg	arginine
Asp	aspartic acid
ATP	adenosine triphosphate
AUC	analytical ultracentrifugation
BCG	bacille Calmette–Guérin
B. napus	*Brassica* napus
B. subtilis	*bacillus subtilis*
CoA	coenzyme A
CIP	calf intestinal alkaline phosphatase
Cys	cystiene
D	aspartic acid
DD-AcpM	*trans*-2-Dodecenoyl AcpM
DD-CoA	*trans*-2-dodecenoyl CoA

DNA	deoxyribonucleic acid
DTNB	5,5-dithiobis-(2-nitrobenzoic acid)
DTT	dithiothreitol
ε	extinction coefficients
E	glutamic acid
ECF	ethyl chloroformate
E. coli	***es****cherichia coli*
EMB	ethambutol
ENR	enoyl-ACP reductase
EnvM	enoyl-ACP reductase from *E. coli*
ESI-MS	electrospray ionization mass spectrometry
F	phenylalanine
FAB	fatty acid biosynthesis
FabA	β-hydroxyacyl-ACP dehydratase
FabB	β-ketoacyl-ACP synthase
FabD	malonyl-CoA:ACP transacylase
FabF	β-ketoacyl-ACP synthase
FabG	β-ketoacyl-ACP reductase
FabH	β-ketoacyl-ACP synthase III
FabI	enoyl-ACP reductase
FabK	enoyl-ACP reductase
FabL	enoyl-ACP reductase

FabZ	β-hydroxyacyl-ACP dehydratase
FAS	fatty acid synthesis
FPLC	fast performance liquid chromatography
G	glycine
Glu	glutamic acid
Gly	glycine
GPE	glycerophosphoethanolamine
HIV	human immunodeficiency virus
HPLC	high performance liquid chromatography
Ile	isoleucine
INH	isoniazid
InhA	enoyl-ACP reductase from *M. tuberculosis*
IPA	isopropanol
IPTG	isopropyl β-D-thiogalactoside
K	lysine
KasA/KasB	β-ketoacyl-ACP synthase from *M. tuberculosis*
KatG	catalase-peroxidase from *M. tuberculosis*
L	leucine
LAM	lipoarabinomannan
Leu	leucine
Lys	lysine
M. bovis	*mycobacterium bovis*

MALDI	matrix-assisted laser desorption/ionization
MabA	NADPH-dependent reductase from *M. tuberculosis*
MD	molecular dynamics
MDR-TB	multidrug-resistant tuberculosis
Met	methionine
M. Leprae	*mycobacterium leprae*
MIC	minimum inhibitory concentration
M. tb	*mycobacterium tuberculosis*
NAC	N-acetylcysteamine
NAD^+	nicotinamide adenine dinucleotide, oxidized form
NADH	nicotinamide adenine dinucleotide, reduced form
NADPH	nicotinamide adenine dinucleotide phospate, reduced form
NMR	nuclear magnetic resonance
PAGE	polyacrylamide gel electrophoresis
Phe	phenylalanine
PPD	purified protein derivative
PPTase	phosphopantetheinyl transferase
PZA	pyrazinamide
Q	glutamine
R	arginine
RIF	rifampicin
S	serine

S. aureus	*saphylococcus aureus*
SAR	structure activity relationship
SDR	short chain dehydrogenase/reductase
SDS	sodium dodecyl sulfate
SE	sedimentation equilibrium
Ser	serine
SM	streptomycin
TB	tuberculosis
TCN	triclosan
TEA	triethylamine
Thr	threonine
Tyr	tyrosine
UV	ultraviolet
V	valine
Val	valine
XDR-TB	extensively drug resistant TB
Y	tyrosine

Acknowledgements

It is a pleasure to thank the many people who made this thesis possible.

I would like to express deep gratitude to Professor Tonge for giving me the opportunity to do research in his laboratory. With his enthusiasm, his inspiration, and his great efforts to explain things clearly and simply, he always provided guidance, encouragement, support, and environment to do independent research. In addition, he was always accessible and willing to help his students with their livings, job hunting. As a result, research life became smooth and rewarding for me.

I would like to take this opportunity to thank Professor Arnold Wishnia, the chairman of my committee, for his valuable advice and suggestions throughout my studies. I would also like to express my appreciation to Professor Erwin London for being a member on my committee as well as for his genuine interest in my progress as a graduate student. I want to thank Professor Todd Miller for the valuable input he has provided for my research project as well as for agreeing to be my “outside” member. I wish to express my warm and sincere thanks to Professor Dale G. Drueckhammer for his guidance of my research and for serving on my committee.

It has been a real pleasure to work in the Tonge research group. I would like to

thank everyone for contributing to a very enjoyable working environment. I would like to thank Dr. Carl Machutta and Dr. Salma Rafi for their companionship, and help with my research. Also I would especially like to express my appreciation to Huaning Zhang, Hua Xu, Rong Zhou, HueiJiun Li, Hao Lu, Xiaokai Li, and Nina Liu for being friends, whose optimism helped me through many tough situations. I want to thank Deborah Stoner-Ma, Edward H. Melief, Janine Borgaro, and Allison Haigney for their help with my thesis.

Lastly, and most importantly, I wish to thank my family for their constant support and encouragement. They bore me, raised me, supported me, taught me, and loved me. To them I dedicate this thesis.

List of Publications

1. Substrate recognition by Enoyl-ACP reductase. Zhang, X; Rafi, S; Tonge, P; (2008) Processing for submission.
2. Inhibiting enoyl-ACP reductase (FabI) across pathogenic microorganisms by linear sesquiterpene lactones from *Anthemis auriculata*, Karioti, A; Skaltsa, H; Zhang, X; Tonge, P; Perozzo, R; Kaiser, M; Franzblau, S; Tasdemir, D, *Phytomedicine* (2008), in press.
3. Marine natural products from the Turkish sponge Agelas oroides that inhibit the enoyl reductases from *Plasmodium falciparum*, *Mycobacterium tuberculosis* and *Escherichia coli*. Tasdemir, D; Topaloglu, B; Perozzo, R; Brun, R; O'Neill, R; Carballeira, N; Zhang, X; Tonge, P; et al. *Bioorganic & Medicinal Chemistry* (2007), 15(21), 6834-6845.
4. Evidence from Raman Spectroscopy That InhA, the Mycobacterial Enoyl Reductase, Modulates the Conformation of the NADH Cofactor to Promote Catalysis. Bell, A; Stratton, C; Zhang, X; et al. J. *Journal of the American Chemical Society* (2007), 129(20), 6425-6431.
5. Structure of Acyl Carrier Protein Bound to FabI, the FASII Enoyl Reductase from *Escherichia coli*. Rafi, S; Novichenok, P; Kolappan, S; Zhang, X; et al. *Journal of Biological Chemistry* (2006), 281(51), 39285-39293.
6. High affinity InhA inhibitors with activity against drug-resistant strains of Mycobacterium tuberculosis. Sullivan, T; Truglio, J; Boyne, M; Novichenok,P; Zhang, X; et al. *ACS Chemical Biology* (2006), 1(1), 43-53.

Chapter 1: Tuberculosis and fatty acid synthesis

1.1 Tuberculosis overview

Tuberculosis (TB) describes an infectious disease that has plagued humans since Neolithic times. Two organisms cause TB, *Mycobacterium tuberculosis*（*M. tb*） and *Mycobacterium bovis (M. bovis)* (1). *M. bovis* is pathogenic for many animal species, especially bovidae, cervidae, and occasionally carnivores. Most cases of TB are caused by *M. tb* (2). *M. tb* is thought to be a human-specialized form of *M. bovis* developed among milk-drinking Indo-Europeans who then spread the disease during their migration into western Europe and Eurasia. By 1000 BC, *M. tb* and pulmonary TB had spread throughout the known world (*3*). The WHO estimates the two million deaths annually are caused TB. There are around one third of the world's population is infected with *M. tb*. The tubercle bacillus was first isolated and established as an infectious disease by Robert Koch in 1882. He won the Nobel Prize for his contribution in 1905.

The search for a cure of TB began after the cause was established. In the 19th century, patients were isolated in sanatoriums and given treatments such as injecting air into the chest cavity. In addition, attempts were made to decrease lung size by a surgery called thoracoplasty. No effective treatment was available during the first half of the 20th century. Streptomycin was the first antibiotic to fight TB in 1946. All of

the current first-line drugs were discovered in the following 20 years, such as isoniazid (Laniazid, Nydrazid) (*4-11*).

M. tb is a rod-shaped, slow-growing, gram positive bacterium. The *M. tb* cell wall has a high fatty acid content, which makes it hydrophobic and resistant to oral fluids. The cell wall absorbs a methylene-blue dye and maintains a red color despite attempts at decolorization, hence the name acid-fast bacilli.

TB is a highly contagious disease and can be passed from person to person via droplets. Tiny droplets of saliva or mucus are expelled into the air which are then inhaled by another person when someone with TB infection coughs, sneezes, or talks. Once infectious particles reach the alveoli in the lungs, the TB bacteria are engulfed by macrophages. Generally, a cough with a progressive increase in production of mucus, coughing up blood, fever, loss of appetite, and weight loss are common symptoms of TB. Purified protein derivative (PPD) is an easy way to detect if a person has been exposed to TB. PPD skin test-negative individuals (i.e. individuals who do not develop an indurative reaction in the 48–72 h following the intradermal injection of a standardized amount of PPD) have long been described among immune-competent subjects previously vaccinated with bacille Calmette–Guérin (BCG) or infected *M. tb.* Additionally, a chest X-ray is the most common diagnostic test that can confirm suspicion of infection. A combination of a positive PPD result with a negative chest X-ray is indicative of a latent or inactive form of the disease.

Most immunologically healthy persons who are infected with *M. tb* do not develop active TB but remain infected with inactive organisms (latent TB infection); only about 10% of infected persons develop active disease during their lifetimes. Persons with HIV infection have much higher rates of active TB and develop active diseases at a rate approximating 10% per year. HIV and TB cause more deaths than any other infectious diseases worldwide, each claiming millions of lives annually. A biologic synergy exists between these infections: HIV-induced immunosuppression increases susceptibility to TB infection, and active TB infection enhances HIV replication through immunologic stimulation. The populations infected by these two pathogens overlap in many respects, creating epidemiologic synergy. Poverty, crowded living conditions, and inadequate efforts to reduce transmission combine to enhance the transmission of both organisms. The recent emergence of multidrug-resistant tuberculosis (MDR-TB) strains of the bacteria can occur when drugs are misused or mismanaged, which adds to the severity of the disease.

1.2 Treatment of TB

TB is usually treated with four different antimicrobial first line drugs which last from 6-9 months. The most commonly used drugs are rifampicin (RIF) (*12-14*), isoniazid (INH), pyrazinamide (PZA) (*15-18*), and ethambutol (EMB) (*19-22*) or streptomycin (SM) (*23-25*) (Figure 1.1). When adherence to this four-drug is assured, it is highly effective. Based on the prevalence and characteristics of drug-resistant organisms, at least 95% of patients will receive an adequate regimen (at least two drugs to which their organisms are susceptible) if this four-drug regimen is used at the beginning of therapy. Furthermore, a patient who is treated with the four-drug regimen, but who defaults therapy, is more likely to be cured and not relapse when compared with a patient treated for the same length of time with a three-drug regimen.

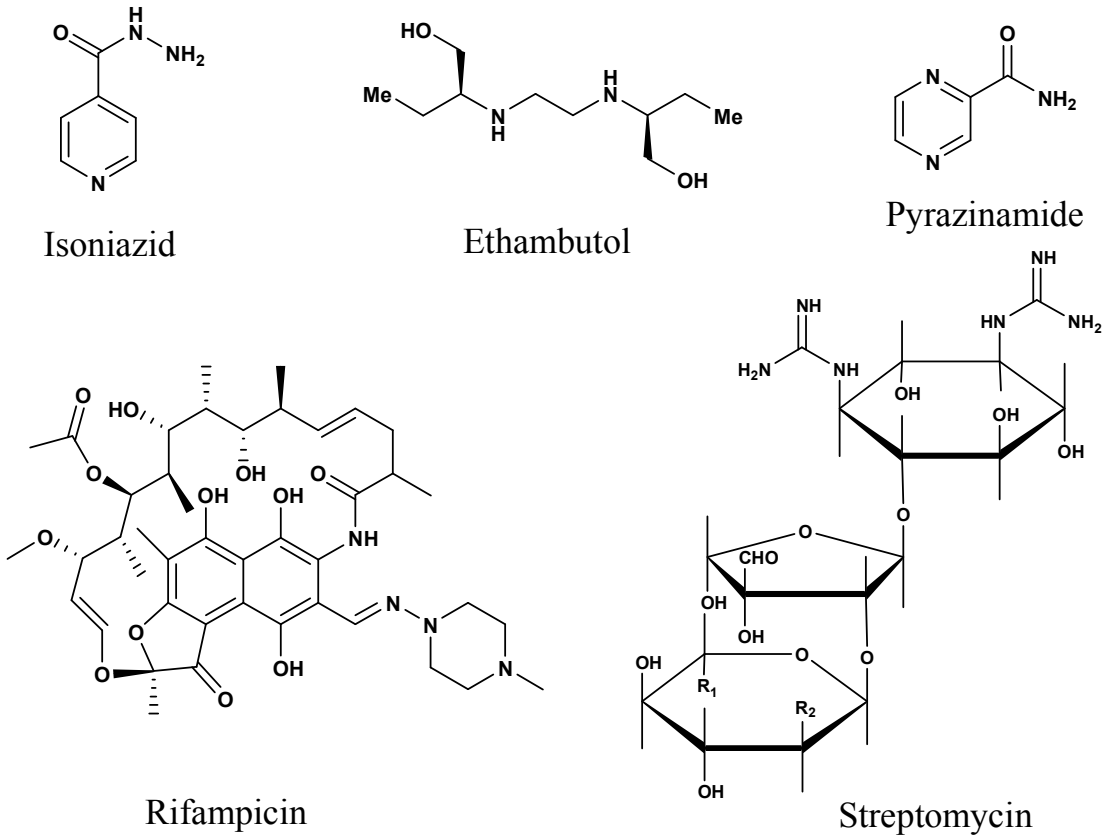

Figure 1.1. The five first-line anti-TB antibiotics: Isoniazid, Ethambutol, Pyrazinamide, Rifampicin, and Streptomycin.

Streptomycin, introduced in 1943 by England's Medical Research Council, is the first antibiotic remedy for TB. Streptomycin binds to the 16S rRNA of the bacterial ribosome to interfere with the binding of formyl-methionyl-tRNA to the 30S subunit so that it stops bacterial growth by inhibiting cell membranes and protein synthesis. However, it can result in temporary hearing loss because of its toxicity.

Isoniazid was discovered in 1952 by Roche and is a first-line anti-TB medication used. Isoniazid (*26*) is a potent, highly selective agent that is still a centrepiece of therapy (*27-29*) some 50 years after its discovery yet with mechanisms of action that

have remained contentious. It is a prodrug and must be activated by catalase-peroxidase enzyme KatG to form the isonicotinic acyl-NADH complex (Figure 1.2) (*9, 30*). The complex binds tightly to enoyl reductase known as InhA and inhibits the natural enoyl-AcpM substrate so it can prevent the synthesis of mycolic acids in the mycobacterial cell wall.

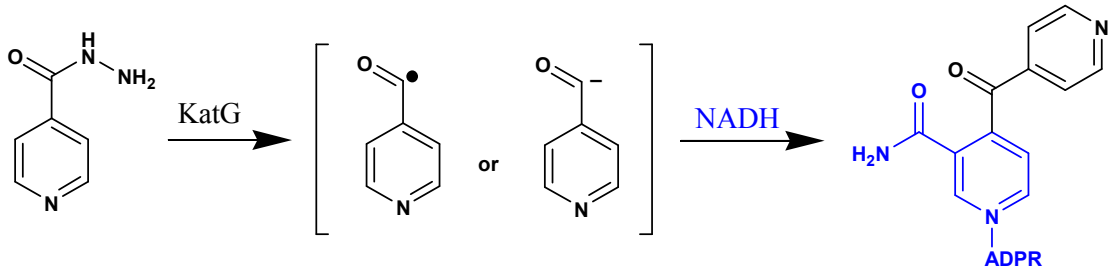

Figure 1.2. Activation of isoniazid.

It has been shown that around 50% of all isoniazid-resistant clinical isolates contain mutations in the KatG gene (*31, 32*). Therefore, a lot of inhibitors have been developed which do not require activation by KatG, such as triclosan (2, 4, 4'-trichloro-2'-hydroxydiphenyl ether) (*31-34*).

Pyrazinamide was proposed to inhibit *M. tb* in 1954. Pyrazinamidase converts pyrazinamide to the active form, pyrazinoic acid (*35, 36*). Pyrazinoic acid is thought to inhibit the enzyme fatty acid synthetase I, which is required by the bacterium to synthesise fatty acids, although this has been disputed (*35, 37*).

Ethambutol and rifampicin were discovered in 1964 and 1967, respectively. Ethambutol is a bacteriostatic antimycobacterial drug (*38, 39*). Traditionally, mycolic acids attach to the 5'-hydroxyl groups of D-arabinose residues of arabinogalactan and form mycolyl-arabinogalactan-peptidoglycan complex in the cell wall. Disruption of the arabinogalactan synthesis inhibits the formation of this complex and leads to increased permeability of the cell wall. Rifampicin is a semisynthetic compound derived from *Amycolatopsis rifamycinica.* It is a transcriptional inhibitor that binds to the RNA polymerase β-subunit *rpo*B.

Standard therapy for active TB consists of a 6-9 month regimen including 2 months with Rifater (isoniazid, rifampicin, and pyrazinamide) following by 4 months of isoniazid and rifampicin (rifamate, rimactane). Ethambutol (myambutol) or streptomycin will be added until the drug sensitivity is known. Treatment takes that long because the disease organisms grow very slowly and, unfortunately, also die very slowly. Furthermore, MDR-TB has emerged as a possible threat to global TB control efforts in recent years (*40-46*). It is a challenge not only from a public health point of view but also in the context of global economy, especially in the absence of treatment for MDR-TB at national-level programs in developing countries (*47*). MDR-TB is defined as TB that is resistant at least to isoniazid and rifampicin. Isolates that are multiply-resistant to any other combination of anti-TB drugs but not to INH and RIF are not classed as MDR-TB (*48*). The treatment and prognosis of MDR-TB are much more akin to that for cancer than to that for infection. It has a mortality rate of up to

80%. MDR-TB is more difficult to treat than drug-susceptible strains of TB. The success of treatment depends upon how quickly a case of TB is identified as drug resistant and whether an effective drug therapy is available. The second-line drugs used in cases of MDR-TB are often less effective and more likely to cause side effects. According to WHO, it estimates that up to 50 million persons worldwide may be infected with drug resistant strains of TB which bring the urgency for the development of novel drugs to cure TB.

More recently, extensively drug resistant TB (XDR-TB) has emerged and is a relatively rare type of MDR-TB (*49-53*). XDR-TB is defined as TB which is resistant to isoniazid and rifampin, plus resistant to any fluoroquinolone and at least one of three injectable second-line drugs (i.e., amikacin, kanamycin, or capreomycin). It has been shown that 10% of MDR-TB isolates are in fact XDR-TB (*53*). Because XDR-TB is resistant to first-line and second-line drugs, patients are left with less effective treatment options, and cases often have worse treatment outcomes. Proper treatment and new drug discovery are critical with the development of resistant strains to more of the anti-TB drugs. A Global Plan to Stop TB has been developed with the objective to save 14 million lives between 2006 and 2015 by the Stop TB Partnership.

1.3 Fatty acid biosynthesis

M. tb has a unique cell wall which is a major determinant of virulence for the bacterium (*54*). Cell wall biosynthesis is a good drug target of antibacterial agents. The mycobacterial cell wall complex contains a very thick waxy, complex lipid-rich membrane which consists of a covalently linked complex of peptidoglycan, arabinogalactan, and mycolic acids (Figure 1.3), which are α-alkyl, β-hydroxy branched long chain fatty acid (C60-C90). The mycolic acids are attached to the mycolylarabinogalactan polymer, which is attached to peptidoglycan by diglycosylphosphoryl (*54*). Immunogenic lipoarabinomannan (LAM) is another major component of the cell wall to which is attached via a phosphatidylinositol anchor (*55*).

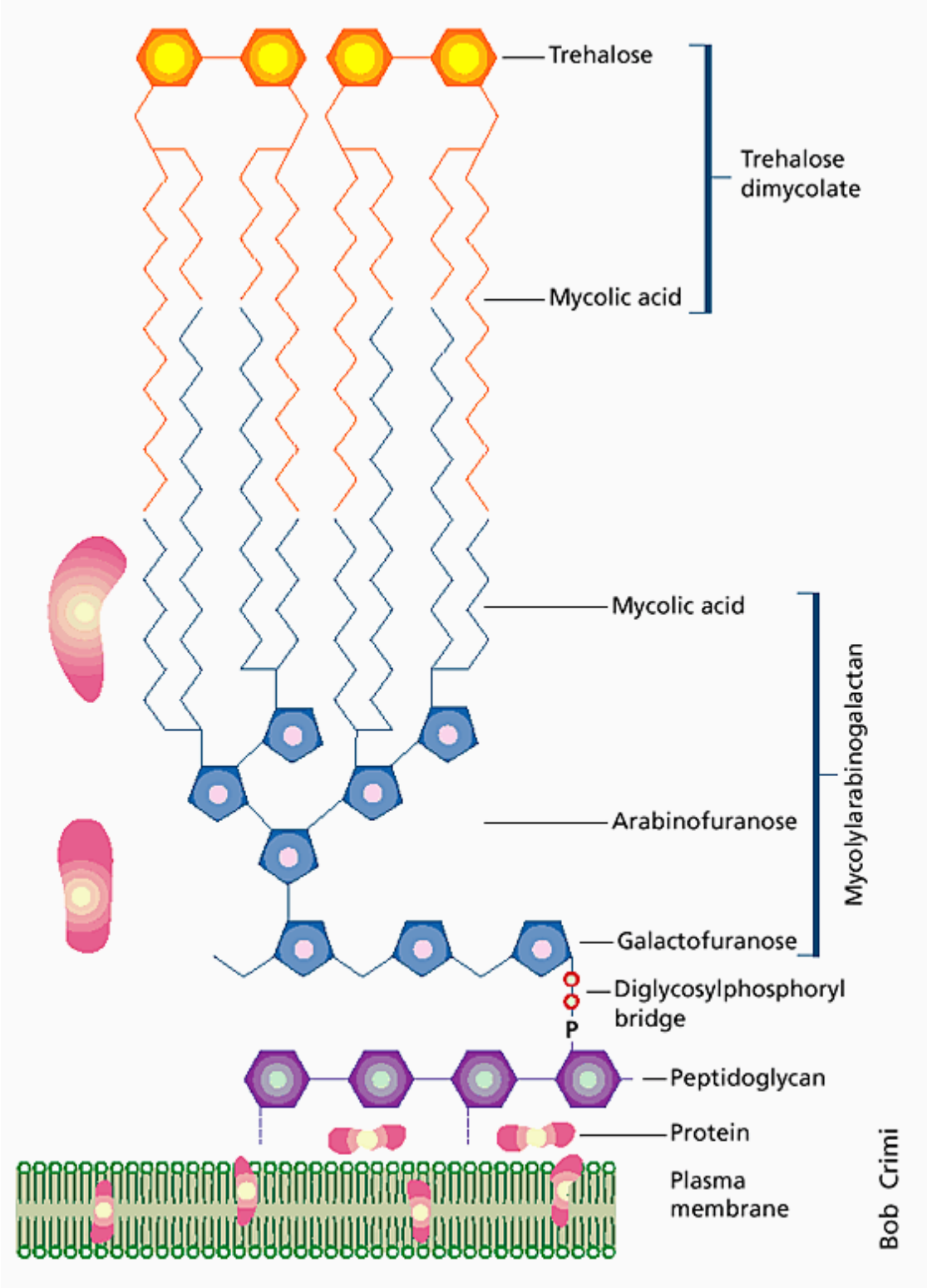

Figure 1.3. structure of mycobacterial cell wall.

They are strong hydrophobic molecules to be slow growing, facilitate survival in the hostile environment of the macrophage (*56*), and retain acid-fast staining. Also, mycolic acids are thought to be the virulence in *M. tb* by cationic proteins, oxygen radicals, and lysozyme to prevent attack of the mycobacteria. Common antibiotics are ineffective against *M. tb* because of the permeability barrier presented by this cell envelope (*54, 57*). Mycolic acids are synthesized from long chain lipid produced by the fatty acid synthesis (FAS) pathway (Figure 1.4). Fatty acid synthesis is critical for the survival and can be divided into two distinct types, FAS-I and FAS-II.

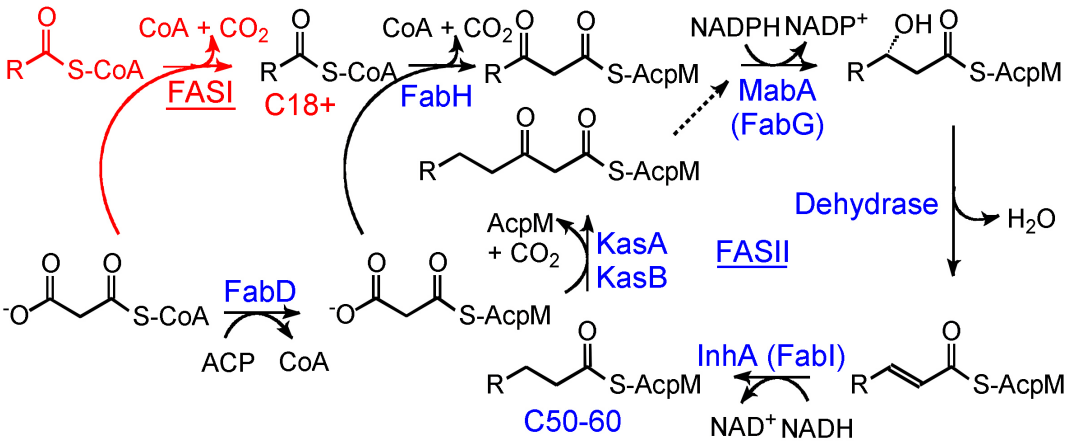

Figure 1.4. FASII system in *M. tb*. The cycle consists of four steps β-keto reduction, dehydration, enoyl reduction and condensation after the initial condensation by FabH.

The fatty acid synthase (FASI) (*58, 59*), typically found in eukaryotes, is a large multifunctional polypeptide composed of distinct enzyme domains, each having a different enzymatic function, including β-ketoacyl synthase, β-ketoacyl reductase, dehydrase, and enoyl reductase (*60-63*). C24-C26, short chain acyl-CoA precursors which are released from the complex by thioesterase (*64, 65*), are produced by this

pathway which utilizes both acetyl-CoA and malonyl-CoA substrates. Mammalian FASI, known as the "associated" system, is a 550 kDa homodimer with multiple structural and functional domains including an acyl carrier protein (ACP) domain.

In contrast, in FASII, found in bacteria, plants, and parasites, fatty acid synthesis is carried out by a series of separate polypeptide, each performs one enzymatic process to elongate the products of the FASI pathway (*66, 67*). Initially, acetyl-CoA is carboxylated by AccABCD (*68*) to form malonyl-CoA, which is, in turn, transferred to AcpM (*69*) by FabD (*70*). Fatty acid synthesis is initiated by the condensation of malonyl-AcpM and acetyl-CoA to yield β-ketobutyryl-AcpM and CO_2. The reaction is catalyzed by FabH, the β-ketoacyl-AcpM synthase III (*71*) supplying substrates (acetoacetyl-AcpM) to the fatty acid elongation cycle, which includes MabA (*72*), InhA (*73-75*), and KasA/B (*76, 77*). In the cycle, the keto group of β-ketoacyl-AcpM is reduced to a hydroxyl group by NADPH-dependent reductase MabA and then the β-hydroxyacyl-AcpM is dehydrated by an unknown dehydratase. The double bond of *trans*-2-enoyl-AcpM is reduced by NADH-dependent reductase InhA, which feeds the substrate back to KasA/B, which in turn adds an additional acetate unit (two carbons), and the cycle iterates (*58*). In the FASII pathway, the growing fatty acids are attached to the phosphopantetheine through a thioester bond.

The last reaction in the elongation cycle is catalyzed by the enoyl-ACP reductase. InhA in which the *trans* double bound between the C2 and C3 of the fatty acyl is

reduced (Figure 1.5). Bacterial enoyl ACP reductases (ENR) belong to the SDR family which shares the signature tyrosine and lysine residues in the active sites. The structure of enoyl-ACP reductase has been determined from different organisms, *E. coli* (*34, 78-80*), *B. napus* (*81*), and *M. tb* (*75, 82*). Their structure and active sites are very similar. Rafferty and coworkers (*81*) suggested a hydride was transferred to the C3 carbon of the C2-C3 double bond and an enolate anion on the C1 carbonyl oxygen accepted a proton from the tyrosine hydroxyl. Tonge and coworkers (*83*) utilized isotope substitute to indicate that hydride transfer is promoted by pseudoaxial positioning of the NADH pro-4S bond. The resulting enol yields the final product by undergoing tautomerization.

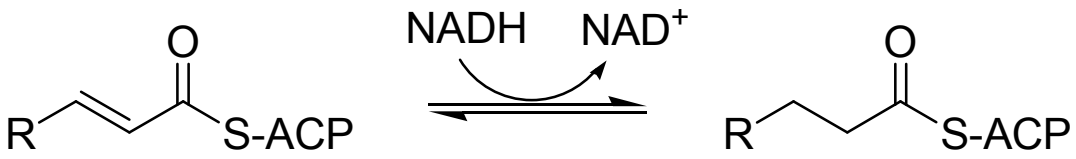

Figure 1.5. Reduction catalyzed by Enoyl-ACP reductase.

FabI, the enoyl ACP reductase in *E. coli*, shares 37% sequence identity with InhA. FabI has been demonstrated to be the only enoyl-ACP reductase in *E. coli* (*70*) which makes this pathway a good drug target for TB (*59*). There are three types of enoyl-ACP reductase inhibitors: diazaborines, triclosan, and isoniazid. All three inhibitors bind to ENRs in a similar way by forming a tight complex with the cofactor NADH. Diazaborines contain a heterocyclic 1,2-diazine ring and inhibit maturation of

rRNAs for the large ribosomal subunit. Triclosan (2, 4, 4'-trichloro-2'-hydroxydiphenyl ether) has been used in soaps, deodorants, toothpastes, shaving creams, and cleaning supplies as the proprietary microban treatment for 30 years. Triclosan is a small hydrophobic molecule and is assumed to cause a general and non-specific membrane disruption to make the bacterial envelop more porous and prevent the uptake of nutrients. In the triclosan bound FabI complex, the chlorine atom on the phenol ring corresponds to the beginning of the growing acyl chain. Diazaborines and triclosan bind to the ENR·NAD^+ form of the enzyme and interact with the 2'-hydroxyl group of the cofactor. The structure of the InhA·NAD^+·isoniazid complex reveals that isoniazid occupies slightly different position in the active site of InhA in which the isonicotinic moiety forms a covalent adduct with the 4-position of the nicotinamide ring which is believed to participate as a hydride donor in catalysis. Similar to diazaborines, isoniazid forms covalent bonds with the cofactor, while triclosan does not.

1.4 Acyl Carrier Protein (ACP)

1.4.1 Background and significance

The acyl carrier protein (ACP) plays an important role in a diverse array of metabolic pathways including the biosynthesis of fatty acids (*84, 85*), polyketides (*86*), membrane-derived oligosaccharides (*87*), lipopolysaccharides (*88, 89*) and phospholipids (*90*). ACP is in all the fatty acid synthase reactions and transfers the growing fatty acyl chain between the enzyme active sites. It was first demonstrated that a protein can act as a coenzyme in the fatty biosynthesis system (*91, 92*). All enzymatic components in the FAS system have been identified since 1961. Lynen and coworkers proposed that FAS intermediates are protein bound after a series of experiments to isolate the free intermediates in the synthetic process catalyzed by a purified fatty acid (*93*). This protein was later designated acyl carrier protein. Studies to elucidate ACP structure and function were initiated once the importance of ACP in fatty acid synthesis was realized.

The carrier proteins attach the growing substrate via a thioester to the ACP phosphopantetheine group via a central serine residue. The carrier proteins interact with a wide variety of enzymes to load carbon units, condense these units and modify the product. ACPs functioning in FASII mediated biosynthesis vary in molecular mass

from 7.5 kDa (*E. coli*) to 13 kDa (*M. tb*). The solution structure of ACP has been resolved by NMR spectroscopy (*94*) (Figure 1.6). In addition, based on X-ray crystallographic analysis, ACP has been demonstrated to adopt two major conformations: either as an integral domain to deliver the acyl chain to the target enzyme (type I) or as a discrete protein to transport the growing acyl chain to constitute a multienzyme synthase complex (type II) (*95*). Because of its flexibility in solution, ACP has lower affinity for target proteins, so the structural analysis of ACP protein complex is sparse. Somers and coworkers (*96*) have determined the crystal structure of ACP in complex with holo-ACP synthase (AcpS). AcpS catalyzes the addition of a 4'-phosphopantetheine group from a CoA molecule to a conserved serine reside to produce the holo or modified form of AcpM (*97, 98*). It is upon the phosphopantetheine moiety which initial malonyl group or the growing acyl chain is attached via a thioester bond (*99*).

In each case the growing substrate is attached via a thioester to the ACP phosphopantetheine group. ACPs must therefore be able to recognize and interact, in an acyl group-dependent manner, with a wide variety of enzymes. In eukaryotic type I fatty acid synthesis (FASI) and in polyketide biosynthesis, the ACP occurs as part of a larger polypeptide that is also associated with other catalytic activities. In contrast, in bacterial type II fatty acid biosynthesis (FASII), each of the enzyme activities as well as the ACP are encoded by separate polypeptide chains. ACPs that function in FASII-mediated biosynthesis are small, highly soluble, acidic proteins that vary in

molecular weight.

AcpM, the acyl carrier protein in *M. tb*, has an extended C-terminal tail to solubilize and accommodate the longer acyl chain which makes it is distinct from other ACPs, such as the *E. coli* ACP. AcpM is 115 amino acid in length and composed four α helices (*100*).

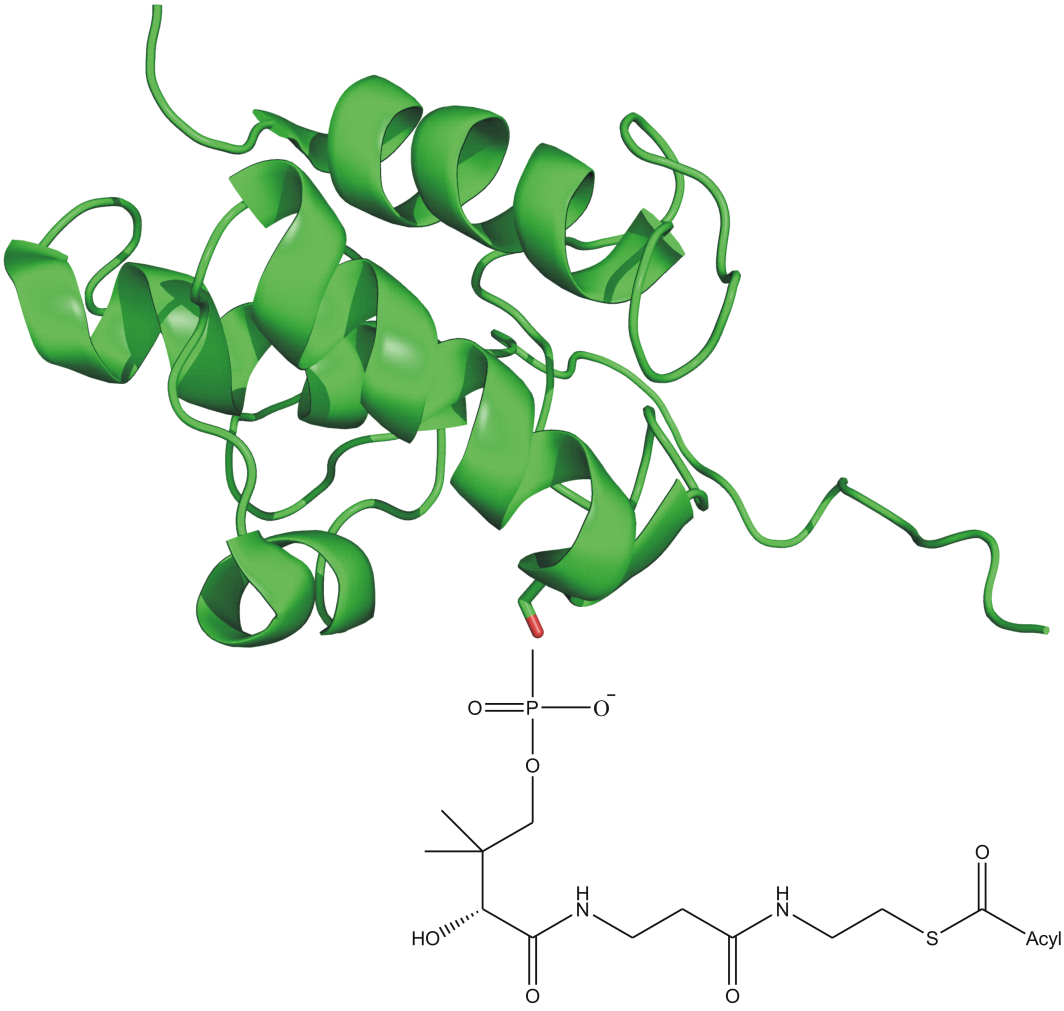

Figure 1.6. The growing fatty acid chain attached to phosphopantetheine prosthetic group linkage to Serine 41 of Acyl Carrier Protein (AcpM) in *M. tb*.

1.4.2 Role of ACP in fatty acid biosynthesis

Due to its central importance, there is a great deal of interest in ACP. ACP is a necessary cofactor in all FAS reaction and it is responsible for acyl group activation (*62, 101-103*). The structure of the Acyl-AcpM molecule with an acyl phophopantetheine chain attached to S41 is given in Figure 1.6. The 4'-phophopantetheine moiety serves as a point of attachment of the acyl groups and provides a flexible chain that can reach into the active sites of ACP-recognizing enzymes (*104*).

It is important to understand protein-protein interaction in a variety of biological processes like cellular structure, signal transduction, immune response, and apoptosis to programmed cell death (*105*). ACP has been identified as being essential for the survival of *E. coli* (*106*). The fact that no crystal structures of ACP in complex with any FAS enzymes are available means that it is difficult to understand the details of the molecular recognition of ACP by the FAS enzymes. Since, fatty acid biosynthesis enzymes are important antibacterial target by a great deal of genetic, biochemical, and crystallographic evidence. Hence, drug development is an exciting new area to identify the specific interaction which governs ACP recognition by the FAS enzymes. Designing small molecules or small peptide antagonists of ACP·protein interfaces would result in the inhibition of fatty acid synthesis and eventually in bacterial growth inhibition.

1.5 overview of my research

My research has focused on three areas. I have used kinetics to study the interaction of the *E. coli* FabI with ACP. FabI-ACP model has been constructed by X-ray crystallography and molecular dynamics simulation. I have extended the study of ACP-protein recognition to the FASII from *M. tb* system. In addition, I have studied the dehydratase in the FASII pathway.

1.5.1 Elucidation of the structure of Acyl Carrier Protein bound to FabI, the FASII enoyl Reductase from *E. coli* using site-direct mutagenesis, UV-kinetics and fluorescence titration.

Out of a total of 77 residues in *E. coli* ACP, 14 are glutamic acids and 8 are aspartic acids, which correspond to about 29% of the total amino acid composition. Here we report the protein-protein interface between the ACP and the *E. coli* fatty acid biosynthesis enoyl reductase enzyme (FabI) and how the enzyme recognizes the substrate based on a combination of site-direct mutagenesis, UV kinetics, and fluorescence titration. The kinetics data are in agreement with the structural studies and reveal how the acyl carrier protein interacts with FabI through acidic residues in the ACP helix α2 and a patch of basic residues adjacent to the FabI substrate-binding loop. FabI is a good target for drug discovery and the present structure provides insight into the molecular determinants that regulate the interaction of ACPs with

target proteins. This study was collaborated with Salma Rafi and Polina Novichenok.

1.5.2 Understanding the substrate binding loop in the *M. tb* enoyl reductase InhA with the natural substrate:AcpM

Keen observation of the different crystal structures and crystal contacts led us to identify a patch of basic residues in InhA which may play an important role in interaction with AcpM. AcpM has a very high structure similarity to the ACP in *E. coli*, and it is predicted that they have similar binding modules with the FabI-ACP system. However, site-direct mutagenesis and kinetics show they have different binding loops. This is very important as the residues participating in this key interaction are different to than those participating in the similar interaction of FabI with ACP, the protein that brings the substrate to FabI. Why the similarly functioning proteins have different binding modules will elucidate the importance of protein-protein interaction in FAS.

1.5.3 Protein engineering dehydratase in FASII pathway.

The enzyme responsible for dehydration of (3R)-hydroxyacyl-ACP during the elongation cycles of the mycobacterial FASII pathway is unknown (*107*). In *E. coli* bacterial, FabZ and FabA, catalyze the dehydration step (*108*), but no such proteins are present in *M. tb* (*109*). It was challenging to identify the candidate protein cluster

by bioinformatics analyses and an essentiality study. *Rv0635-Rv0636-Rv0637* has been cloned as the long-sought (3R)-hydroxyacyl-ACP dehydratases, which belongs to the hydratase 2 family (*107*). The four enzymes corresponding to the four steps β-keto reduction, dehydration, enoyl reduction and condensation have now been cloned and expressed, so it is possible to initiate the FASII cycle reaction in vitro by introducing the four enzymes.

Chapter 2: Biochemical studies of FabI·ACP complex

2.1 Introduction

Acyl carrier protein (ACP) is a small protein that interacts with diverse enzymes in both fatty acid and polyketide biosynthesis with the growing chain bound during synthesis as a thiol ester at the distal thiol of a 4'-phophopantethiene moiety (*110-115*). The protein is expressed in the inactive apo form and the 4'-phophopantethiene moiety must be post-translationally attached to a conserved serine residue on the ACP by the action of holo-acyl carrier protein synthase (AcpS), a phosphopanththeinyl transferase (*70, 116*). AcpS transfers the 4'-phosphopantetheine group from CoA to apo-ACP and ACP phosphodiesterase cleaves the prosthetic group from the protein. AcpS is a homotrimer and forms a tight complex with apo-ACP and it was stimulated as a potential drug target (*117, 118*). The role of the acyl carrier protein as a necessary cofactor in fatty acid biosynthesis has been extensively reviewed (*85, 91, 93, 103, 119-121*). ACP first sequesters the growing acyl chain from the aqueous environment, and second, it releases its grip in the fatty acid to insert into the active site cavity of the enzyme when it binds to one of the type II proteins (*112*).

The ACPs are a group of highly related, small acidic proteins with molecular weights of about 9 kDa (*100*). The *E. coli* ACP has been the most extensively studied among the ACPs. The protein consists of helical elements and is refolded to native

conformation after heating or pH-induced denaturation (*122*). Furthermore, ACP makes up 0.25% of the total soluble protein in *E. coli* (*122*).

James and coworkers first reported the NMR structure of *E. coli* ACP in the late 1980s (*94, 118, 123-125*). The structures of eight other ACPs have been studied by both NMR and X-ray crystallography methods (*126-129*). They have very similar secondary structure elements. *E. coli* ACP is a rod-shaped protein consisting of a preponderance of acidic residues grouped into four α helices with a long but structured loop which links the first and the second helices (*100*) (Figure 2.1).

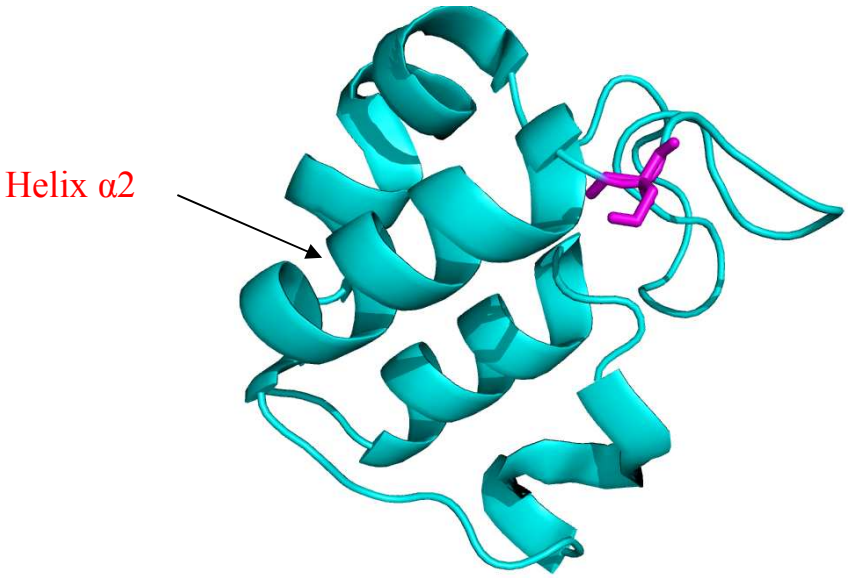

Figure 2.1. The NMR and X-ray structure of *E. coli* ACP.

The acyl intermediates of fatty acid biosynthesis are bound to ACP through a thioester linkage attached to the terminal sulfhydryl of the 4'-phosphopantetheine prosthetic group(*100, 101*). The sulfhydryl group is the only thiol group of *E. coli*

ACP and is attached to Ser36 of the Asp-Ser-Leu motif at the end of helix α2 via a phosphodiester linkage (*94, 122, 125*). The Asp-Ser-Leu motif is conserved in all ACP structures. The prosthetic group rapidly exchanges between a state that is bound to the ACP and another state which is solvent exposed in the holo form of ACP. Chemical shift perturbation experiments have shown that the binding site for the prosthetic group on the surface of the ACP is near the extended hydrophobic pocket around the Ser 36 (*106, 129*).

Molecular modeling was used to dock the NMR structure of ACP with the crystal structure of FabH in an attempt to understand the molecular details that govern the specific interactions between ACP and the type FAS II enzymes (*104*). Rock and coworkers experimentally tested this model by constructing site-directed FabH mutants and using both ACP-dependent and ACP-independent assays. The docking experiment revealed a positively charged/hydrophobic patch exists adjacent to the active tunnel of FabH and clearly showed a conserved arginine (Arg249) on FabH is required for the ACP-FabH interaction. These studies revealed the presence of a positively charged hydrophobic patch adjacent to the active site cavity in each FASII enzyme and that this binds the highly conserved ACP helix containing the invariant Glu41. Furthermore, the crystal structure of ACP-AcpS binary complex shows the same binding interaction between Glu41 of ACP and a surface arginine AcpS (*96*). All the experiments suggest the similarity of the binding mode of ACP to all of the *E. coli* enzymes. In addition, there is a high degree of sequence conservation of negatively

charged residues along helix α2 of ACP (*120*). Fourteen acidic and no positive residues between position 30 and 60 contribute to conformational flexibility of ACP in this very acidic central region by electrostatic repulsion (*111*). The flexibility is important in facilitating rapid association and dissociation of ACP with various enzymes. In conclusion, it has been shown that the conserved acidic helix α2 of ACP is a "recognition helix" for universal enzyme interaction by mutagenic studies and computational docking analyses with *E. coli* fatty acid synthase components and other enzymes (*104, 112, 120, 130*).

Two types of fatty acid biosynthesis pathway are FASI and FASII. Most eukaryotes contain the type I where all the catalytic domains reside on a single polypeptide chain, while, prokaryotes and plants contain the FASII system where each step is catalyzed by different functional enzyme. Mycobacteria contain both FASI and FASII systems. Acetyl-Coenzyme A (CoA) (Figure 2.2) is converted to malonyl-CoA by acetyl-CoA carboxylase (AccABCD) as the starting step (*120*). The malonyl moiety is tranferred from CoA to ACP by malonyl-CoA:ACP transacylase (FabD). The initial condensation reaction is catalyzed to acetoacetyl-ACP by β-ketoacyl-ACP synthase III (FabH). The next enzymes in the following cycle are β-ketoacyl-ACP reductase (FabG) and β-hydroxyacyl-ACP dehydratase (FabA or FabZ), which catalyze the NADHP-dependent formation of β-hydroxyacyl-ACP and enoyl-ACP, respectively. Finally, the last step is catalyzed by the NADH-dependent enoyl-ACP reductase (FabI, FabK or FabL) which reduces the enoyl-ACP to acyl-ACP. The

product is elongated further by β-ketoacyl-ACP synthase FabB or FabF until the appropriate chain length of fatty acid is reached.

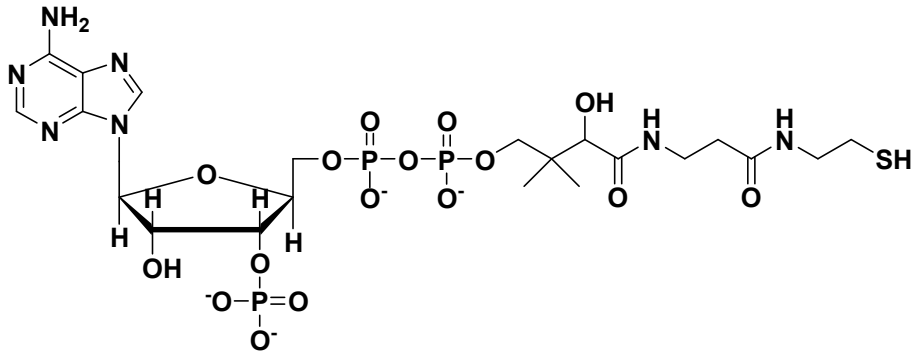

Figure 2.2. Structure of Coenzyme A (CoA)

Acyl carrier protein is synthesized in the cell as apo-ACP which is a biologically inactive form of the protein. AcpS transfers the 4'-phosphopantetheine moiety from Acyl-CoA to Ser36 of apo-ACP in a magnesium-dependent reaction by post-translationally modifying the apo-ACP to its active form, acyl-ACP (*118, 131, 132*) (Figure 2.3). *Trans*-2-Dodecenoyl-CoA (DD-CoA) was synthesized from *trans*-2-dodecenoic acid using the mixed anhydride method (*76, 77*).

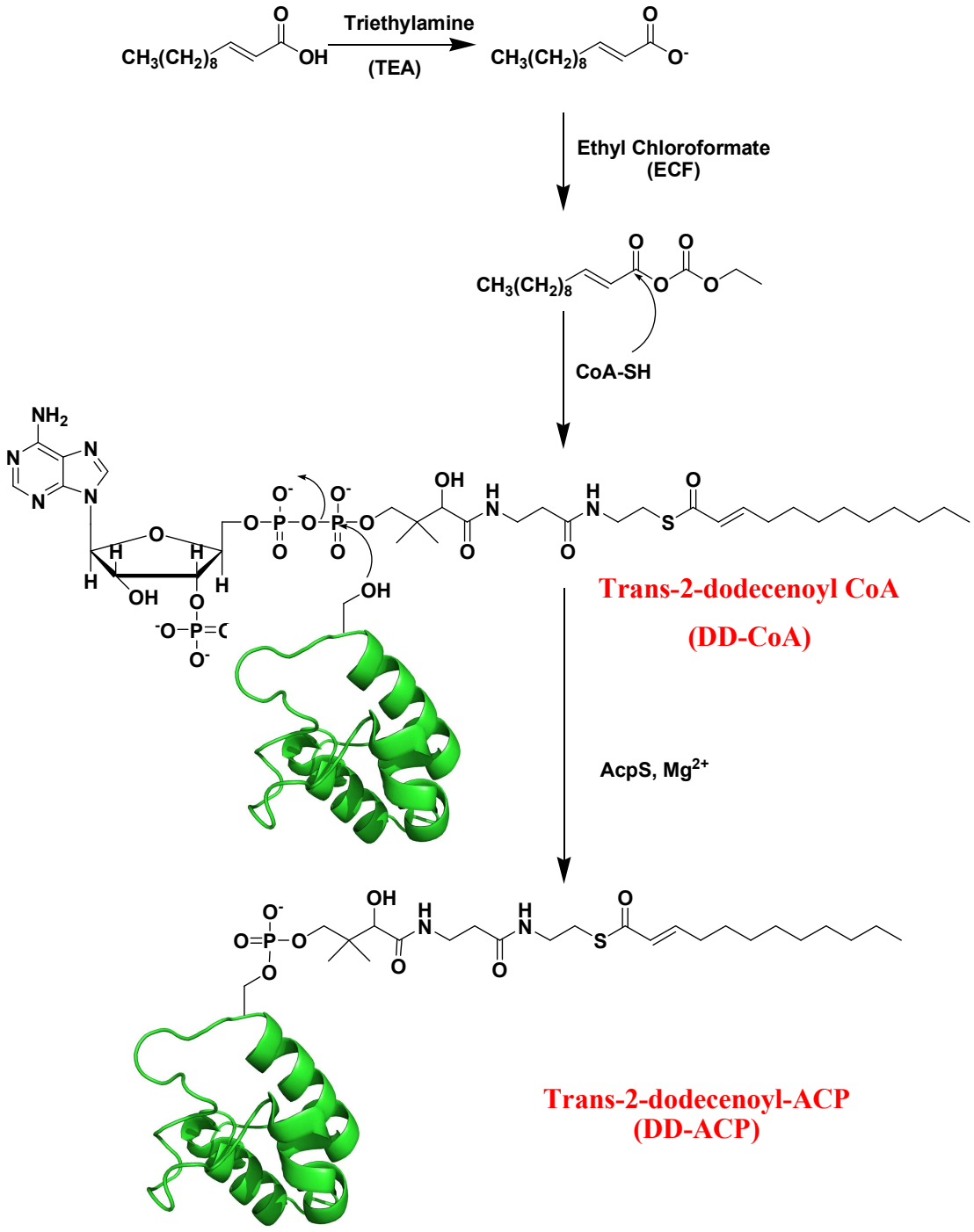

Figure 2.3. The route to synthesize a natural substrate of FabI:

trans-2-dodecenoyl-ACP

A second enzyme, acyl-ACP synthase (Aas), can accomplish the synthesis of acyl-ACP *in vitro*. Aas is an *E. coli* inner membrane protein and functions as a

2-acylglycerophosphoethanolamine (2-acyl-GPE) acyltransferase. It incorporates exogenous fatty acids into membrane phospholipids (*133*).

The efforts in my research are focused on the FASII enoyl reductase enzyme FabI, a target for antibacterial diazaborine compounds and triclosan (*32-34, 80, 134, 135*). Rock and coworkers stated the enoyl-ACP reduction reaction is the rate-limiting step of fatty acid biosynthesis (*70*). FabI, FabK, and FabL genes have been identified as three distinct classes of ENR enzymes (*32, 71, 72*). The structure of FabI has been determined from three organisms, *E. coli*,(*34, 78, 136*) *M. tb* (InhA) (*75, 82*), and the oilseed rape plant *B. napus* (*81*). Their structures and their active sites are very similar. The significant tyrosine and lysine residues, Tyr156 and Lys163, have the usual roles for an SDR family member. A hydride is transferred to the C3 carbon of the C2-C3 double bond and an enolate anion on the C1 carbonyl oxygen accepts a proton from the tyrosine hydroxyl (*81*). The final product is formed by undergoing tautomerization. The conserved critical lysine stabilizes the binding of the cofactor through hydrogen bond interactions with the hydroxyl groups on the nicotinamide ribose. Suitably positioned hydroxyl and amine groups on the two active site residues, two adjacent hydroxyl groups on the nicotinamide ribose, and a number of bound water molecules which communicate with the bulk solvent play an important role in the catalytic mechanism (*100*)

Based on the information provided by the interaction of ACP with

β-ketoacyl-ACP synthase III, FabH and β-ketoacyl-ACP reductase, FabG (*104, 112*), modeling studies suggest that ACP should interact with a cluster of basic residues adjacent to the FabI substrate binding loop (*137*). The loop is disordered in binary FabI-NADH complexes, and becomes ordered in the ternary FabI:NAD^+:triclosan complex (*138*) (Figure 2.4). Two entries into the active site termed the major and minor portals are created by the ordered loop. Sacchettini and coworkers (*75*) have determined the structure of a C16 NAC substrate bound to InhA and proposed that substrates enter the InhA active site through the major portal.

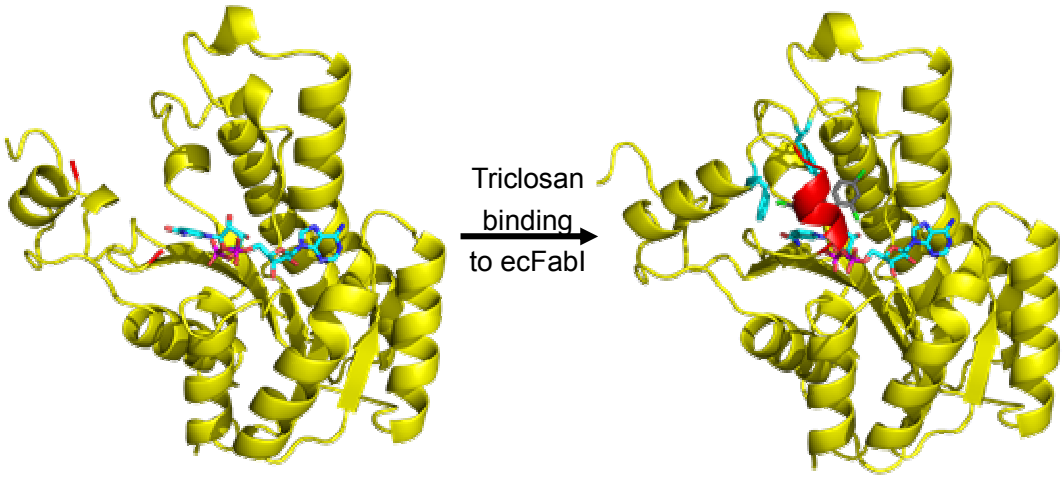

Figure 2.4. Inhibition Of *E. coli* FabI And Ordering Of The Substrate Binding Loop

Kisker and coworkers used X-ray crystallography to study the structure of ACP bound to the *E. coli* FabI enzyme (*137*). Most of the main chain electron density for both FabI and ACP was present. However, Ser36 of ACP is too far from the active site to deliver the substrate through the major portal with the observed relative orientation of ACP and FabI. Computational methods were employed by modeling the missing

details and, importantly, to ascertain how the ACP could deliver substrate into the FabI active site in the complex. Dr. Salma Rafi generated a model for a productive complex between ACP and FabI through molecular dynamics (MD) simulations. This suggested the ACP deliveries substrate through the minor portal and the ACP thioester carbonyl group does not form a hydrogen bond to Y156. Three key basic residues, K201, R204 and K205 located in the helix α8 of FabI, are proposed to interact with the helix α2 acidic patch of ACP's recognition loop. In order to study the model, I used a series of mutagenesis studies to provide the first detailed description of ACP recognition. We used mutagenesis studies to provide the first detailed description of ACP recognition (*137*).

2.2 Materials and Methods

X-ray crystallography and the MD simulations was performed by Dr. Kolappan and Dr. Rafi respetively.

2.2.1 Materials.

Coenzyme A (CoA) as a lithium salt was purchased from Sigma. Triethylamine was purchased from Aldrich (Milwaukee, WI). 15% SDS-PAGE pre-made gels were from Bio-Rad. Q-Sepharose and SP-Sepharose were purchased from Pharmacin Biotech Company. DE-52 resin was from Whatman. *trans*-2-dodecenoic acid was from TCI Chemicals (Portland, OR). β-NADH from *Leuconostoc mesenteroides* (type XXIV), and ethyl chloroformate were purchased from Aldrich. Oligonucleotides(primers) were purchased from IDT, Inc. Restriction enzymes (NdeI and BamHI) were purchased from Stratagene (La Jolla, CA). T4 ligase, calf intestinal alkaline phosphatase (CIP), and T7 cloned *pfu* polymerase were purchased from New England Biolabs Inc. (Beverly, MA). DNA purification and gel extraction kits were from Qiagen Inc. (Valencia, CA). His-Bind Resin, streptavidin-agarose, pET15(b) plasmid and biotinylated thrombin were purchased from Novagen. All other buffer salts (reagent grade or better), solvents (HPLC grade or better), and chemicals were purchased from Fisher Scientific Co.

2.2.2 Preparation of CoA substrates

trans-2-Dodecenoyl-CoA (DD-CoA) was synthesized from *trans*-2-dodecenoic acid using the mixed anhydride method (Figure 2.3) (*77*). Briefly, 252 μM (50 mg) of acid was dissolved in 10 mL of anhydrous THF with 315μM (32 mg) of triethylamine (TEA). Yellow salt crystals formed and the solution was stirred at room temperature under nitrogen for 2 hours followed by 315 μM (34 mg) of ethyl chloroformate (ECF) which was added to the solution very slowly. The mixed anhydride was then filtered and added slowly to a solution of 25 mg CoA in 50 mM Na_2CO_3 (pH 8.0) with stirring at room temperature. The reaction progress was monitored by following the concentration of free thiol in solution using 5,5'-dithiobis(2-nitrobenzoic acid) (DTNB) (*139*). The solution was purified by HPLC (Shimadzu) using a Phenomenex Primesphere 5 C_{18}-HC 250 mm × 4.60 mm (5 μm) preparative column when no free thiol was detected by UV. Chromatography was performed using 20 mM ammonium acetate/ 1.75% acetonitrile as buffer A and running a 0 to 100% gradient of 95% acetonitrile/5% H_2O as buffer B over the course of 60 minutes at a flow rate of 4 mL/min. Shimadzu SPD-10A UV-vis detector was used to monitor the elution at 260 and 285 nm. The fractions containing DD-CoA were pooled and lyophilized. The retention time for DD-CoA was around 23 min. The lyophilized white solid was redissolved in water and relyophilized twice to remove all ammonium acetate. The desired product was obtained in 40% yield as a flaky white powder with UV-vis extinction coefficient (ε_{260}) 20.4 $mM^{-1} \cdot cm^{-1}$. ESI-MS ($[M+H]^+$) was explored to

characterize DD-CoA: calculated 947.2, found 948.2.

2.2.3 Preparation of *E. coli* apo-ACP

The *E. coli* apo-ACP plasmid was a kind gift from Dr. Booker at Pennsylvania State University. Apo-ACP was expressed from plasmid pBHF-5 (*140, 141*). After growing cultures at 37 °C until an *A*600 of 0.6 was reached, casamino acids were added to a final concentration of 2 g/liter and expression was induced by the addition of 500 μM isopropyl β-D-thiogalactoside. Following an additional 4 h of growth at 30 °C, centrifugation yielded 8 g/liter of wet cell paste that was subsequently frozen. Frozen cell pellets (50 g) were then resuspended in 50 ml of 25 mM MES, pH 6.1, containing 200 mM NaCl (buffer A) and sonicated for 6 min using 30-s pulses at 4 °C. Cellular debris was removed by centrifugation at 33,000 rpm for 1 h at 4 °C and the supernatant was loaded onto a Q-Sepharose column (8 ml) preequilibrated with 25 ml of buffer A. The column was washed with 50 ml of buffer A and ACP was eluted using a linear gradient (50 ml) of NaCl from 200 to 850 mM NaCl in buffer A. Fractions were analyzed by 18% SDS-PAGE and ESI-MS, pooled, concentrated using an Amicon membrane (YM3, NMWL 3,000) and stored at -80 °C. Conformationally sensitive SDS-PAGE indicated that the ACP was predominantly in the apo form and ESI mass spectrometry revealed that the apo-ACP sample was comprised of two forms in which the N-terminal Met was present or had been cleaved. The apo-ACP was used without further purification for the synthesis of *trans*-2-dodecenoyl-ACP

(DD-ACP) (*137*).

2.2.4 Overexpression and purification of AcpS

A pET22(b) expression plasmid containing the gene for AcpS was a kind gift from Dr. Drueckhammer at Stony Brook University (Stony Brook, NY). The overexpression and purification of AcpS from *E. coli* has been published previously (*70*). The plasmid encoding its AcpS gene was transformed into *E. coli* BL21(DE3) pLysS cells for overexpression. Cultures were grown in 1 L of 2×YT medium containing 50 μg/mL ampicillin at 37℃ to an optical density of 0.8-1.0. AcpS was expressed in a soluble form by induction of mid-log phase cultures with 0.3 mM IPTG at 30℃ for 3 hours. The cells were harvested by centrifugation at 5000 rpm for 20 min at 4 ℃ and were resuspended (5 mL/g) in 50 mM Tris-HCl, 10 mM $MgCl_2$, 5% glycerol, pH 8 solution and sonicated. Cellular debris was removed by centrifugation at 33000 rpm for 1 hour. Then the cell-free extract was treated with 1 g of DE-52 slurry in 50 mM Tris-HCl buffer (pH 8.0) and mixed gently for 15 min at 4℃. The DE-52 was removed by centrifugation at 33000 rpm for 30 min. This step was repeated twice and the pH of the supernatant was adjusted to 6.5 with a saturated MES solution and the protein was loaded onto an 8 mL SP Sepharose column which preequilibrated with the buffer containing 50 mM MES, 10 mM $MgCl_2$, 5% glycerol (pH 6.1). Three column volumes of the buffer washed the column and AcpS was eluted with a linear gradient of 0-1 M NaCl buffer. SDS-PAGE was used to identify

the fractions containing AcpS. All AcpS fractions were pooled and concentrated with Centricon-10 (Millpore). The concentration of protein was calculated from the UV absorption at 280 nm using a ε_{280} 18.5 $M^{-1} \cdot cm^{-1}$.

2.2.5 Natural substrate synthesis of *E. coli*: *trans*-2-dodecenoyl-ACP (DD-ACP)

DD-ACP was synthesized from DD-CoA and apo-ACP using *E. coli* AcpS (*99*), which was overexpressed and purified from *E. coli* as described previously (*70, 137*). Briefly, 0.9 mg of apo-ACP was incubated with 50 μM DD-CoA (1.4-fold excess) and 50 μg of AcpS in 1.4 ml of 50 mM Tris-HCl, 25 mM $MgCl_2$, 1 mM dithiothreitol, pH 7.5, buffer for 1 h at 30 °C, followed by quenching the reaction by placing it into a dry ice/ethanol bath for 5 min. Subsequently, an equal volume of isopropyl alcohol was added and the reaction mixture was incubated for 2 h at 10 °C. AcpS was removed by centrifugation at 6000 rpm for 15 min and the supernatant was applied to a 1-ml Q-Sepharose column, equilibrated with 20 mM Bis-Tris, 1 mM dithiothreitol, pH 6.5 (Buffer A), containing 50% isopropyl alcohol. The column was washed three times with Buffer B containing 50% isopropyl alcohol, and then five times with Buffer A alone. DD-ACP was eluted with 5 column volumes of Buffer A containing 600 mM NaCl. The fractions containing DD-ACP were identified by SDS-PAGE and ESI-MS, pooled, concentrated, dialyzed into 20mM Tris-HCl, pH 7.0, and stored at -80 °C. The concentration of protein was determined by a kinetic assay.

2.2.6 Construction of Expression Plasmids for Wild-Type and mutual FabI

A pET15(b) expression plasmid containing the FabI gene was used as a template for FabI mutagenesis utilizing the QuikChange mutagenesis kit (Stratagene). A list of primers that were used for mutagenesis is given in Table 2.1. The plasmids encoded wild type and mutant FabI were purified from XL1 blue cells (Stratagene) using a DNA purification and gel extraction kit from Qiagen Inc. All the plasmids were transformed into BL21(DE3)pLysS cells (Novagen) for protein expression.

Table 2.1. Primers used for mutagenesis[a]

Mutant	Primer[b]
K201E (forward, F)	5'-TCCGGTATC**GAA**GACTTCCGCAAAATGCTG -3'
K201E (reverse, R)	5'-GCGGAAGTC**TTC**GATACCGGAGGCCGCCAG -3'
K201A (F)	5'-TCCGGTATC**GCA**GACTTCCGCAAAATGCTG -3'
K201A (R)	5'-GCGGAAGTC**TGC**GATACCGGAGGCCGCCAG-3'
R204E (F)	5'-AAAGACTTC**GAA**AAAATGCTGGCTCATTGC -3'
R204E (R)	5'-CAGCATTTT**TTC**GAAGTCTTTGATACCGGA-3'
R204A (F)	5'-AAAGACTTC**GCC**AAAATGCTGGCTCATTGC -3'
R204A (R)	5'-CAGCATTTT**GGC**GAAGTCTTTGATACCGGA -3'
K205E (F)	5'-GACTTCCGC**GAA**ATGCTGGCTCATTGCGAA -3'
K205E (R)	5'-AGCCAGCAT**TTC**GCGGAAGTCTTTGATACC -3'
K205A (F)	5'-GACTTCCGC**GCA**ATGCTGGCTCATTGCGAA -3'
K205A (R)	5'-AGCCAGCAT**TGC**GCGGAAGTCTTTGATACC -3'

[a]Forward and reverse primers are listed. [b]Mutation site is underlined in bold

2.2.7 Overexpression and purification of wild-type and mutant FabI

Cultures of BL21(DE3)pLysS cells carrying the wild-type and mutant plasmids were growing in 1 L of LB-ampicillin (200 μg/mL) medium at 37 ℃ to an OD_{600} of 1.2 (*31, 32*). FabI was expressed in a soluble form by induction of mid-log phase cultures with 1 mM IPTG at 25℃ overnight. The cells were harvested by

centrifugation, resuspended in 40 mL of His-bind buffer (20 mM Tris-HCl, 0.5 M NaCl, 5 mM imidazole, pH 7.9), and lysed using sonication. Cell debris was removed by centrifugation (33000 rpm for 1 hour) and the supernatant applied to a His-bind resin column (8 mL bed volume). The His-bind column was washed successively with His-bind buffer and His-wash buffer (20 mM Tris-HCl, 0.5 M NaCl, 60 mM imidazole, pH 7.9), and the protein was eluted using a gradient of 0 to 1 M imidazole in 20 mM Tris-HCl and 0.5 M NaCl (pH 7.9). Fractions containing His-tagged FabI were immediately pooled and applied to a 2 cm × 50 cm Sephadex G-25 column (Pharmacia) preequilibrated with 30 mM PIPES, 150 mM NaCl, and 1 mM EDTA (pH 8.0). SDS-PAGE and ESI-MS were used to determine the purity of protein. The eluted protein is not allowed to remain in the high concentration of imidazole elute buffer because it caused the protein to precipitate. Fractions containing the His-tagged protein from the G-25 column were pooled and concentrated with a Centricon-30 (Millpore). The concentration of protein was calculated from the UV absorption at 280 nm using an absorption coefficient of 16.5 $M^{-1} \cdot cm^{-1}$ for the wild type and the mutant enzymes. The protein was stable at 4℃ for 3 months.

2.2.8 Kinetics of DD-CoA and DD-ACP with FabI and mutants

The kinetic measurements were performed on a Cary 300 Bio (Varian) spectrophotometer at 25 ℃ in 30 mM PIPES and 150 mM NaCl (pH 6.8) (*142-144*). Specifically, the enzyme concentration was 10 nM and the DD-CoA concentration

was varied from 5 to 150 μM while NADH was maintained at a fixed concentration of 250 μM. Higher concentrations of DD-CoA could not be used since they result in a decrease in rate due to substrate inhibition (*145*). Steady-state K_m and k_{cat} values for WT FabI were determined at variable concentrations of one substrate and at fixed concentration of NADH. The enzyme concentration of mutants FabI, K201E, K201A, R204E, R204A, K205E and K205A were fixed to 100 nM when the natural substrate was used, no substrate inhibition was detected even DD-ACP concentration was up to 300μM. The initial velocities were obtained by following the oxidation of NADH to NAD^+ at 340 (ε=6.3 mM^{-1} cm^{-1}) or 370 nm (ε=2.4 mM^{-1} cm^{-1}). Each initial velocity was measured in triplicate and at least five different substrate concentrations were used. All the data were plotted to equation 1 using Grafit 4.0 software to determine the K_m and k_{cat} where [S] is the concentration of the varied substrate and $[E]_0$ is the total enzyme concentration.

$$v = k_{cat} [E]_0[S] / (K_m + [S]) \quad (1)$$

2.2.9 Fluorescence Titration of FabI and mutant FabI by DD-ACP

Fluorescence titration (*145*) was conducted with a model PTI spectrofluorimeter. The measurements were carried out in 100 mM PIPES, pH 8.0 and at 25 ℃. FabI and mutants were excited at 290 nm (5 nm slit widths), the emission wavelength was fixed to 340 nm (1 nm slit width). Normally, 1 μL aliquots of 460 μM FabI or mutants was

added to a 1 mL buffer, the titrations were making with concentrated DD-ACP stock solution to the 1 mL buffer cuvette. Dilution of protein caused by InhA was kept to < 1%. Data were fit to a quadratic equation (eq 2) (*76*) instead of a simple hyperbolic function for a second order binding process.

$$Bound = \frac{(K_d + [E]_0 + [DDACP]) - \sqrt{(K_d + [E]_0 + [DDACP])^2 - 4K_d[E]_0}}{2[E]_0} \quad (2)$$

Bound is the fluorescence intensity change when DD-ACP was added, $[E]_0$ is the initial FabI concentration, K_d is the dissociation constant and [DDACP] is the concentration of added DD-ACP. Data fitting was achieved by software programs Grafit 4.0.

2.3 Results

2.3.1 Mutagenesis, overexpression and purification of wild-type and mutant proteins

All proteins were expressed with an N-terminal His-tag sequence which enabled a single-step purification using metal affinity chromatography. 12% SDS-PAGE was used to analysis the purity of all proteins (Figure 2.5). The molecular weight of FabI is 27.7 kDa without a His-tag. The strong bands in the gel are FabI with His-tag, around 30 kDa.

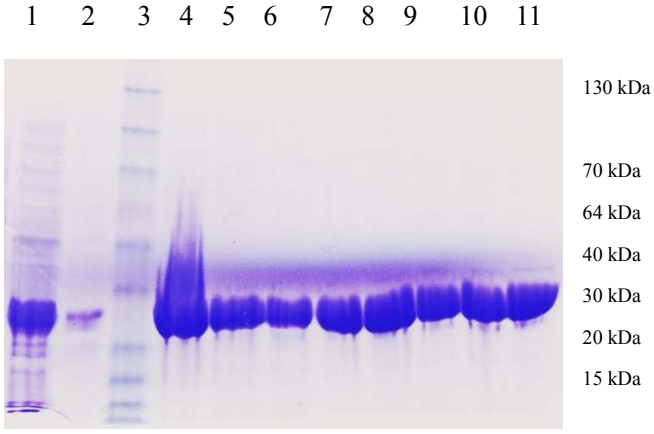

Figure 2.5. 12 % SDS-PAGE of FabI purification. Lane 1 represents original supernatant before His-tag affinity chromatography column; Lane 2: wash solution from His-tag column; Lane 3: MW Ladder; Lane 4-7: Fractions from the His-tag; Lane 5-11: FabI fractions from G-25 column.

2.3.2 Overexpression and purification of AcpS

Holo-ACP synthase (AcpS) catalyzes the conversion of apo-ACP to acyl-ACP which is the substrate for the enoyl reductase enzymes. AcpS is a basic protein (PI 9.3) and it was purified using SP Sepharose cation exchange chromatography. The protein purification was monitored using 15% SDS-PAGE (Figure 2.6). The molecular weight of AcpS is 14 kDa which agrees with the molecular weight shown in the gel.

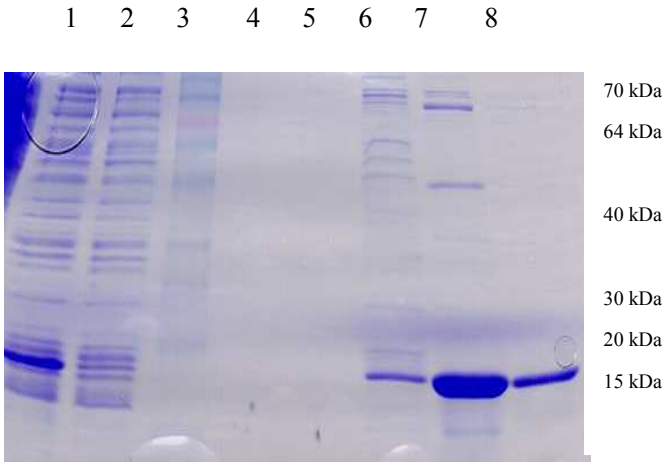

Figure 2.6. 15% SDS-PAGE of AcpS purification. Lane 1: Cells after induction; Lane 2: Cells before induction; Lane 3: MW marker; Lane 4-8: SP-Sepharose elution fractions.

2.3.3 Overexpression and purification of apo-ACP and synthesis of nature substrate of FabI: DD-ACP

E. coli apo-ACP plasmid was cloned into a vector containing the T7 lac promoter for constitutive expression of lac repressor (pBHF-5), cells were capable of growth and expression of ~105 mg L^{-1} ACP (*141*). The culture density reached a maximum

~2 h after induction with lactose at 37 ℃ during the fermentations. The growth period could be extended to ~4 hours by decreasing the temperature to 30 ℃ during induction. The majority of ACP expressed from pBHF-5 cells was in the apo form. 18% SDS-PAGE determined the purity of apo-ACP (Figure 2.7).

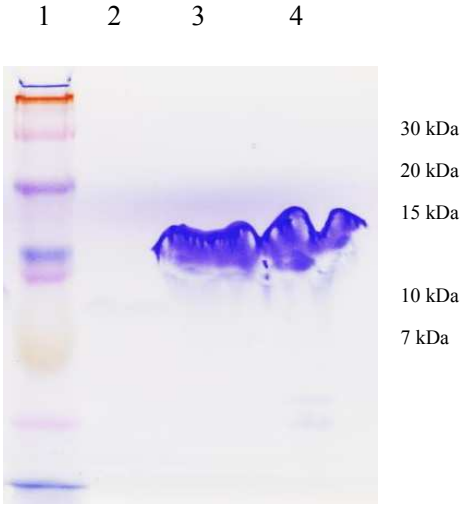

Figure 2.7. 18% SDS-PAGE of apo-ACP. Lane 1: MW ladder; Lane 2-4: Fractions of Apo-ACP from Q-Sepharose column.

ESI-MS also revealed that the purified apo-ACP contained two different molecular weight. Specifically, one with a MW 8637 Da, consistent with apo-ACP with N-terminal Met, and the other is 8506 Da lacking Met (Figure 2.8) (*113, 116*).

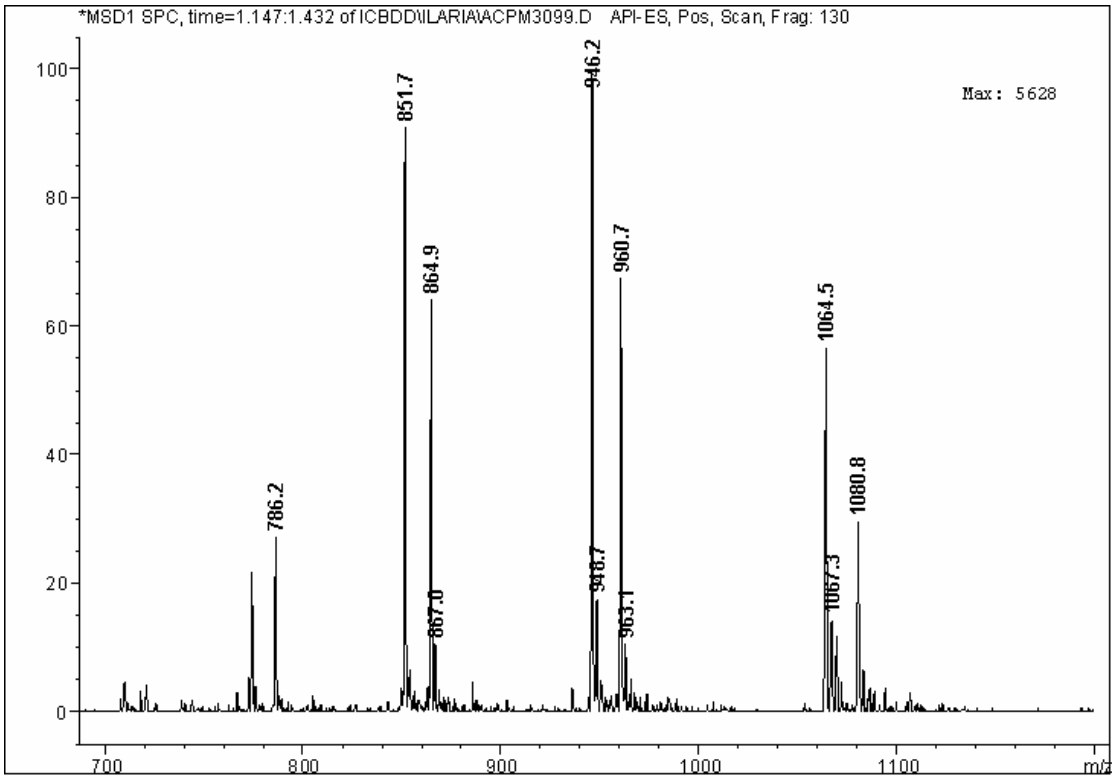

Figure 2.8. ESI-MS data for Apo-ACP. The peaks were deconvolved and assigned. 774.4, 851.7, 946.2, and 1064.5, were deconvolved to 8506 Da and assigned to apo-ACP without Methionine at the N-terminal. 768.2, 864.9, 960.7, and 1080.8, were deconvolved to 8637 Da and assigned to apo-ACP with Methionine residue.

DD-ACP was synthesized from apo-ACP and DD-CoA using AcpS as the transferase and was purified by Q-Sepharose column. ESI-MS characterized the MW of DD-ACP (Figure 2.9). There were two forms DD-ACP (with methionine and without methionine) corresponding to the two forms of apo-ACP. After deconvolution, peaks 821.3, 903.7, 1003.9, 1129.6 were deconvolved to 9027 Da which is 521 Da higher than apo-ACP without methionine.

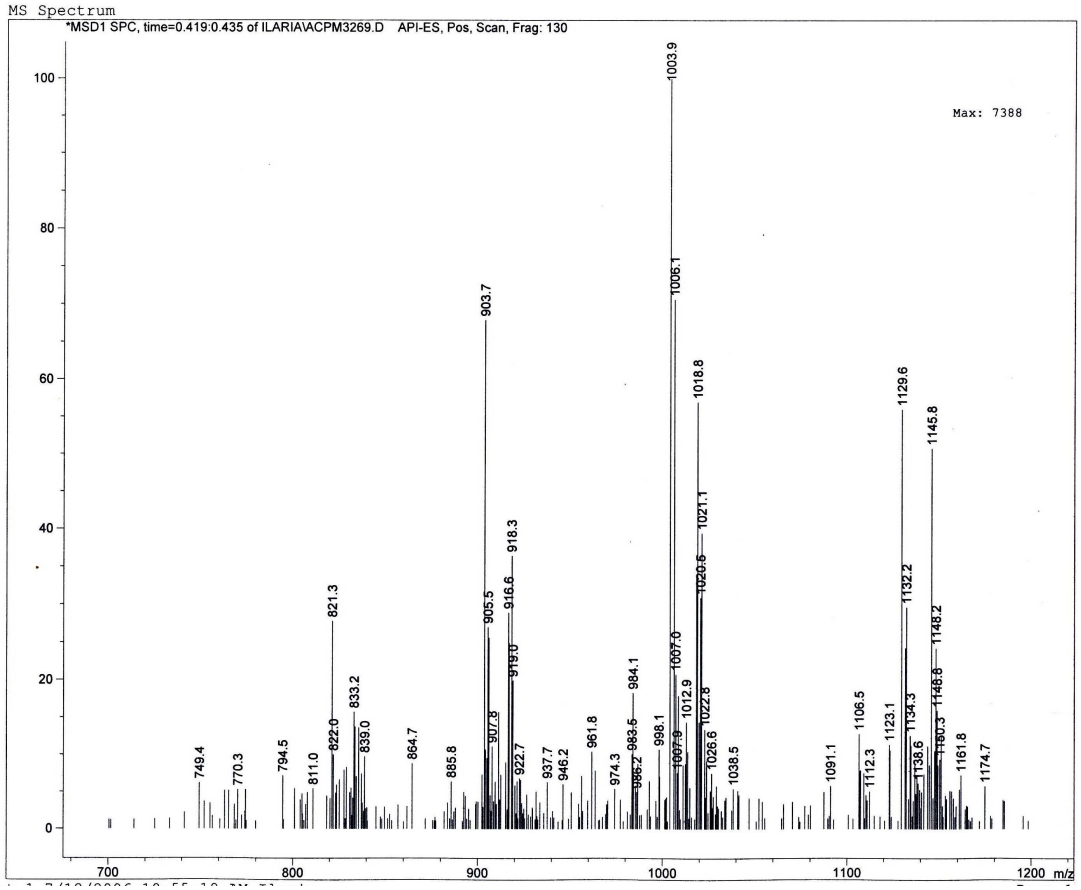

Figure 2.9. ESI-MS data for DD-ACP. The peaks were deconvolved and assigned. 821.3, 903.7, 1003.9, 1129,6, were deconvolved to 9027 Da and assigned to DD-ACP without Methionine at the N-terminal. 833.2, 918.3, 1018.8, and 1145.8, were deconvolved to 9138 Da and assigned to DD-ACP with Methionine residue.

2.3.4 Kinetics analysis of wild type and mutant FabIs

Kinetics parameters for the wild type and the mutant FabIs with DD-CoA and DD-ACP substrate are given in Table 2.2 and 2.3.

Table 2.2: Steady state kinetics data for DD-CoA substrate

FabI	DD-CoA			
	K_m (μM)	k_{cat} (min^{-1})	k_{cat}/K_m ($min^{-1}\cdot\mu M^{-1}$)	Ratio
Wild Type	24.2±3.2	797±37	33±2	1
K201E	29.8 ± 0.2	987±56	33±2	1
K201A	22.3±1.5	733±20	33±2	1
R204E	16.1±2.3	1300±70	80.7±4	2.4
R204A	18±2	1470±53	81±5	2.4
K205E	21.5±1.0	439±8	20.4±0.4	0.6
K205A	24±5	716±38	29.8±2	0.9
Y156F	19±1	1160±35	61±5	1.8
Y146F	10±1	24±1	2.4±0.3	0.07

Table 2.3: Steady state kinetics data for DD-ACP substrate

FabI	DD-ACP			
	K_m (μM)	k_{cat} (min^{-1})	k_{cat}/K_m ($min^{-1}\cdot\mu M^{-1}$)	Ratio
Wild Type	3.3±0.2	896±16	271±5	1
K201A	13.2±0.6	582±12	44±2	0.16
R204E	89.5±8.8	94±4	1.05±0.04	0.004
R204A	291±31	1546±87	5.3±0.5	0.02
K205E	48±2	1027±17	21.3±1	0.07
K205A	14.3±1.5	857±26	57±2	0.2
Y156F	4.6±0.5	1140±50	250±40	0.9
Y146F	2.4±0.2	14±1	6±1	0.02

The data in Table 2.2 and 2.3 demonstrate that replacement of K201, R204, and K205 with Ala or Glu has little or no effect on the kinetic parameters for reduction of DD-CoA, whereas k_{cat}/K_m for reduction of DD-ACP is reduced 5 (K201 and K205) to 50 (R204)-fold. In addition, replacement of R204 and K205 with Glu causes a further reduction in k_{cat}/K_m for reduction of DD-ACP without affecting k_{cat}/K_m for the DD-CoA substrate. Similar to the Ala mutants, substitution of Glu for R204 has a larger impact on substrate reduction (250-fold) compared with K205 (14-fold). Finally, replacement of K201 with Glu resulted in an enzyme with little activity toward either substrate (data not shown) and we were unable to determine accurate

kinetic parameters for this mutant (*137*).

We have also examined the importance of Y156 and Y146, the two active site Tyr residues, in substrate reduction. Replacement of Y156 with Phe has no effect on substrate reduction in agreement with previous studies on both FabI (*32*) and InhA *(33, 76),* which questioned the importance of Y156 (Y158 in InhA) in catalysis (59). In contrast, mutagenesis of Y146 has a larger impact on catalysis, with k_{cat} and k_{cat}/K_m for DD-ACP decreasing by around 50-fold compared with wild-type FabI. A similar decrease in kinetic (*146*) parameters for Y146F was also observed for the DD-CoA substrate (*137*).

2.3.5 Equilibrium Binding of DD-ACP to Wild-Type and Mutant FabI Proteins

The direct binding data were measured using a fluorimeter and analyzed using a quadratic equation (eq 3). The results are shown in Table 2.4. FabI binds tightly with DD-ACP from the direct binding experiments. When K201, R204, and K205 are mutated, the K_d decrease 4-5 fold binding affinity with ACP.

Table 2.4: Fluorescence titration of FabI and mutants by DD-ACP

	FabI	K201E	K201A	R204E	R204A	K205E	K205A
K_d (nM)	38.3±6.4	171±17	99±19	200±21	158±15	139±47	73±35

2.4 Discussion

The formation and dissociation of protein complexes plays an important role in numerous biological processes (*147*). Questions have been addressed including how the binding site on a protein can be identified and how a protein-protein interface can be predicted. Improved shape complementarity, van der Waals contacts, hydrogen bonding, increased buried surface area, and entropic restriction of interacting residues have been addressed to increase affinity of protein-protein complex (*148*). The accurate prediction of protein complex structure can provide the direct information for drugs or inhibitor design and for protein engineering (*149*). However, the principles of protein-protein interactions still are unclear because protein interfaces vary greatly in size, composition, shape and solvent content (*150*).

ACPs are small, acidic proteins that fulfill an essential role in metabolism through their interactions with a diverse array of target enzymes. Despite their central role, the nature of the proper recognition and precise alignment between the protein moieties of ACP and its many interactive proteins is not understood (*130*). Residues conserved among ACPs from numerous plants and bacteria were predicted as being crucial to ACP's function, protein-protein interaction (*151, 152*). Based on a combination of X-ray crystallography, computational modeling, and site-direct mutagenesis, we report first structural data for the direct interaction of an acyl-ACP substrate with the FASII FabI enzyme. The FabI:ACP structure not only gives us a general insight into

how target proteins recognize and bind to ACP, but also provides a foundation for the development of novel FabI inhibitors that antagonize the fatty acid biosynthesis pathway.

The structure of the final FabI-ACP structure is shown in Figure 2.10. ACP interacts with FabI helix α8 and delivers the substrate to the active site between helix α8 and a loop comprised of FabI residues 152-156 (*137*).

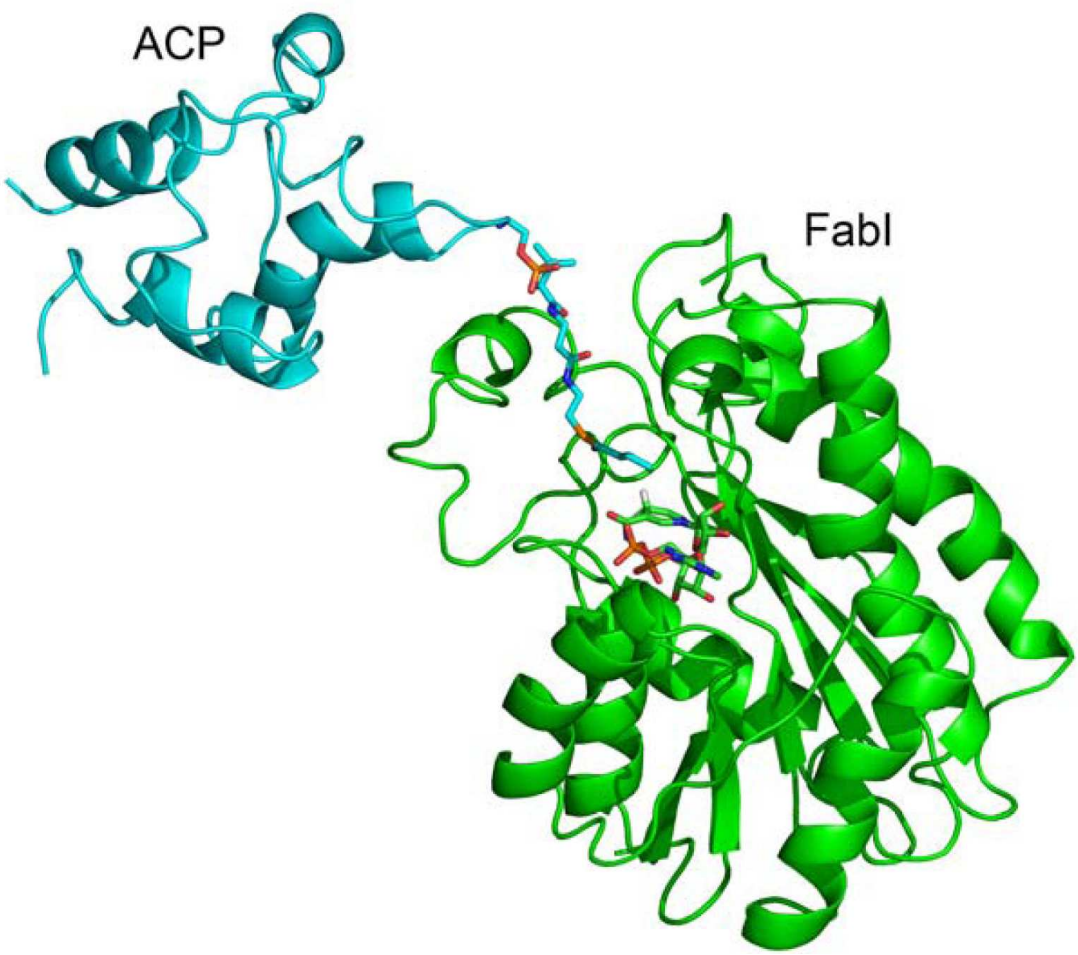

Figure 2.10. The Structure of ACP Bound to FabI Following MD Simulations

Several important interactions at the FabI-ACP interface and also between the phosphopantetheine and the FabI protein were revealed by the analysis of the structure (Figure 2.11). Residues K201, R204, and K205 from helix α8 of FabI interact with residues D35, D38, E41, and E48 of ACP helix α2, while FabI K201 also interacts with Q14 in ACP. The side chain amino group of FabI K205, which interacts with D35 in ACP helix α2, is hydrogen bonded to the phosphopantetheine phosphate (O-7). In addition, the backbone carbonyl of FabI K205 forms a hydrogen bond to the pantetheine hydroxyl group (O-10) while Hε2 of H209 is hydrogen bonded to the pantetheine 4" amide carbonyl oxygen. Finally, the pantetheine 2" amide nitrogen forms a hydrogen bond to the backbone carbonyl of D202 (Figure 2.11). The FabI-ACP complex is stabilized by these interactions between the ACP pantetheine which positions the substrate within the active site. In the final structure, the distance between the crotonyl C3 and the NADH pro4(*S*) proton is 3 Å. Analysis of the structure also reveals that the crotonyl thioester carbonyl is located 4 Å from the Y146 hydroxyl group, suggesting that Y146 may form a hydrogen bond to the thioester during substrate reduction (Figure 2.11) (*137*).

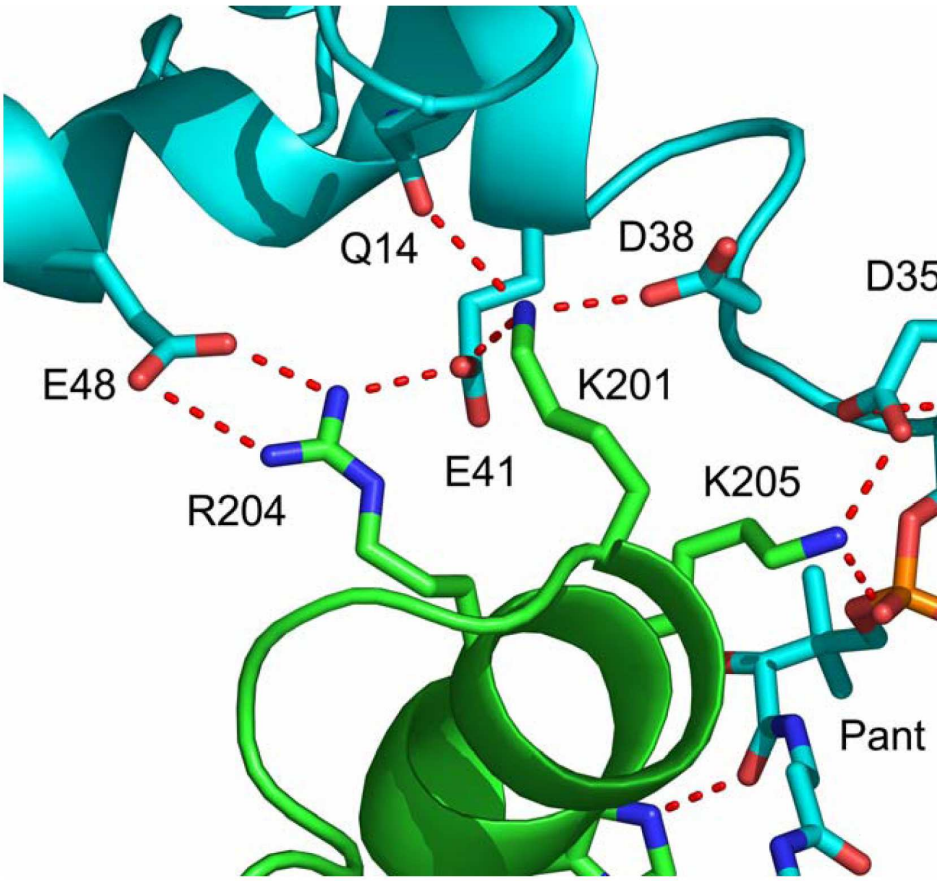

Figure 2.11. Interactions between FabI and ACP. Interactions between ACP (*cyan*) and FabI (*green*) at the helix2 (ACP) and helix8 (FabI) interface.

Sacchettini and coworkers have stated there were two entry points for substrates into the active sites of enoyl reductases, the major and minor portals (*75, 137*). The present structure indicates that binding of ACP to FabI delivers the acyl-pantetheine to the active site between loops comprised of residues 192-206 and 152-156 so that the fatty acid enters the active site through the minor portal. Rock and coworkers also proposed the same ACP-FabI binding interface which is consistent with our mutagenesis and fluorescence data (*104, 112*). The experimental results confirmed the hypothesis that K201, R204, and K205 of FabI are important for binding ACP. The

mutants retained the same k_{cat} and K_m values for the CoA bound substrate which indicated that the enzymes were still catalytically active and that these residues are not important for CoA binding. However, when tested with DD-ACP, the binding of ACP is much weaker to R204E and K205E than to the wild type FabI.

In summary, the crystal structure of *E. coli* enoyl reductase, FabI in complex with *E. coli* DD-ACP has been determined and it has been showed that the basic patch located in helix α8 of FabI interacts with the acid patch located in helix α8 of ACP by hydrogen bonding interaction. The conclusion from the crystallography analysis has been confirmed by mutagenesis and steady state kinetics studies. Future studies on the interaction of *M. tb* AcpM with InhA leads us to the question of whether all enoyl-ACP reductase interact with ACP in the same way.

Chapter 3: Substrate recognition of AcpM with InhA

3.1 Introduction

The mycobacterial FASII system is responsible for the elongation of fatty acids to form mycolic acids which are very long chain (60-90 carbons) α-alkyl, β-hydroxy fatty acids (*55, 56*). The specifics of mycolic acid synthesis are not known. The enzymes of the FASII pathway in *M. tb* use an acyl carrier protein, AcpM, for substrate delivery (*99, 153-155*). Thus, AcpM plays an important role in the production of mycolic acids. AcpM shares a high degree of similarity to typical bacterial ACPs, especially around the serine residue where the 4'-phophopantethiene moiety is attached and along helix α2. Solution structures derived from NMR indicate that AcpM contains the standard four-helix ACP fold along with an unfolded C-terminal extension. This random coil at the C-terminal is the most obvious difference between AcpM and the ACPs of most other organisms. An exception is the ACP from *Rhizobium leguminosarum*. The C-terminal tail of this organism's ACP functions in the biosynthesis of long chain Acyl-ACPs which are used to synthesize the nodulation factor (*156, 157*).

The random coil at the C-terminal of AcpM is a natively unfolded domain. There are two possible roles for the this extension in the function of AcpM. The C-terminal domain may interact with the long chain fatty acid intermediates which are carried by

the protein. More than half of the residues of AcpM are hydrophobic and are proposed to sequester the long acyl chain from solvent. Another possible function for this long C-terminal tail is in protein-protein interactions. The *M. tb* genome contains at least three ACP sequences. AcpM gene (*Rv2244*) is located in an operon together with several other FASII genes all involved in the FASII mycolic acid elongation system (*158, 159*). The biosynthesis and assembly of these structures offer potential targets for chemotherapeutic intervention because mycolic acids are essential for the intracellular survival of *M. tb* (*121, 153*). Targeting the mycolic acid biosynthetic pathway has been validated. InhA, the enoyl-reductase from *M. tb*, is already the target of several antimicrobial drugs (*160, 161*).

ACPs interact with a wide variety of enzymes to load carbon units, condense them and modify the product. ACPs function in FASII mediated biosynthesis and vary in molecular mass from 7.5 kDa (*E. coli*) to 13 kDa (*M. tb*) (*93, 103, 121*). The structures of ACP and AcpM have been solved by both X-ray crystallography and NMR spectroscopy (*94*). The structures reveal a common four-helix with a long loop I connecting helices I and II (*106, 162*). In contrast to Ser36 of ACP from *E. coli,* the Ser41 of *M. tb* AcpM attaches the 4'-phosphopantetheine prosthetic group to the active site of InhA (*129*). In addition, based on X-ray crystallographic analysis, ACP has been shown to adopt two major conformations: either as an integral domain to deliver the acyl chain to the target enzyme (type I) or as a discrete protein to transport the growing acyl chain to constitute a multi-enzyme synthase complex (type II) (*95*).

Because of its flexibility in solution, ACP has a lower affinity for the target protein, so the structural crystallography of ACP interacting with target proteins is sparse. Somers and coworkers (*96*) have determined the crystal structure of ACP in complex with Holo-ACP synthase (AcpS). AcpS connects the phosphopantetheine to the serine of ACP. They confirmed the importance of some acidic residues located at the ACP recognition helix α2 in interacting with a patch of basic residues on the *E. coli* β-ketoacyl-ACP synthase (FabH) and the β-ketoacyl-ACP reductase (FabG) enzymes (*104, 112*).

InhA (*163-172*) catalyzes the last step of the fatty acid synthesis pathway (*77*). FabI in *E. coli* and InhA in *M. tb* are both members of the short chain dehydrogenase/reductase (SDR) family of enzymes, which are in turn members of the well-established family of oxidoreductase enzymes. Over 30 three-dimensional structures of SDR enzymes have been published in the protein sequence database. They display highly similar α/β folding patterns with a central β-sheet even through their sequence identity is low (about 15-30%). Most of the SDR enzymes are 250-350 amino acid residues in length. Furthermore, the cofactor binding domain and the active site residues of SDRs are highly conserved as seen by sequence alignment of the different enzymes in the SDR family. The glycine rich T-G-X_3-G-X-G motif near the N-terminal is the cofactor binding region. Another Y-X_{3-7}-K motif is found at the active site where the reaction is catalyzed (*33, 144, 173*).

All members of the SDR family contain a conserved catalytic triad which includes a tyrosine and a lysine residue. In InhA, these residues are Y158 and K165. The tyrosine residue forms a hydrogen bond with the thioester carbonyl moiety to interact with the substrate directly. Sacchettini and coworkers solved the crystal structure of InhA in complex with NAD^+ and the substrate analog, *trans*-2-hexadecenoyl-(N-acetylcysteamine)-thioester (C16-NAC) (*75*). Similar to FabI, there is a hydride transfer from the C4 position of NADH to the C3 position of the substrate double bond which yields an enolate intermediate. An enol is formed when a proton is added to the enolate oxygen. Tyr158 of InhA does not function as a proton donor in the reaction but is proposed to serve as an electrophilic catalyst stabilizing the transition state for hydride transfer by hydrogen bonding to the substrate carbonyl (*76*). Similar to the dehydrogenases, structural and kinetic studies have revealed that K165 in InhA functions primarily in cofactor binding, forming hydrogen bonds with the nicotinamide ribose 2' and 3' hydroxyl groups (Figure 3.l) (*76, 83, 174*).

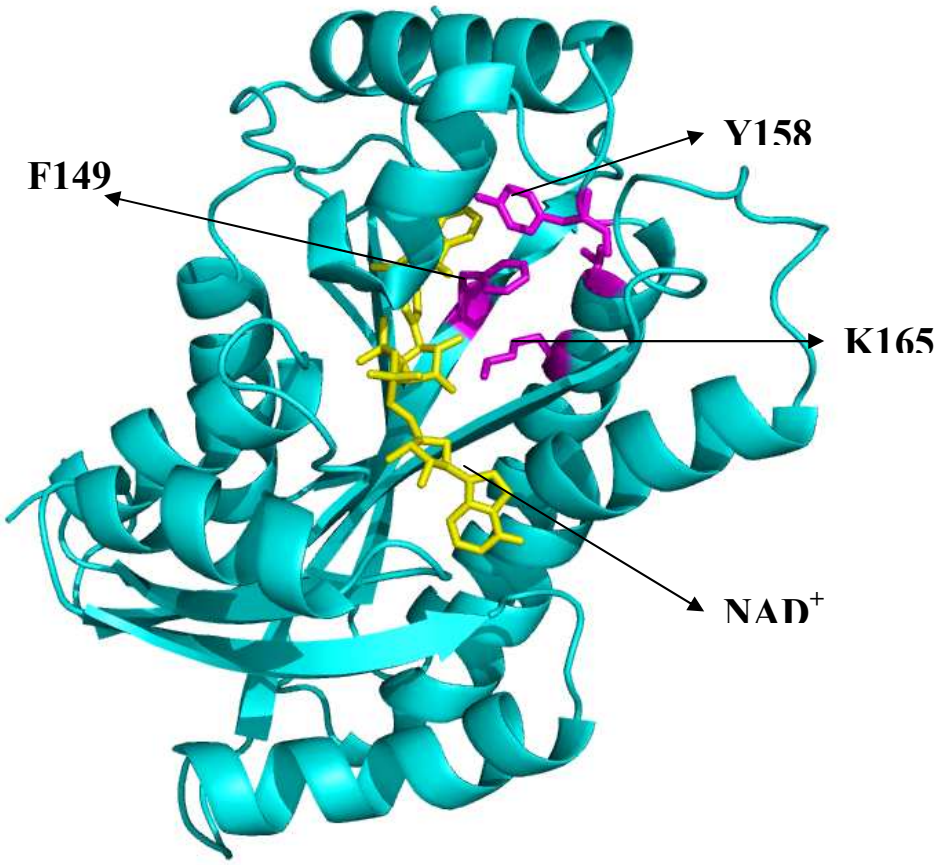

Figure 3.1. Crystal structure of the isonicotinic acyl-NADH adduct bound inside the InhA active site.

The third residue in the catalytic triad of the dehydrogenases is a Ser or Thr residue in dehydratases or a Phe or Tyr (F149 in InhA) in the enoyl reductases. The role of the conserved Phe/Tyr in the reductases is less clear. The side chain of F149 is above the nicotinamide ring from the crystal structure of NADH-InhA complex. Our lab used Raman spectroscopy and isotope effect to investigate the role of F149 in the catalytic reaction (*83*).

The chain length substrate specificity of the two reductases is different, where FabI catalyzes no more than 16 carbons but the maximum carbon substrate can reach

60-90 for InhA. Rock et al. proposed an ACP-FabI binding interface (*104, 112*). We have determined the structure of ACP bound to the FabI enzyme (*137*) using X-ray crystallographic data and computational methods to model in the missing details. However, the ACP Ser36 residue is too far from the active site to deliver the substrate. Modeling studies show that ACP interacts with a patch of basic residues located in the helix α8 of FabI. They showed that Lys201, Arg204, and Lys205 in FabI hydrogen bond with the Asp35, Asp38, and Glu41 of ACP. Mutation studies agree with the model. Replacement of Lys201, Arg204, or Lys205 by Ala or Glu shows a significant decrease in k_{cat}/K_m for DD-ACP reduction and without affecting the kinetics parameters for DD-CoA substrate (*137*).

Similar to ACP, AcpM contains lot of acidic Glu and Asp residues. The importance of these acidic residues in the α-helix binding has been confirmed and the basic residues on the *M. tb* InhA identified. The interaction of four important acidic residues, Asp53, Glu46, Asp40, and Asp38 with the basic patch of helix α8 of InhA has been investigated.

We already have analyzed the FabI-ACP interaction. The question must be addressed is whether InhA interacts AcpM in the same way. However, InhA does not have the same basic patch as FabI. Arg195, Arg 225, and Lys233 are very close to the helix α8 of InhA. In addition, InhA has other basic patches, Arg53, Arg49, Arg45, and Arg43 are located at helix α2 of InhA, another basic patch is located at helix α6 of

InhA including Lys181, Arg177 and Arg173 (Figure 3.2). All these residues will be investigated using kinetics and fluorescence.

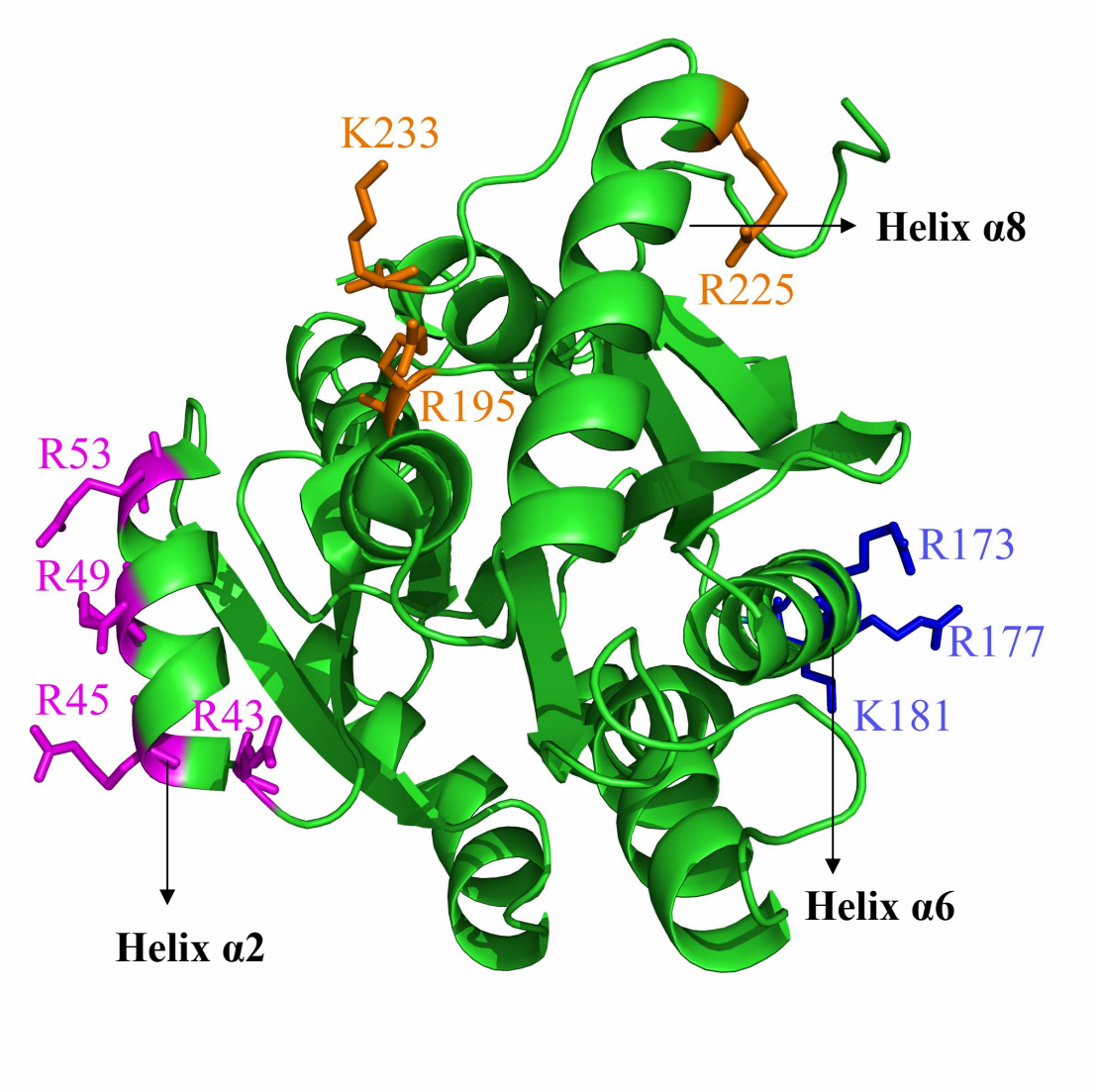

Figure 3.2. The basic patches around InhA. R195, R225 and K233 are located near the minor portal. R45, R49 and R53 are adjacent to major portal and another three basic residues (R173, R177 and K181) in another α helix opposite to the major portal.

Our lab focuses on the binding experiments between the FASII enoyl reductase

enzyme InhA with the natural substrate AcpM. Our previous studies on InhA have utilized *trans*-2-dodecenoyl-CoA (DD-CoA), an unsaturated C12 fatty acid which is esterified to coenzyme A. However, in order to make the assay system as relevant as possible, we want to extend the studies to the natural substrate AcpM. This is challenging because there are three forms AcpM: Apo-, Holo- and Acyl-AcpM (Figure 3.3).

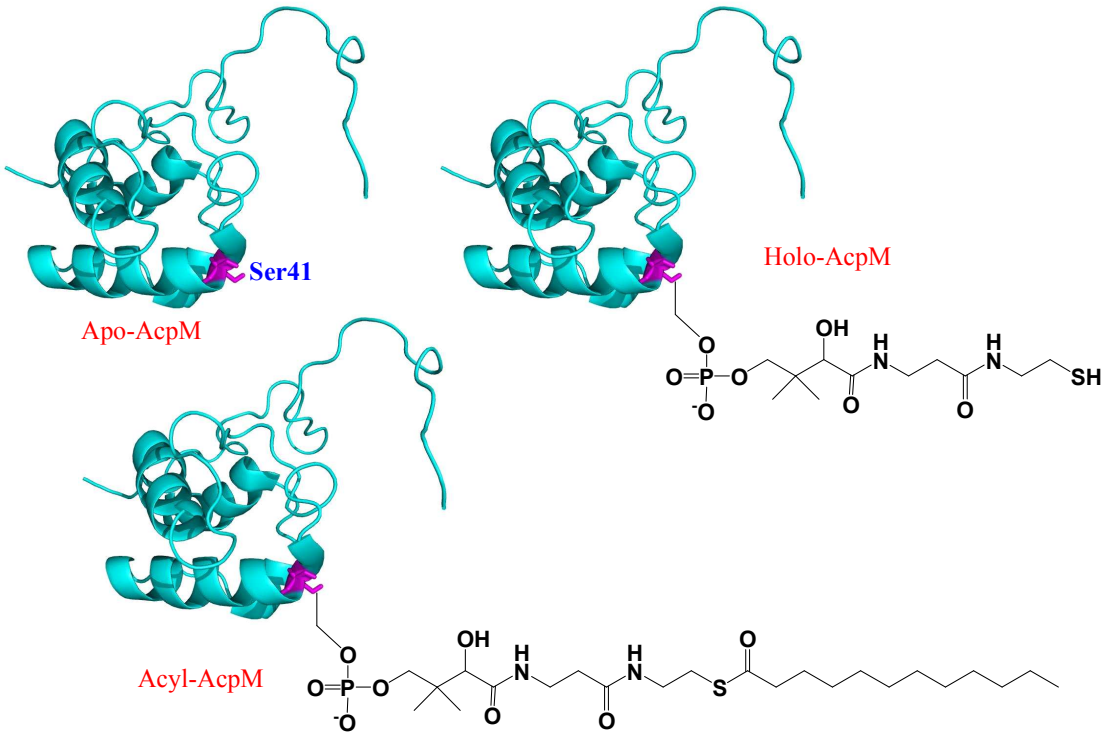

Figure 3.3. Three forms AcpM: Apo-, Holo-, Acyl-AcpM

Purification methods (such as HPLC, FPLC etc.) to separate the three different AcpM forms are needed because Apo-AcpM is the only active form to synthesize a natural substrate of InhA, DD-AcpM. We can then synthesize DD-AcpM substrates

using the Holo-ACP synthase to transfer the acyl-pantetheine from DD-CoA to Apo-AcpM. The method to synthesize DD-AcpM is the same as DD-ACP (Figure 2.3).

Kinetics studies using UV spectroscopy and the cofactor NADH support the detailed interaction of AcpM with InhA and mutants. Fluorescence is another direct method to determine the dissociation constant between the InhA and AcpM in the absence of NADH. Mutagenesis studies demonstrate the details of the interaction between AcpM with InhA in the resulting models.

3.2 Materials and Methods

3.2.1 Materials.

Coenzyme A (CoA) as a lithium salt was purchased from Sigma. 15% SDS-PAGE pre-made gels were from Bio-Rad. Q-Sepharose and SP-Sepharose were purchased from Pharmacia Biotech Company. DE-52 resin was from Whatman. *trans*-2-Dodecenoic acid was from TCI Chemicals (Portland, OR). β-NADH from *Leuconostoc mesenteroides* (type XXIV), and ethyl chloroformate were from Aldrich. Oligonucleotides(primers) were purchased from IDT, Inc. His-Bind Resin, streptavidin-agarose, pET15b plasmid and biotinylated thrombin were purchased from Novagen. All other buffer salts (reagent grade or better), solvents (HPLC grade or better), and chemicals were purchased from Fisher Scientific Co.

3.2.2 Preparation of Substrates: *trans*-2-Dodecenoyl-Coenzyme A and dodecenoyl-AcpM

trans-2-Dodecenoyl-CoA (DD-CoA) was synthesized from *trans*-2-dodecenoic acid using the mixed anhydride method (*76*). A stock of pET24 AcpM plasmid was transformed into BL21(DE3) cells (*99*). AcpM was expressed in a soluble form by induction of mid-log phase cultures (A_{600}=0.7) with 0.3 mM IPTG at 37℃ for 2.5 hours. Cells were harvested by centrifugation at 5000 rpm for 20 min at 4 ℃,

resuspended in 20 mL buffer C (20 mM Bis-Tris, 200 mM NaCl, 1 mM DTT, pH 6.5) and lysed by 3 cycles of freezing and thawing after adding 2 mg/mL lysozyme. The pH of the cell-free supernatant was adjusted to 8.5 using 1 M Tris base, and $MgCl_2$ and $MnCl_2$ were added to final concentrations of 10 and 2 mM, respectively. The lysate was centrifuged at 11,000 rpm for 30 min following 2 hour incubation at 35℃. An equal volume of isopropanol (IPA) was added slowly to the supernatant which was then stirred for 2 h at 4 ℃. The sample was centrifuged at 6000 rpm for 10 min at 4 ℃ to remove the precipitate. The pH of the 50 % IPA-soluble lysate was adjusted to 6.5 with acetic acid and loaded onto an 8 mL Q Sepharose column, which had been pre-equilibrated with buffer C. The column was washed with 5 column volumes of buffer C and eluted with a 60 mL linear gradient of buffer D (20 mM Bis-Tris, 700 mM NaCl, 1 mM DTT, pH 6.5). Fractions containing AcpM were identified on 15% SDS-PAGE gels and ESI-MS. The concentration of AcpM was determined by measuring the absorption at 276 nm using an extinction coefficient of 2900 $M^{-1}cm^{-1}$. The enzyme was concentrated using a Centricon-10 and was dialyzed into buffer E (20 mM Tris-HCl, pH 8.0) to remove the salt in the sample. Subsequently, the sample was injected onto a Pharmacia Biotech Mono Q FPLC column and chromatography was performed with buffer E and running 0 to 100% gradient of buffer F (20 mM Tris-HCl contains 1 M NaCl, pH 8.0) over 100 min at a flow rate of 1.8 mL/min. The concentration of the fractions was determined by UV and the species were characterized by 15% SDS-PAGE gels. Pure Apo-AcpM was dialyzed overnight against 2L buffer G containing 50 mM Tris-HCl, 25 mM $MgCl_2$, 5 mM DTT pH 7.5.

In a typical assay (26), dialyzed Apo-AcpM, 50 μM DD-CoA, 100 μg AcpS in a final volume of 1.9 mL were incubated at 37 ℃ for 30 min in a 2 ml microcentrifuge tube. The reaction was quenched by placing it into a dry ice/ethanol bath. AcpS was removed by centrifugation at 5000 rpm for 10 min after 2 hours stirring on 4 ℃ when 1.9 mL isopropanol was slowly added to the solution. The mixture sample was dialyzed in the InhA buffer (30 mM pipes, 150 mM NaCl, 1 mM EDTA pH 6.8) to remove IPA. Dodecenoyl-AcpM (DD-AcpM) was concentrated with Centricon-10. ESI and InhA assay were used to characterize DD-AcpM.

3.2.3 Overexpression and purification of wild-type and mutant InhAs

Plasmid for wild-type InhA was available from a previous study (*32, 135*). The R195E, R195Q, R195A, R225E, R225Q, K233E, Q214E, Q224E, E220K, K181E, R177E, F149A, R53E, R53A, R49E, R49A, R45E, R45A and R43E InhA mutations were introduced using the QuikChange mutagenesis kit (Stratagene). The primers are listed in Table 3.1. Wild-type and mutant InhA proteins were overexpressed and purified as described previously (*76*). The concentration of the protein was calculated using an ε_{280} of 37.5 mM^{-1} cm^{-1}.

Table 3.1: Primers used for mutagenesis	
Mutant	Primer[b]
R195E (forward, F)	5’-GCCGCAGGCCCTATC**GAG**ACGCTGGCGATG-3’
R195E (reverse, R)	5’-CATCGCCAGCGT**CTC**GATAGGGCCTGCGGC-3’
R195Q (F)	5’-CCTATC**CAA**ACGCTGGCGATGAGTGCGATC-3’
R195Q (R)	5’-CGCCAGCGT**TTG**GATAGGGCCTGCGGCAAC-3’
R195A (F)	5’-CCTATC**GCC**ACGCTGGCGATGAGTGCGATC-3’
R195A (R)	5’-CGCCAGCGT**GGC**GATAGGGCCTGCGGCAAC-3’
R225E (F)	5’-GATCAG**GAG**GCTCCGATCGGCTGGAACATG-3’
R225E (R)	5’-CGGAGC**CTC**CTGATCCCAGCCCTCCTCGAG-3’
R225Q (F)	5’-GATCAG**CAA**GCTCCGATCGGCTGGAACATG-3’
R225Q (R)	5’-CGGAGC**TTG**CTGATCCCAGCCCTCCTCGAG-3’
K233E (F)	5’-AACATG**GAA**GATGCGACGCCGGTCGCCAAG-3’
K233E (R)	5’-CGCATC**TTC**CATGTTCCAGCCGATCGGAGC-3’
Q214E (F)	5’-GCCGGCGCC**GAG**ATCCAGCTGCTCGAGGAG-3’
Q214E (R)	5’-CAGCTGGAT**CTC**GGCGCCGGCCTCCTCGCC-3’
Q224E (F)	5’-GGCTGGGAT**GAG**CGCGCTCCGATCGGCTGG-3’
Q224E (R)	5’-CGGAGCGCG**CTC**ATCCCAGCCCTCCTCGAG-3’
E220K (F)	5’-CTGCTCGAG**AAG**GGCTGGGATCAGCGCGCT-3’
E220K (R)	5’-ATCCCAGCC**CTT**CTCGAGCAGCTGGATCTG-3’
K181E (F)	5’-GAGGCCGGC**GAA**TACGGTGTGCGTTCGAAT-3’
K181E (R)	5’-CACACCGTA**TTC**GCCGGCCTCGCGCGCCAC-3’

R177E (F)	5’-TTCGTGGCG**GAA**GAGGCCGGCAAGTACGGT-3’
R177E (R)	5’-GCCGGCCTC**TTC**CGCCACGAACCTGTTGAC-3’
F149A (F)	5’-GGCATGGAC**TAC**GACCCGAGCCGGGCGATG-3’
F149A (R)	5’-GCTCGGGTC**GTA**GTCCATGCCGACGATGGA-3’
R53E (F)	5’-ATCACCGAC**GAG**CTGCCGGCAAAGGCCCCG-3’
R53E (R)	5’-TGCCGGCAG**CTC**GTCGGTGATGCGCTGAAT-3’
R53A (F)	5’-ATCACCGAC**GCC**CTGCCGGCAAAGGCCCCG-3’
R53A (R)	5’-TGCCGGCAG**GGC**GTCGGTGATGCGCTGAAT-3’
R49E (F)	5’-CTGATTCAG**GAG**ATCACCGACCGGCTGCCG-3’
R49E (R)	5’-GTCGGTGAT**CTC**CTGAATCAGCCGCAGCCG-3’
R49A (F)	5’-CTGATTCAG**GCC**ATCACCGACCGGCTGCCG-3’
R49A (R)	5’-GTCGGTGAT**GGC**CTGAATCAGCCGCAGCCG-3’
R45E (F)	5’-GACCGGCTG**GAG**CTGATTCAGCGCATCACC-3’
R45E (R)	5’-CTGAATCAG**CTC**CAGCCGGTCGAACCCGGT-3’
R45A (F)	5’-GACCGGCTG**GCC**CTGATTCAGCGCATCACC-3’
R45A (R)	5’-CTGAATCAG**GGC**CAGCCGGTCGAACCCGGT-3’
R43E (F)	5’-GGGTTCGAC**GAG**CTGCGGCTGATTCAGCGC-3’
R43E (R)	5’-CAGCCGCAG**CTC**GTCGAACCCGGTGAGCAC-3’
R43A (F)	5’-GGGTTCGAC**GCC**CTGCGGCTGATTCAGCGC-3’
R43A (R)	5’-CAGCCGCAG**GGC**GTCGAACCCGGTGAGCAC-3’

[a]Forward and reverse primers are listed. [b]Mutation site is underlined in bold

3.2.4 Kinetics of DD-CoA and DD-AcpM with InhA and mutants

Kinetic studies were performed using a Cary 300 Bio (Varian) spectrophotometer at 25 ℃ in 30 mM PIPES and 150 mM NaCl (pH 6.8). The enzyme concentration was 60 nM and NADH was maintained at 250 μM. The DD-CoA concentration was varied from 5 to 150 μM. Higher concentrations of DD-CoA could not be used due to substrate inhibition possibly due to competition between the adenine of DD-CoA and that of the NADH cofactor (*145*). Steady-state K_m and k_{cat} values for WT InhA were determined at variable concentration of one substrate and several fixed concentrations of the other. The enzyme concentration of mutants InhA, R53E, R53A, R49E, R49A, R45E and R45A was fixed at 200 nM when natural substrate was used. No substrate inhibition was detected even when the concentration of DD-AcpM reached 300μM. The initial velocities were determined by following the oxidation of NADH to NAD^+ at 340 (ε=6.3 mM^{-1} cm^{-1}) or 370 nm (ε=2.4 mM^{-1} cm^{-1}). Each initial velocity was measured in triplicate and at least five different substrate concentrations were used. The data were plotted using Grafit 4.0 software to determine the K_m and k_{cat}. Data was plotted in Lineweaver-Burk reciprocal form and fitted to eq 1.

$$v = VA/(K + A) \quad (1)$$

The data for intersecting initial velocity patterns were fitted to eq 2 (*77*).

$$v = VAB/(K_{ia}K_b + K_aB + K_bA + AB) \quad (2)$$

Equation 1 can be reduced to equation 3 if K>>A.

$$k_{cat}/K_m = v/(E_0A) \quad (3)$$

k_{cat} and K_m values were obtained by fitting the data to eq 2, V is the V_{max} of the reaction and K_a and K_b are the K_m of substrate A and B respectively, K_{ia} is the K_d of for substrate A. A, B are concentrations of substrate A and B, respectively. E_0 is the initial enzyme concentration.

3.2.5 Synthesis of 4(S) and 4(R)-NADD

4(*S*)-NADD was synthesized enzymatically by the reduction of NAD^+ with *L. mesenteroides* glucose-6-phosphate dehydrogenase as described previously (*175, 176*). 4(*R*)-NADD was synthesized from NAD^+ and ethanol-*d6* in the presence of equine liver alcohol dehydrogenase as described previously (*83*). Both reduced nucleotides were purified as described previously (*76*) except that the stability of the NADD during purification was improved by performing the anion exchange chromatography (FPLC, MONO Q HR10/10) at pH 9.0 using 10 mM triethanolamine, rather than pH 7.8.

3.2.6 Kinetic Isotope Effects

Primary kinetic isotope effects on *V* (^{D}V) and *V*/*K* ($^{D}(V/K)$) were determined at 25 °C in 30 mM PIPES and 150 mM NaCl (pH 6.8) at a fixed, saturating concentration of NADH or 4(*S*)-NADD (250 μM) and by varying the concentration of DD-ACP (0-24 μM). Alternatively, the kinetic isotope effects were determined at a fixed, saturating concentration of DD-ACP (24 μM) and by varying the concentration of NADH or 4(*S*)-NADD (0-250 μM). Kinetic isotope effects were calculated by fitting the initial velocity data to equation 4 using Grafit 4 10.

$$v_i = V[A]/(K_A(1+fi.E_{V/K})+[A](1+fi\cdot E_V)) \quad (4)$$

In equation 4, V is V_{max}, [A] is the concentration of the varied substrate, fi is the fraction of deuterium in NADD, and $E_{V/K}$ and E_V are the isotope effects minus 1 on V/K and V, respectively. A value of 0.95 was used for fi.

3.2.7 FluroAcpM Preparation and Fluorescence Titration Experiments

The fluorescent maleimide 7-diethylamino-3-(4'-maleimidylphenyl)-4-methylcoomarin (*177-179*) was dissolved in DMSO at 10 mM concentration, and 400 μL solution was added to a solution of coenzyme A disodium salt (4 mg) in 1.6 mL Tris-HCl and 25 mM $MgCl_2$ at pH 7.5.

The resulting solution was vortexed briefly and reacted at room temperature for 2 hours. 400 μL Apo-AcpM (600 μM stock) and 200 μL AcpS (450 μM stock) were added to the solution and incubated at 35℃ with shaking for another 2 hours. 50:50 IPA was added to the reaction mixture and incubated in ice for 2 hours followed by centrifugation to remove the precipitate. The supernatant was applied to a 2 mL Q sepharose column. The column was washed by 5 column volumes of 20 mM Bis-Tris containing 1 mM DTT (pH 6.5). FluroAcpM was eluted with 3 column volumes of 20 mM Bis-Tris, 600 mM NaCl containing 1 mM DTT (pH 6.5). The fluroAcpM was characterized by 20% SDS-PAGE gel and mass spectrometry.

Fluorescence titration was conducted with a model PTI spectrofluorimeter. The measurements were carried out in 100 mM PIPES, pH 7.0 and at 25 ℃. FluroAcpM was excited at 360 nm (5 nm slit width) and fluorescence was detected using an emission wavelength 412 nm (1 nm slit width). Standard assay involved the addition 1 μL aliquots of 460 μM fluroAcpM to a 1 mL buffer containing 5 μM NADH, the titrations were making with concentrated Wild-type InhA or mutant stock solution to the 1 mL buffer cuvette. Dilution of protein caused by InhA was kept < 1%. The control experiments were determined, following exactly the same procedure, by omitting the fluorescence changed by InhA titrated to NADH. Data were fit to a quadratic equation (eq 4) (*180, 181*) instead of a simple hyperbolic function for a second order binding process.

$$Bound = \frac{(K_d + [E]_0 + [InhA]) - \sqrt{(K_d + [E]_0 + [InhA])^2 - 4K_d[E]_0}}{2[E]_0} \qquad (4)$$

Bound is the fluorescence intensity change when InhA or mutants were added, $[E]_0$ is the total fluroAcpM concentration, K_d is the dissociation constants and [InhA] is the concentration of added enzymes. Data fitting was performed by Software programs Grafit 4.0.

3.2.8 2,4,6-Octatrienoic-AcpM Preparation and Analytical Ultracentrifugation (AUC)

2,4,6-Octatrienoic-CoA was synthesized using 2,4,6-octatrienoic acid as stating material. The method is similar to the preparation of DD-CoA (*77, 139*). The desired product was obtained in 40% yield as a flaky white powder with UV-vis ε_{260} 16.3 $mM^{-1}\cdot cm^{-1}$. ESI-MS ($[M+H]^+$) was explored to characterize 2,4,6,-octatrienoic-CoA: calculated 988.1, found 988.2. 2,4,6-octatrienoic-AcpM was synthesized from 2,4,6-octatrienoic-CoA and Apo-AcpM using *E. coli* holo ACP synthase (AcpS) which was overexpressed and purified from *E. coli* as described previously (*97*). The fractions containing 2,4,6-octatrienoic-AcpM were identified by SDS-PAGE and ESI-MS, pooled, concentrated, dialyzed into 20mM Tris-HCl, pH 7.0, and stored at -80 °C. The concentration of protein was calculated from the UV absorption at 330 nm using a ε_{330} 16.5 $M^{-1}\cdot cm^{-1}$.

All protein samples were dialyzed into 20 mM Na_2HPO_4, 150 mM NaCl, pH 7.5, immediately prior to analysis. AUC experiments were performed at 20 ℃ using a Beckman Coulter Optima XL-1 analytical ultracentrifuge equipped with a scanning UV/VIS spectrometer to monitor absorbance during the scans. Sedimentation equilibrium (SE) was run using an 8 cell, An-45 Ti analytical rotor with six-channel, charcoal-filled Epon centerpiece. Samples were analyzed at different compositions: 60 μM InhA, 30 μM 2,4,6-octatrienoic-AcpM and 60 μM InhA, 30 μM 2,4,6-octatrienoic-AcpM and 60 μM InhA plus 60 μM NADH. SE was run at 10 k rpm to 25 k rpm and the data were collected for 72 h when scans at A_{330} nm remained constant. Partial specific volumes (0.7406) and solvent density (1.00727) were calculated using HeteroAnalysis software.

3.3 Results

3.3.1 Comparison of AcpM with other ACPs

A sequence alignment of the ACPs from *M. tb* and *E. coli* with other typical bacterial ACPs is shown in Figure 3.4. ACPs have a high degree of similarity, especially DSL motif around the serine residue where the phosphopanteheine is attached.

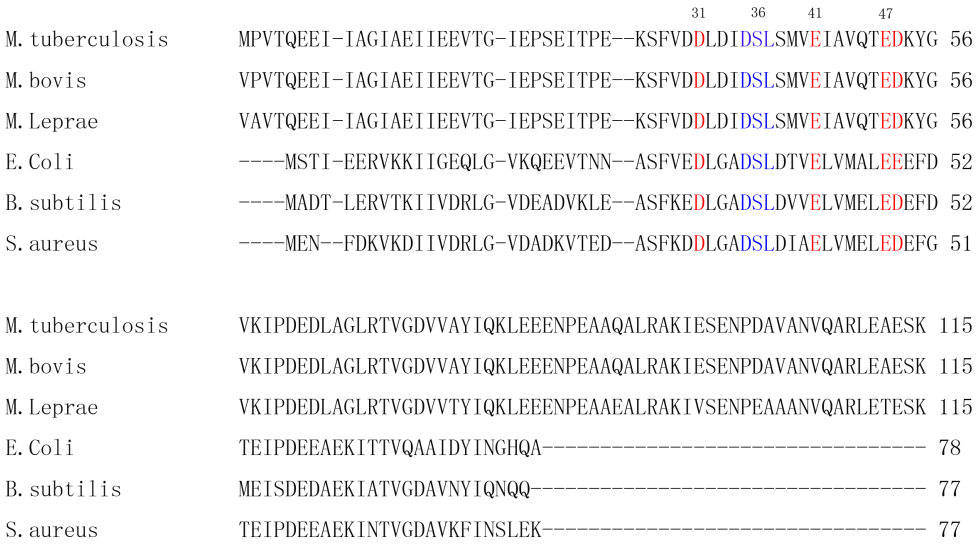

Figure 3.4. Sequence alignment of ACP and AcpM. Sequences were aligned using Clustalw software. Primary sequences of ACP from representative prokaryotes and eukaryotes were compared, and the region containing the residues proposed to be the important amino acid for the interaction colored red. Abbreviations: *M. tuberculosis*, *Mycobacterium tuberculosis*; *M. bovis*, *Mycobacterium bovis*; *M. Leprae*, *Mycobacterium leprae*; *E. coli*, *Escherichia coli*; *B. subtilis*, *Bacillus subtilis*; *S. aureus*, *Staphylococcus aureus*.

AcpM differs from the *E. coli* ACP by the presence of a carboxyl terminal domain that extends 35 amino acids as a random coil. The alignment of AcpM with *E. coli* ACP reveals the important Ser41 of AcpM which corresponds to Ser36 of ACP from *E. coli.* Docking and site-directed mutagenesis (*80, 104*) have analyzed the interaction of ACP with two FASII enzymes, FabG (*E. coli* β-ketoacyl-ACP reductase) and FabH (*E. coli* β-ketoacyl-ACP synthase). It demonstrated the helix α2 of ACP is important for ACP target protein recognition. Some acidic residues which are important to the interaction with enoyl-ACP reductase, Glu 41, Glu 47 and Glu48 of *E. coli* ACP are replaced by Glu46, Glu52 and Asp 53. All ACPs have conserved acidic residues, such as ASP35, Glu41 and Glu47 (Figure 3.5).

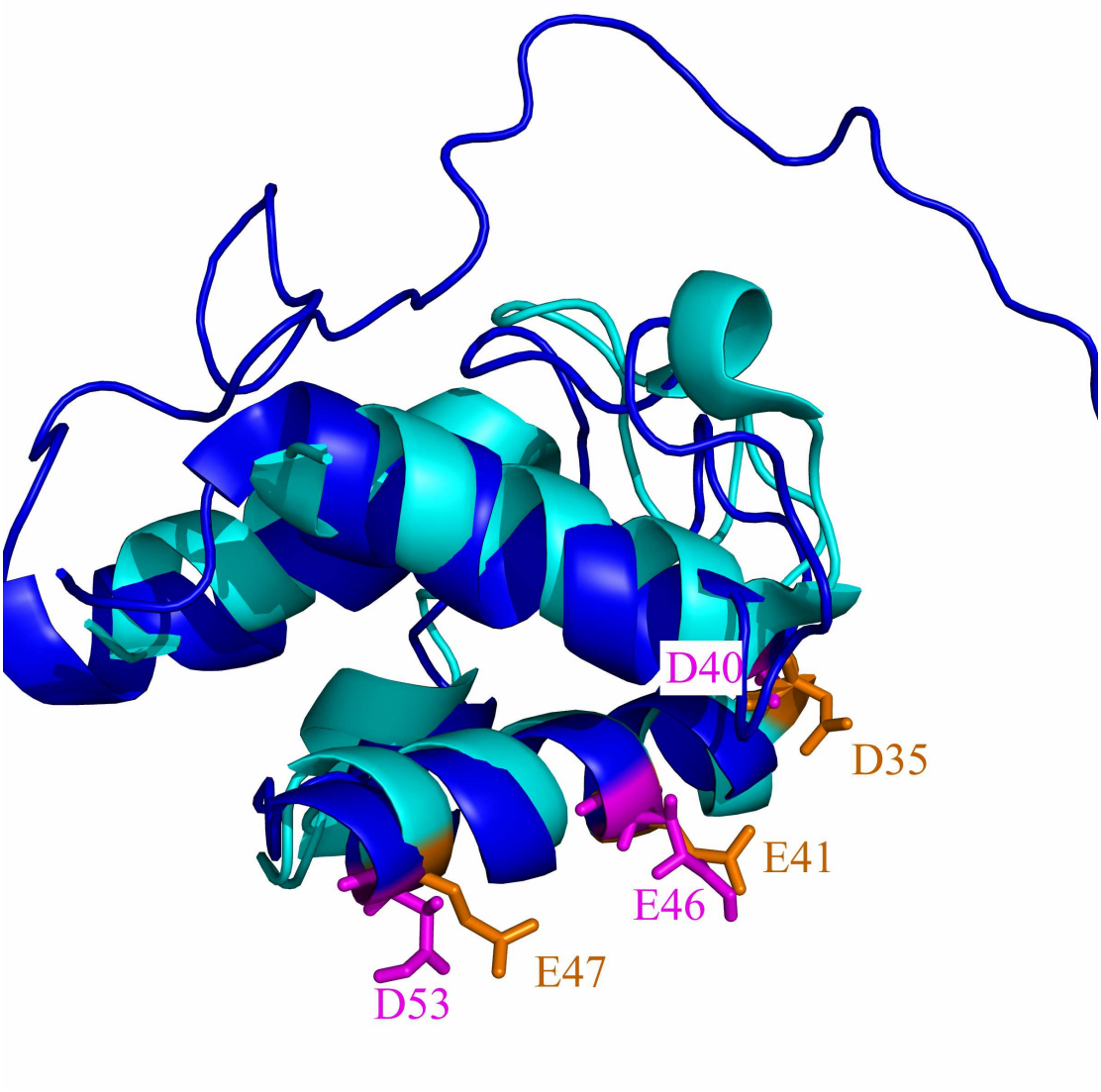

Figure 3.5. Superposition of ACP (cyan) with AcpM (blue). The three acidic residues (D35, E41, and E47) located in helix α2 of ACP interact with basic residues of FabI. The corresponding residues in AcpM are D40, E46, and D53.

3.3.2 AcpM overexpression and Apo-AcpM purification

Unlike the *E. coli* ACP which was predominantly in the apo form and used for the synthesis of *trans*-2-dodecenoyl-ACP without further purification (*137*), AcpM was expressed as a mixture containing Apo-, Holo- and Acyl-AcpM when expressed in *E.*

coli cells at 37℃ under the control of the T7 promoter system. To minimize the conversion of Apo- to Holo-AcpM, the induction time was shortened to only 2.5 h at 37 ℃. Treatment of the lysate to induce the activity of an endogenous phosphodiesterase that is required to convert Holo- or Acyl-AcpM to Apo-AcpM was performed to further increase the yield of Apo-AcpM (*182*). Anion exchange chromatography was utilized to purify AcpM by eluting the Q Sepharose-bound protein with a linear gradient of 200 to 700 mM NaCl. The fractions were analyzed by conformational sensitive 15% SDS-PAGE gel (Figure 3.6) and characterized by ESI-MS (Figure 3.7).

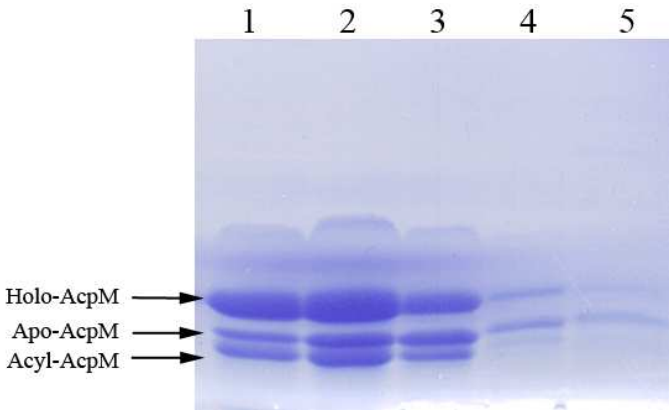

Figure 3.6. SDS-PAGE of AcpM fractions from Q Sepharose column. Lanes 1-5 represent fractions containing significant amounts of AcpM.

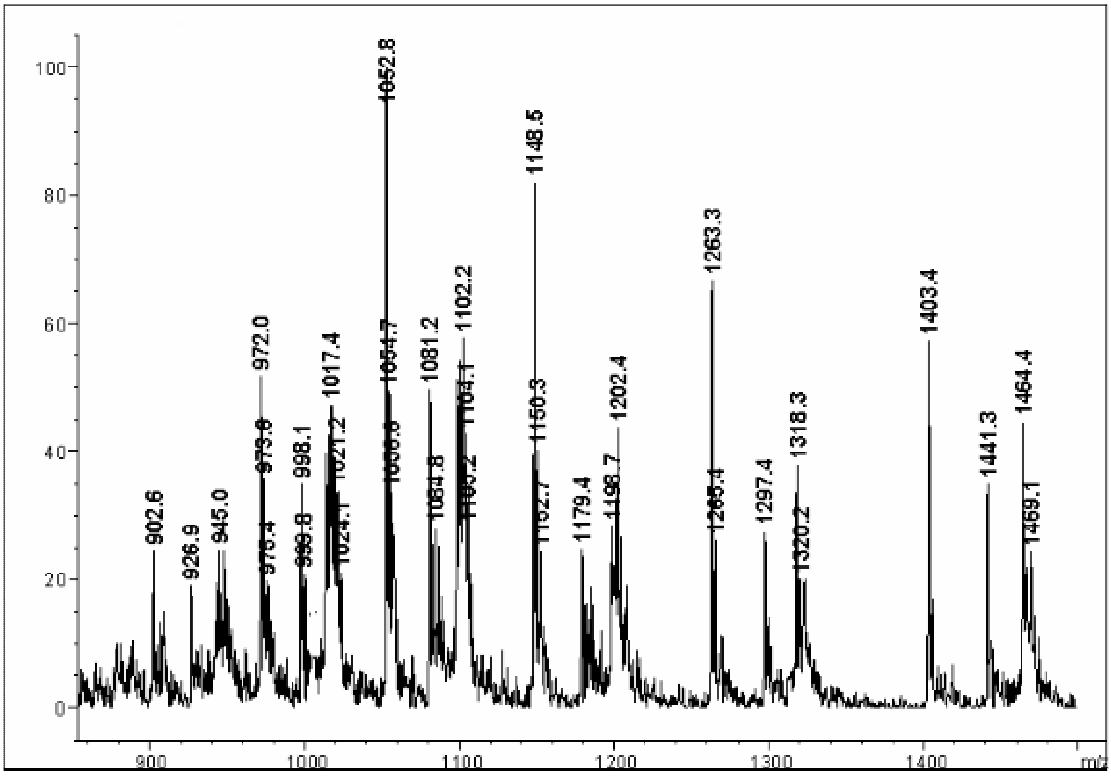

Figure 3.7. ESI mss spectrometry of AcpMs species. Apo-, Holo-, Acyl-AcpM eluted from Q-sepharose column were analyzed by ESI. The peaks were deconvolved and assigned. 902.6, 972.0, 1052.8, 1148.5, 1263.3, and 1403.4 were deconvolved to 12 622.3 Da and assigned to Apo-AcpM. Holo-AcpM, 926.9, 998.1, 1081.2, 1179.4, 1297.4, and 1441.3 were deconvolved to 12 962.6 Da and assigned to Holo-AcpM. 945.0, 1017.4, 1102.2, 1202.4, 1318.3, and 1464.4 were deconvolved to 13 206.3 Da and assigned to Acyl-AcpM

AcpM can be further purified by Fast Performance Liquid Chromatography (FPLC) to separate the three species of AcpM, Apo-, Holo- and Acyl-AcpM as shown in the 15% SDS-PAGE gel (Figure 3.8) and as characterized by ESI-MS (Figure 3.9).

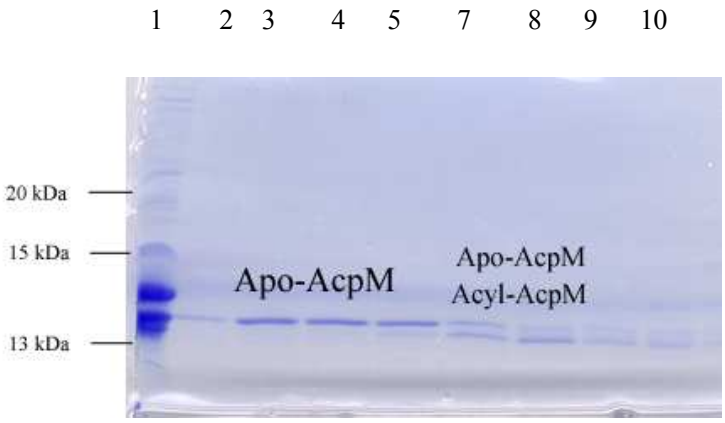

Figure 3.8. SDS-PAGE of AcpM fractions from FPLC. Lanes 1 represent original concentrated AcpM mixture. Lane 2-4 represent Apo-AcpM which came first then followed by Acyl-AcpM showed in lane 5-7. Holo-AcpM was last one to wash out which showed in lane 8-9.

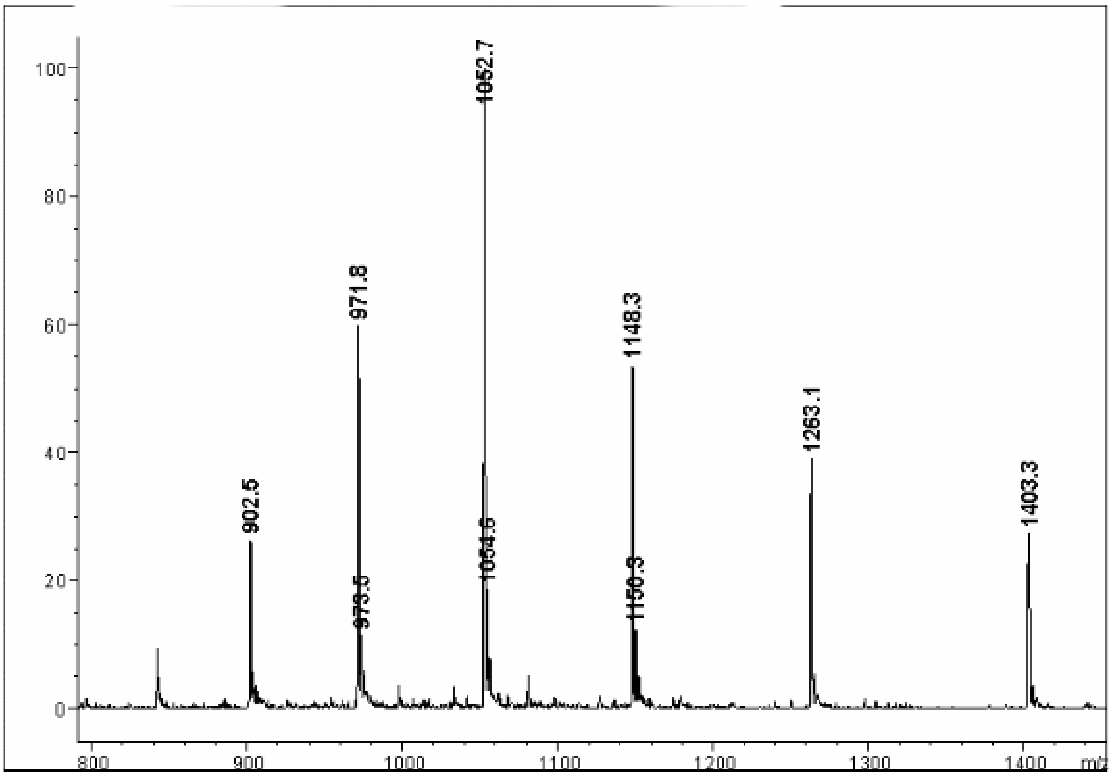

Figure 3.9. Apo-AcpM purified by FPLC was characterized by ESI. 902.5, 971.8, 1052.7, 1148.3, 1263.1, and 1403.3 were deconvolved to 12 620.5 Da and assigned to Apo-AcpM

The three AcpM species (apo, holo and acyl) which were eluted in the lane 1-3 of Figure 3.6 and Figure 3.8 were characterized by ESI-MS (Figure 3.7 and Figure 3.9 respectively). The experimentally determined masses of AcpM match the predicted values from the gene sequence. The Apo-AcpM can be separated purely by Mono-Q FPLC which showed in the Figure 3.8, Apo-AcpM was eluted first, followed by Acyl-AcpM, then the Holo-AcpM mixtures.

The acylated Holo-AcpM (DD-AcpM) was synthesized from Apo-AcpM and DD-CoA using the Holo-ACP synthase and analyzed by 15% pre-made SDS-PAGE gels (Figure 3.10).

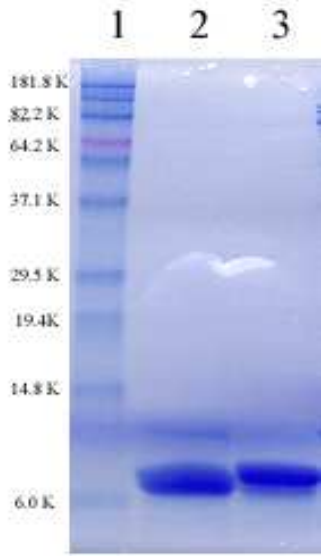

Figure 3.10. SDS-PAGE of dodecenoyl-AcpM reaction. Lane 1, Protein Ladder; Lane 2, pure Apo-AcpM; Lane 3, after reaction mixture (DD-AcpM and ACPS).

The product (DD-AcpM) migrated faster than Apo-AcpM because the acyl chain interacts with SDS(*183*). Consequently, DD-AcpM appears to have a lower MW than

Apo-AcpM. Apo-AcpM exhibited a mass of 12,621 Da, while the DD-AcpM exhibited a mass of 13,142 Da, as expected for the addition of the dodecenoate and the phosphopantetheine moiety (mass 521) to the Ser 41 of Apo-AcpM. Holo-AcpM had a MW of 12,962 Da (Figure 3.11), 341 Da higher than apo- form corresponding to the covalently bound phosphopantetheine unit. FluroAcpM had a MW of 13,364 Da mass, 402 Da mass higher than holo- form as expected for the addition of the maleimide moiety.

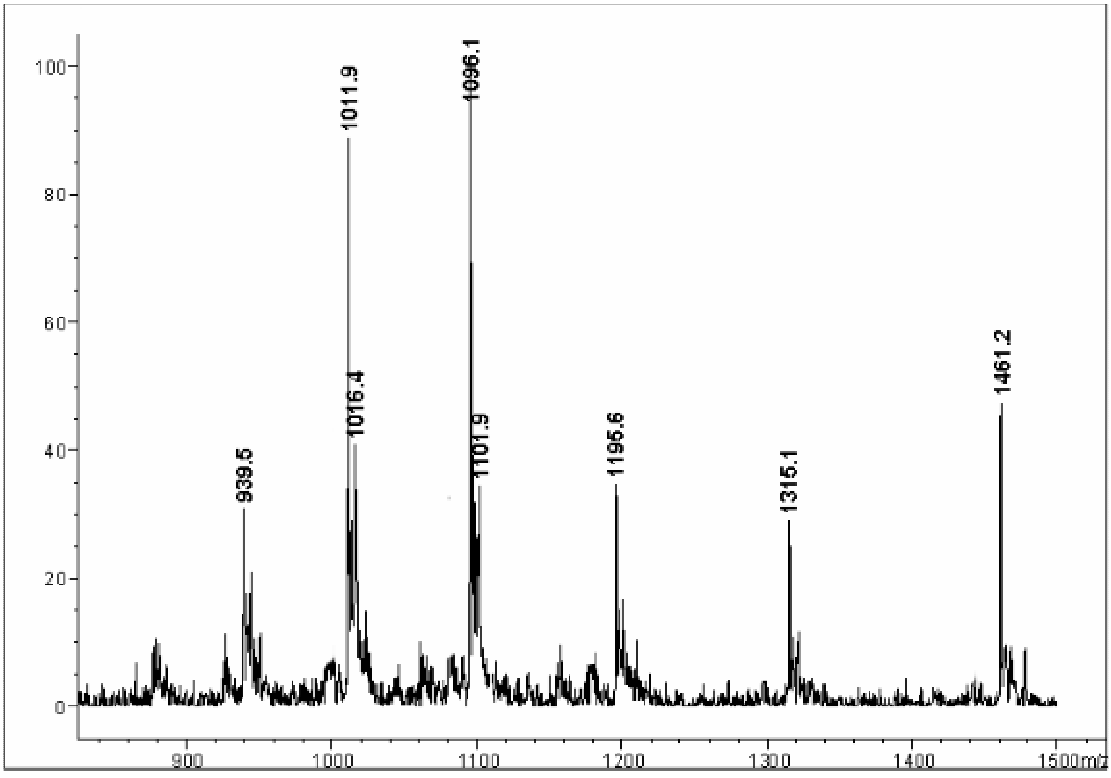

Figure 3.11. DD-AcpM synthesized by DD-CoA and Apo-AcpM was characterized by ESI mass spectrometry. 939.5, 1011.9, 1096.1, 1195.6, 1315.1 were deconvolved to 13 140.6 Da (confirmed by MALDI MS) which contributed to DD-AcpM.

3.3.3 Binding loop between ACP and enoyl ACP reductase

In the previous chapter, FabI, the homolog of InhA in *E. coli*, was shown to a tetramer with a central β-sheet that contains seven β-strands. Molecular dynamics simulation and X-ray crystallography were used to determine the structure of ACP bound to FabI, in which, four acidic residues interact with three basic residues of FabI. Lys201, Arg204 and Lys205 are located outside of helix α8 have the hydrogen bonding with the Asp35, Asp38, Glu41 and Glu48 of ACP helix α2. Some mutants of Lys210, Arg204 and Lys205 to Glu of FabI showed a significant reduction in k_{cat}/K_m of DD-ACP but not any effect for the DD-CoA substrate. InhA is an 114 KDa tetramer and has 37.3% similarity with FabI. Based on the crystal structure of ACP binding with FabI, we superimposed the AcpM with ACP and FabI with InhA (Figure 3.12).

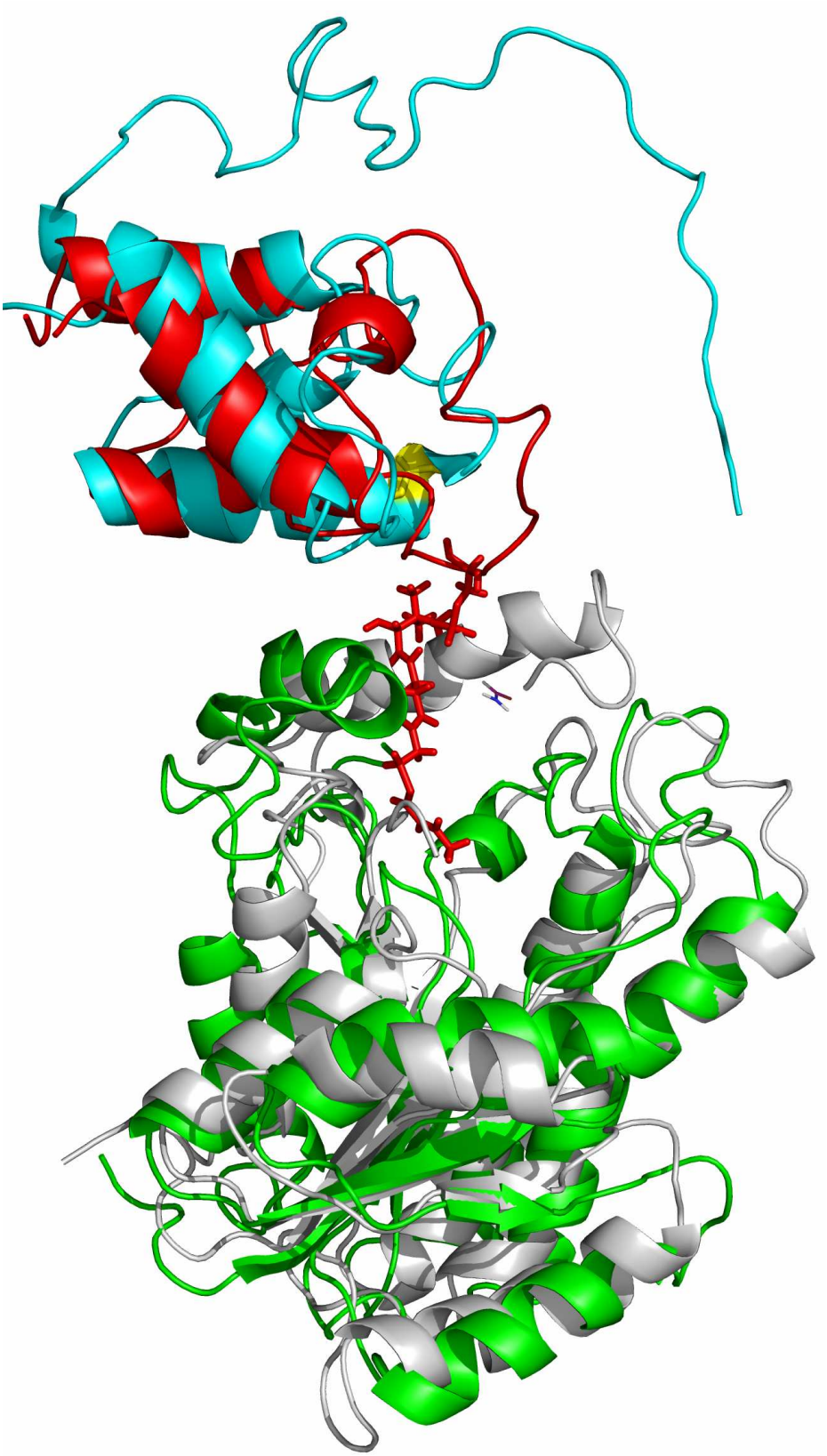

Figure 3.12. Superposition of ACP with AcpM and FabI with InhA. Red, ACP; blue, AcpM; grey, FabI; green, InhA.

From the overlay, AcpM superimposes very well with ACP but has a long tail which will be flexible in solution. Helix α8 of FabI is not in the same conformation with helix α8 of InhA. Comparing the interface between ACP with FabI, it was expected that some residues located in the helix α8 of InhA should interact with AcpM residues. This included Gln224, Glu220 and Gln214 located adjacent to helix α8 of InhA. In addition, there are additional basic residues close to this α helix, including Arg195, Arg225 and Lys233 (Figure 3.13).

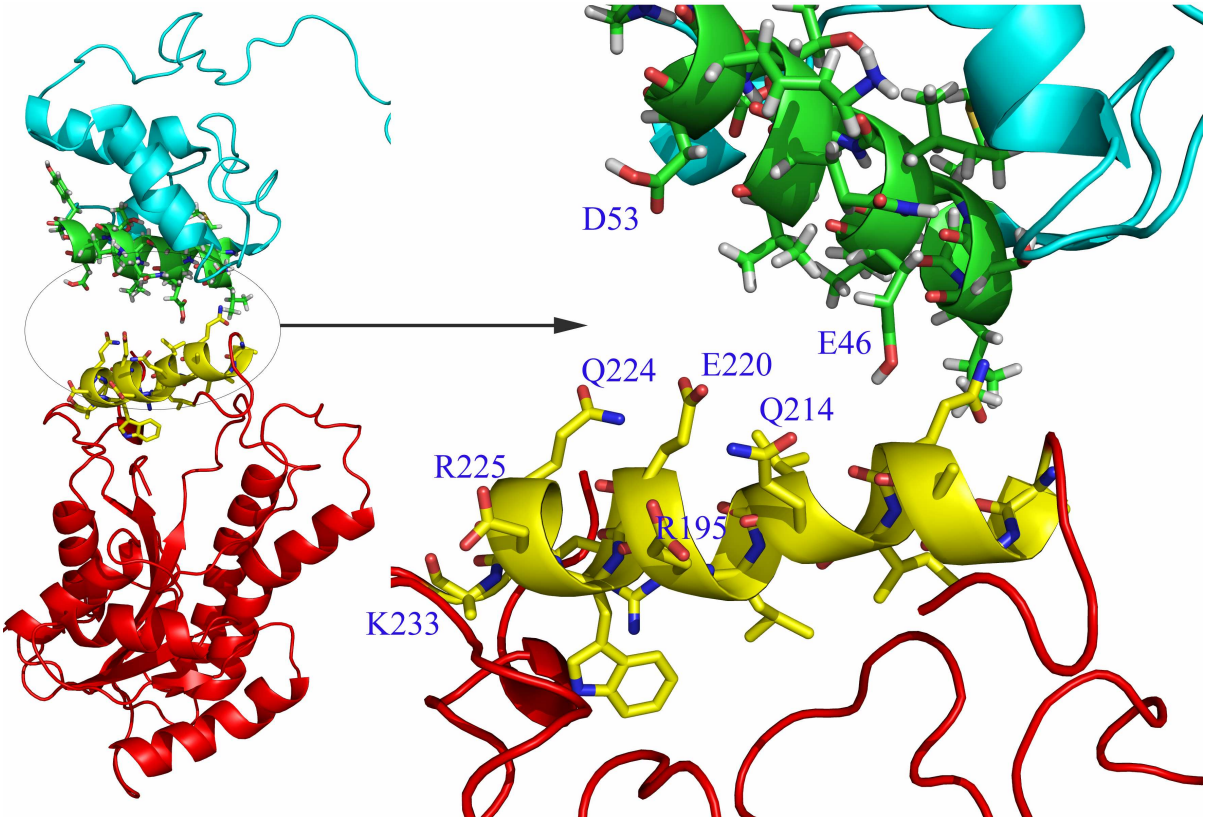

Figure 3.13. Interface between InhA with AcpM. The residues of Gln214, Glu220 and Gln224 located outside of the helix α8 of InhA. Another three basic residues Arg195, Arg225 and Lys233 near the α helix where Arg195 and K233 locate at the beginning and the end of the loop respectively and R225 is in the helix α8 of substrate binding loop.

Arg225 is located in helix α8 but Arg195 is at the beginning of the loop and Lys233 is at the end of the loop. All these residues have been mutated to Glu or Ala and the kinetic results are shown in Table 3.2.

	DD-CoA				DD-AcpM			
	K_m μM	k_{cat} min^{-1}	k_{cat} / K_m	Ratio[a]	K_m μM	k_{cat} min^{-1}	k_{cat} / K_m	Ratio[a]
WT	17.8±2.4	215±12	12±2	1	2.4±0.4	227±8	95±5	1
Q214E	20.9±3.0	153±11	7.3±1.8	0.6	3.0±0.4	215±8	71±13	0.75
Q224E	17.8±6.6	145±25	8.2±4	0.68	3.5±0.4	209±6	60±8	0.65
E220K	16.6±3.3	132±13	8.0±2.4	0.67	N/D[b]			
R195E	18.5±1.2	208±4	11.2±0.5	0.93	37.8±3	263±8	6.9±1	0.07
R225E	15.0±2.4	144±11	9.5±2	0.8	44.8±2.1	272±6	6.0±0.5	0.06
K233E	17.9±1	101±2	6.0±0.5	0.5	25.3±3.5	167±8	6.6±1.3	0.07
R195Q	26.1±4.2	297±21	11.4±2	0.94	7.9±1.3	212±12	26.8±1.5	0.28
R225Q	36.5±2.3	343±11	9.4±1.2	0.8	9.44±1.0	125±5.7	13.2±0.8	0.14
R195A	36.1±2.4	340±10	9.4±1.2	0.8	6.89±0.5	214±6.1	31±2	0.33
R195E/R225E	No activity							

[a] Ratio of k_{cat}/K_m values of wild type and mutant FabIs.

[b]ND = not determined

Table 3.2. Kinetics data of wild-type InhA and all mutants by DD-CoA and DD-AcpM substrates.

The data in Table 3.2 demonstrates that replacement of the three residues located in the proposed interface between InhA and AcpM with acidic residues or basic residues (E220K) has no effect on the kinetics parameters for reduction of DD-CoA and DD-AcpM. Another three basic residues near the helix α8, Arg195, Arg225 and Lys233 reduced k_{cat}/K_m of DD-AcpM about 15 fold with no effect in reduction of the DD-CoA substrate. Replacement of Arg195 with Ala has a small impact (3 fold) on reduction of DD-AcpM substrate, while k_{cat}/K_m of R195Q and R225Q is reduced 3 to 7 fold, respectively.

3.3.4 Steady State Kinetics Analysis of Wild-Type InhA

To distinguish between a sequential or a ping-pong mechanism, the initial velocity were determined using either DD-AcpM or NADH as variable substrates. Analysis of the Lineweaver-Burk reciprocal plots showed intersecting patterns for both substrates (Figure 3.14), suggesting a ternary complex mechanism with a sequential kinetic mechanism. The K_m values of the recombinant InhA for DD-AcpM and NADH were 2.4 ±0.4 μM and 19.0 ±2.5 μM, respectively at pH 6.8 and k_{cat} was 227 min^{-1}.

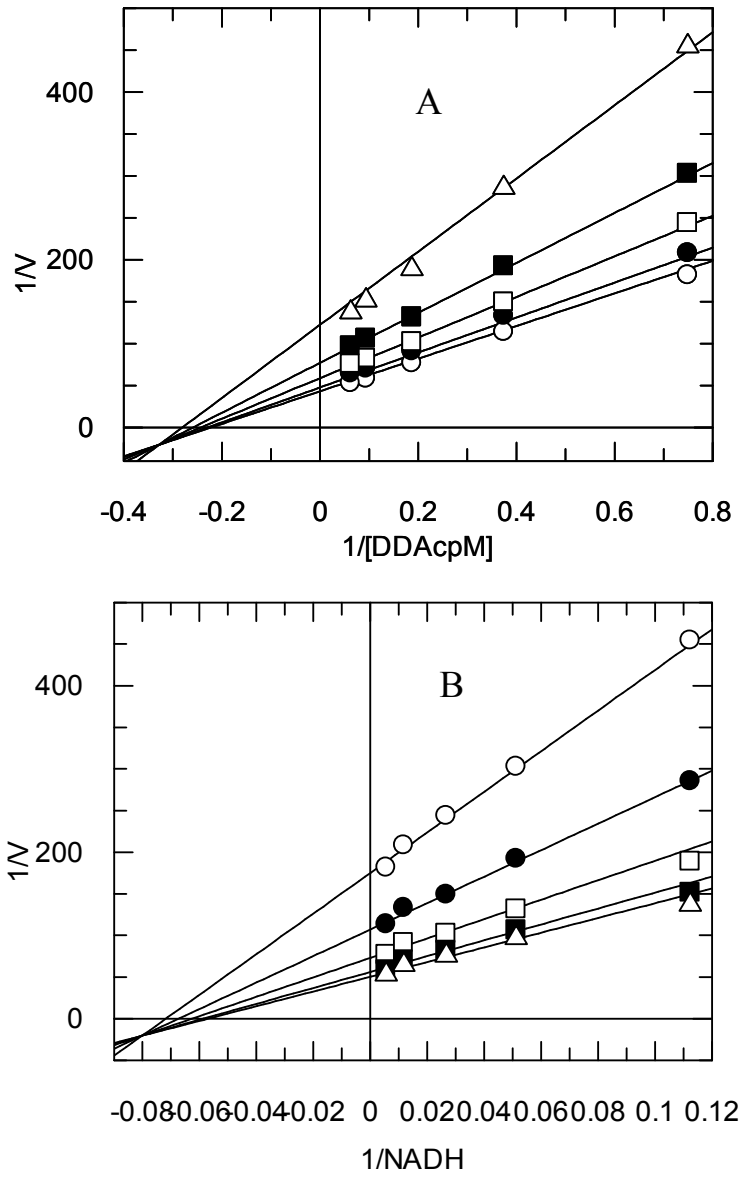

Figure 3.14. Initial velocity patterns for InhA with either DD-AcpM (A) or NADH (B) as the variable substrate. A, The DD-AcpM concentrations varied from 1.3 to 16.0 μM, and fixed NADH concentration were 8.9 (△), 19.5 (■), 37.5 (□), 85 (●), and 177 μM (○). B, The NADH concentrations various from 8.9 to 177 μM, and fixed DD-AcpM concentration were 1.34 (○), 2.67 (●), 5.34 (□), 10.7 (■), and 16.0 μM (△).

3.3.5 Kinetics Analysis of Mutant InhA Enzymes

Compared to the model of FabI binding with ACP, Arg204 and Lys205 are the

most important residues corresponding the interaction with the substrate, the maximum reduction decreases 250 fold of k_{cat}/K_m for the mutant R204E. However, none of the mutants had the dramatic effect on k_{cat}/K_m this was previously observed to FabI-ACP. Consequently, InhA structure is identified additional surface basic residue that could interact with AcpM. Arg53, Arg49, Arg45 and Arg43 are located in the same helix α2 adjacent to the active site of InhA (Figure 3.15).

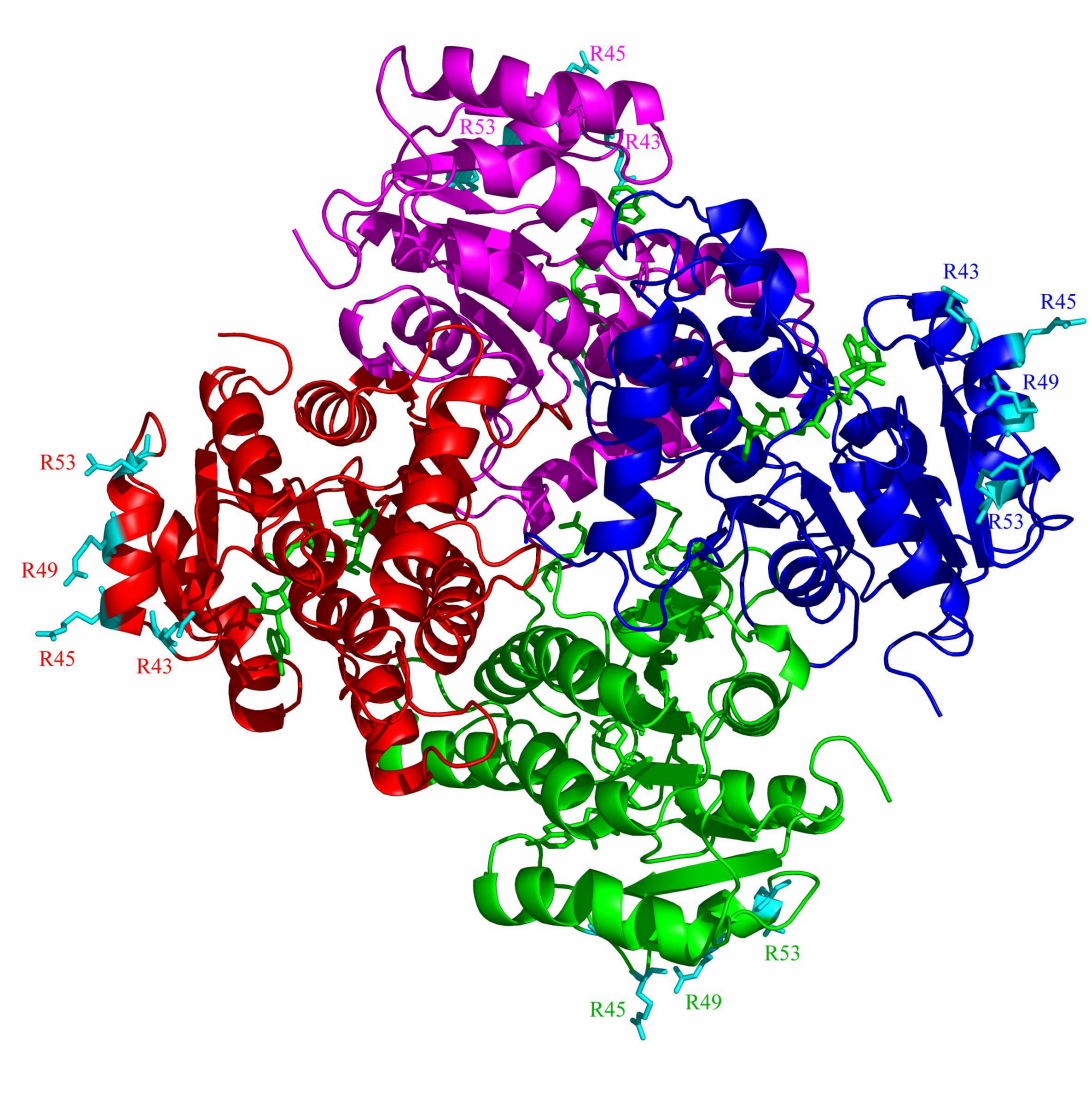

Figure 3.15. InhA tetramer (PDB 1BVR). Four basic patch in the helix α2 of each

monomer InhA, Arg53, Arg49, Arg45 and Arg43 which near the active site and the cofactor NADH.

Furthermore, there is another basic patch opposite to the major portal of InhA, R173, R177, and K181 (Figure 3.2).

All of the important basic residues were mutated to glutamates to introduce electrostatic repulsion between InhA and AcpM and to test whether AcpM associates with InhA over the entire system. Furthermore, the same positive residues were mutated to alanines to determine which residue significantly promotes the binding to AcpM. Because the high K_ms of such mutants and paucity of DD-AcpM substrate, we only detected k_{cat}/K_m result using eq 3 by Grafit 4.0 and shown in Table 3.3.

	DD-CoA				DD-AcpM			
	K_m μM	k_{cat} min^{-1}	k_{cat} / K_m	ratio	K_m μM	k_{cat} min^{-1}	k_{cat} / K_m	ratio
WT	17.8±2.4	215±12	12±2	1	2.4±0.4	227±8	95±5	1
R53E	27.8±1.8	330±11	11.8±0.4	0.98	ND	ND	0.46±0.12	0.005
R53A	30.8±5.6	373±29	12.1±1	1	ND	ND	1.1±0.4	0.011
R49E	38±11	358±55	9.4±1.4	0.8	ND	ND	0.4±0.1	0.004
R49A	36.6±2.8	407±15	11.1±0.5	0.9	ND	ND	10.1±0.8	0.106
R45E	35.2±7.1	353±35	10±1	0.83	ND	ND	1.55±0.12	0.016
R45A	39.5±4.7	462±26	11.7±0.6	1	ND	ND	11.2±0.6	0.117
R177E	22.5±3.9	210±14	9.3±1.9	0.76	3.2±0.5	292±28	91±2	0.96
K181E	18.5±1.5	151±12	8.2±1.2	0.68	2.4±0.2	260±16	108±10	1.13
R43E	50±13	129±17	2.6±0.4	0.2	ND			

Table 3.3. Kinetics data of wild-type InhA and all mutants by DD-CoA and DD-AcpM substrates.

The data in Table 3.3 shows that replacement of Arg53, Arg49 and Arg43 with Glu did not have impaired activity with DD-CoA, but k_{cat}/K_m for reduction of DD-AcpM is reduced 62 (Arg45), 200 (Arg53) to 250 (Arg49) fold. In addition, replacement of Arg53, Arg49 and Arg45 with Ala causes a smaller reduction in k_{cat}/K_m of DD-AcpM without affecting k_{cat}/K_m for the DD-CoA substrates. For example, substitution of Ala for Arg49 only has a reduction 9 fold compared with Glu

substitution (250 fold). Arg43 residue has 5 fold decrease reduction of k_{cat}/K_m of DD-CoA, so we believed R43 involved the chemical step. The other basic patch (R181, R177, and R173) do not important for the substrate interaction since the k_{cat}/K_ms are not change for CoA and AcpM substrate.

3.3.6 Equilibrium Binding of FluroAcpM to Wild-Type and Mutant InhA Proteins

The direct binding data were measured using fluorescence titration and plotted using the quadratic equation (eq 4). The results are given in Table 3.4. In the presence of cofactor NADH, InhA binds tightly with AcpM. Mutation of the three residues, R53, R49, and R45 showed a 16-18 fold decrease binding affinity with AcpM if mutated to alanines. No obvious fluorescence change was found for R53E and R49E mutants because the two mutants significantly decrease the binding affinity with AcpM. R43, which is not located in the binding interface between AcpM with InhA, doesn't show a big effect when mutated to Glu.

	WT	R53E	R53A	R49E	R45E	R45A	R43E
K_d (μM)	0.3±0.1	ND	4.8±0.3	ND	9.1±0.2	5.5±0.7	0.34±0.2
Ratio	1	ND	16	ND	30	18	1.1

Table 3.4. Fluorescence measures the dissociation constants of wild-type InhA and mutants.

3.3.7 Steady-state kinetics of F149A InhA protein and Kinetics isotope effects

DD-ACP was used in the present work in order to facilitate evaluation of ^{D}V. Steady-state kinetic parameters obtained using DD-ACP synthesized from *E. coli* ACP showed that the F149A InhA mutant had a k_{cat} value that was reduced 30-fold compared to wild-type InhA. The F149A mutation had only a small affect on the K_m values for the two substrates and the k_{cat}/K_{DDACP} and k_{cat}/K_{NADH} values were reduced 23 and 13, fold respectively, compared to wild-type InhA. To further investigate the role of F149 in substrate reduction, we measured the primary kinetic isotope effects for wild-type and F149A InhA (Table 3.5). While the ^{D}V and $^{D}(V/K_{DDACP})$ values for wild-type and F149A InhA were the same, within experimental error, $^{D}(V/K_{NADH})$ was increased two-fold for the F149A mutant.

Enzyme	^{D}V	$^{D}(V/K_{NADH})$	$^{D}(V/K_{DDCoA})$
Wild-type	1.87±0.36	2.16±0.82	2.23±0.21
F149A	1.54±0.25	4.74±0.8	2.1±0.87

Table 3.5. Primary Kinetic Isotope Effects for Wild-Type and F149A InhA

3.3.8 Analytical Ultracentrifugation (Sedimentation equilibrium)

Analytical ultracentrifugation (AUC) is a powerful technique that utilizes real time monitoring of protein sedimentation through the detection of protein concentration via a sensitive optical detection system. Sedimentation equilibrium (SE) is performed at lower speeds and measures the equilibrium between sedimentation of proteins and diffusion, equilibrium is defined when successive scans reveal a static

boundary. SE analysis was performed to determine the stoichiometry of InhA with AcpM. It has been shown that 2 ACP monomers bind to 1 tetramer of FabI from *E. coli* modeling studies. In the presence of NADH, 2,4,6-octatrienoic-AcpM will bind to AcpM (Figure 3.16)

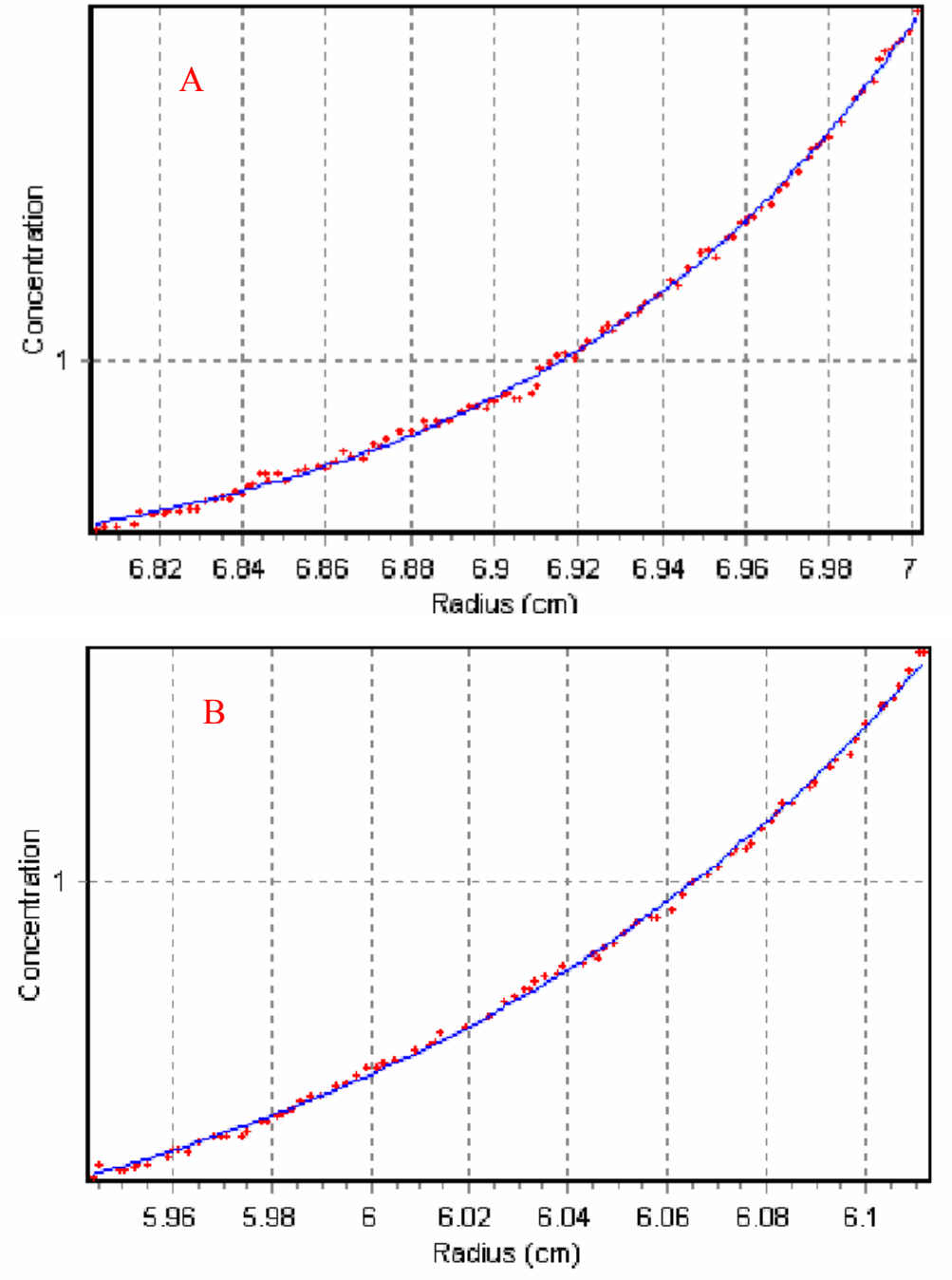

Figure 3.16. SE-AUC analysis shows unbound and bound forms of InhA. (A) InhA with NADH only. (B) InhA, 2,4,6-octatrienoic-AcpM, and NADH together

In the top case, data analysis gave a MW (122.5 ± 2.3 kDa) within 5% of that expected for tetramer in the presence of NADH. The apparent molecular weight doesn't change when 2,4,6-octatrienoic-AcpM is mixed with InhA in the absence of NADH. The MW was found to be around 148 kDa (Figure 3.16B) when 30 μM 2,4,6-octatrienoic-AcpM and 60 μM InhA plus 60 μM NADH were mixed. It clearly shows the 2 AcpM monomers bind with 1 tetramer InhA in the presence of NADH, which agrees with the result of FabI:ACP system.

3.4 Discussion

M. tb AcpM is similar to other ACPs, and the sequence identity between *E. coli* ACP and *M. tb* AcpM is 37%. Overlay studies show a high degree of structural similarity. However, AcpM is larger than most ACPs and has an about 35 amino acids on the carboxyl terminal which forms a random coil in the solution (Figure 3.4). Three acidic residues located in helix α2 of ACP are D35, E41, and E47, the corresponding residues in AcpM are D40, E46, and D53 (Figure 3.5). Two possible roles of the C-terminal random coil of AcpM have been considered (*153*). One possible function of the AcpM carboxyl terminal random coil is important for its interaction with very long chain mycolic acid intermediates carried by the protein. The random coil of AcpM contains more than half hydrophobic amino acids which may sequester the long acyl chain attached to the prosthetic group from the solvent. On the other hand, Rock and coworkers proposed another possibility that the C-terminal extension may be involved in protein-protein interaction.

The yield of AcpM is low, one reason is that overexpression and induction of AcpM in *E. coli* cells is toxic to the cells, as expected *E. coli* ACP and other heterologous ACPs (*184, 185*). Another reason is the purity of AcpM. As seen with others ACPs, the majority of *E. coli* ACP is apo- form in its when expressed in *E. coli* (*140, 141*). However, expression of AcpM results in significant amount of holo- and acyl- forms (Figure 3.6). Only the unmodified apo- form can be used for the synthesis

of DD-AcpM, so purification of Apo-AcpM (FPLC) will further reduce the yield.

We have determined the primary isotope effects on ^{D}V and $^{D}(V/K)$ using NADD as a substrate. We used DD-ACP to replace DD-CoA since the DD-ACP does not cause substrate inhibition. F149A mutant only gives significant change in the measure primary isotope effects on $^{D}(V/K_{NADH})$. The $^{D}(V/K_{NADH})$ can be accounted for by proposing the mutation has both decreased the external commitment factor for NADH and destabilized the transition state for hydride transfer, resulting in an increase in the primary kinetic isotope effect for this step (*83*). Raman data showed a direct link between the conformation of the NADH ring and the hydride transfer reaction. In addition, kinetics isotopes effect data indicate that the F149A is associated with the increase in energy barrier for a step following hydride transfer and it plays a key role in lowering the energy of the transition state (*83*).

In our previous study, it was difficult to deliver the substrate through the major portal of ACP and FabI because the ACP Ser36 which connects with a long phosphopantetheine group was too far from the active site. So we used computational methods to model missing details and reconstruct how the ACP could deliver the long chain to the FabI active site. The residues in FabI interacting with ACP are K201, R204 and K205. But in the InhA-AcpM complex, there are no consecutive basic residues located at the helix α8. Compared with FabI, three amino acids (Q214, E220, and Q224) located in the α8 of InhA which are in the same position as three basic

residues (K201, R204, and R205) of FabI, another three basic residues are near the helix α8 of InhA, R195 and K233 locate in the beginning and the end of helix α8 loop respectively (Figure 3.13). R225 is in the helix α8 of InhA. No significant k_{cat}/K_m reduction was detected when three basic residues (R195, R225 and R233) were mutated to Glu residues. Furthermore, another three residues (N224, E220 and N214) have no any effect of the kinetic reduction of k_{cat}/K_m when mutated to acidic residue (N224E and N214E) or basic residue (E220K). Another basic patch (R173, R177, and K181) is not involved the interaction from the kinetics results.

The NMR structure of AcpM (PDB code 1KLP) and crystal structure of InhA (PDB code 1ZID) were overlapped with the complex ACP binds with FabI by MD simulations respectively by Pymol (Figure 3.12). ACP overlaps with AcpM very well only a long C terminal random coil of AcpM which be flexible in the solution. InhA overlaps with FabI except for the helixes α8 are not in the same conformation. The optimal angle for this type protein protein interaction is a relative angle of -60° (*186*). The closest contact between the recognition helix α2 of AcpM with helix α8 of InhA is oriented at a round of -75°. Sacchettini et al. confirmed that the location of the substrate binding loop significantly differs between InhA with FabI (*75*). They mentioned the size of the substrate binding loop is a primary determinant of the enzymes ability to distinguish between shorter with longer chain substrates. From the crystal structure, they determined the long chain C16 fatty acyl substrate binds in the major portal instead of the minor portal for *E. coli* FabI (PDB code: 1BVR). So we

supposed the interaction interface between InhA and AcpM will be different with FabI and ACP. Another possibility is the amino acid Gln45. Zhang et al. proposed the Ala45 of *E. coli* ACP plays a key role on the surface of ACP that allows the target protein to approach more closely. However, it is Gln50 in *M. tb* AcpM compared with ACP. The polar residue breaks the enzyme-ACP interaction in AcpM. So it suggests that AcpM may interact differently with its target protein compared with *E. coli* ACP. In addition, Schaeffer et al. measured the apparent k_{cat} for *E. coli* ACPS with apo-form AcpM was slower than that for *E. coli* Apo-ACP. This gives additional evidence than mycobacterial enzymes interact differently with *E. coli* ACP.

In the FabI-ACP system, three acidic residues (D35, D38, and E41) in and close to the helix of α2 of ACP form strong hydrogen bonding interaction with three basic residues (K201, R204, and R205) located in the helix α8 of FabI binding interface. Kinetics showed an overall 250 fold decrease in k_{cat}/K_m for reduction of DD-ACP for the R204E mutants, but no any effect for the CoA substrate. Three similar acidic residues (D40, E46, and E52) located in the helix α2 of AcpM. There must be some consecutive basic residues in the InhA have interaction with AcpM compared with FabI-ACP complex. Two α helixes are in the each side from InhA tetramer. Four basic amino acids (R53, R49, R45 and R43) located in each α helix (Figure 3.2). The side chains of R53, R49, and R45 are outward of the tetramer and R43 is toward the tetramer. As mentioned before, it was too far for the Serine to deliver phosphopantetheine group to the active site of InhA (F149, Y158, and K165) if AcpM

binds with helix α8 of InhA. It is only 15 Å from the R45 to pro4(S) of cofactor NADH, so it was easy for Ser41 to deliver the phosphopantetheine group to the active sites to react. Kinetic results prove such binding position. Replacement of R53 and R49 by glutamic acid results an overall 200-250 fold decrease in k_{cat}/K_m for reduction of DD-AcpM, no effect of the corresponding DD-CoA substrate, which is similar as the R204 of FabI. A 62 fold decrease of k_{cat}/K_m for reduction of DD-AcpM was found for the R45E mutant. R43E has showed 5 fold decrease of an overall k_{cat}/K_m when using DD-CoA as substrate, so it was supposed not involved in the binding interaction with InhA. It was further proved by directly fluorescence binding results. R53E, R49E, and R45E have showed at least 16 fold's decrease binding affinity compared with wild type InhA. The InhA-AcpM interaction position Ser41 carries the phosphopantetheine group to the active site through the minor portal and formed by the substrate binding loop. It was further discovered by kinetics of *E. coli* DD-ACP with InhA. Using DD-ACP which doesn't have long random coil in C-terminal as the substrate, we measured the K_m and k_{cat} and calculated k_{cat}/K_m with WT InhA, the mutants in R53, R49 and R45, and the mutants in R225, R195. We found the similar results compared with *M. tb* DD-AcpM (data not shown). Based on all the results, we proposed the binding residues for InhA should be R53, R49 and R45.

More interesting observation was found in Figure 3.17. There are two types of basic patch with InhA and FabI respectively. FabI has a basic patch (K201, R204, and K205) adjacent to the minor portal but has an acidic patch (D42, E49, E50 and D58)

in helix α2 adjacent to major portal. However, InhA has the basic and acidic patch in the opposite way. Instead of basic patch in helix α8, InhA has the acidic patch (E209, E210, E209, and E220). The basic patch for InhA interacting with AcpM is located in helix α2.

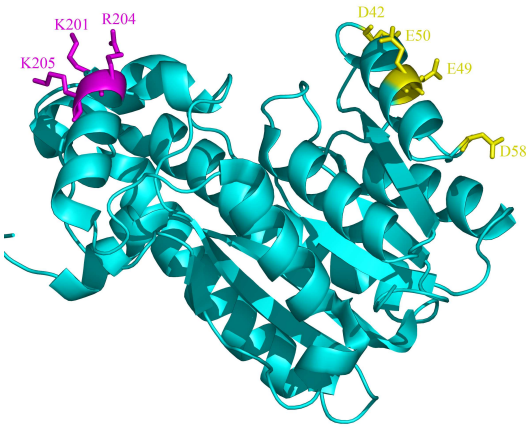

(A)

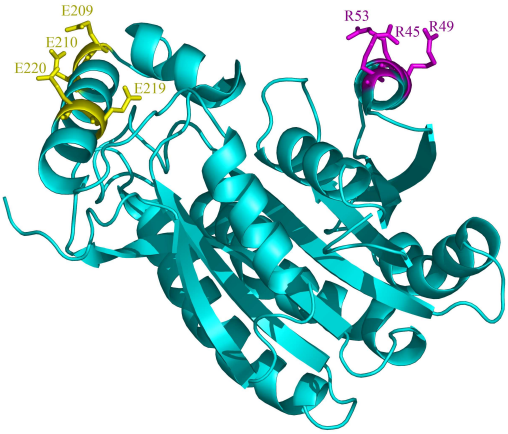

(B)

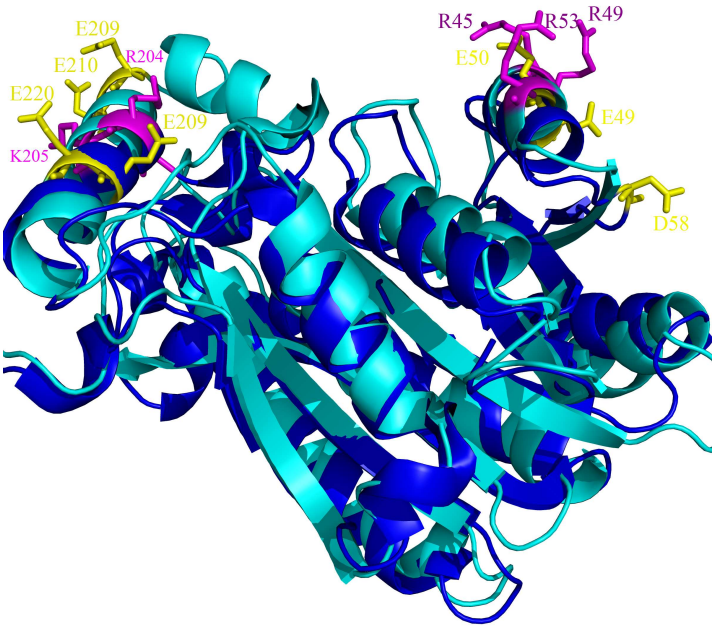

(C)

Figure 3.17. The basic and acidic patch of FabI and InhA. (A) The acidic and basic patch of FabI, 3 basic residues (K201, R204, and K205 colored magenta) and 4 acidic residues (D42, E49, E50 and D58 colored yellow). (B) The acidic and basic patch of InhA, 4 basic residues located in the helix α2 (R43, R45, R49, and R53 colored magenta) and 4 acidic residues located in the helix α8 adjacent to minor portal (E209, E210, E219, and E220 colored yellow). (C) Overlay the basic and acidic patch of InhA and FabI.

The three basic residues correspond to R45, R49, and R53. Sequence alignment of FASII system enoyl-ACP reductases was shown in Figure 3.18 by ClustalW. All InhAs (such as *M. leprae* and *M. tuberculosis* InhA) which have longer carbon chain (up to 90) carried by ACP have a basic patch (R53, R49, and R45) in helix α2 instead of the basic patch located in substrate binding loop of helix α8 of FabI which has shorter carbon chain (up to 20) carried by ACP substrate (such as *E. coli* and *S. aureus*). Furthermore, all InhAs have the exactly same basic patch and acidic patch as *M. tb* InhA. FabIs share the similar basic patch and acidic patch in helix α8 and helix α2 respectively. In the SDR superfamily, the third residue in the catalytic triad is either a Phe (F149 in all InhAs) or a Tyr (around Y146 in all FabIs), which plays a key role in modulating both the structure and reactivity of NADH when bound to reductase (*83*).

```
                                                                43 45    49    53
M.tuberculist_InhA      -----MTGLLDGKRILVSGIITDSSIAFHIARVAQEQGAQLVLTG-FDRLRLIQRITDRL 54
M.bovis_InhA            -----MTGLLDGKRILVSGIITDSSIAFHIARVAQEQGAQLVLTG-FDRLRLIQRITDRL 54
M.marimum_InhA          -----MAGLLEGKRILVSGIITDSSIAFHIARVAQEQGAQLVLTG-FDRMRLIQRIVDRL 54
M.ulcerans_InhA         -----MAGLLEGKRILVSGIITDSSIAFHIARVAQEQGAQLVLTG-FDRMRLIQRIVDRL 54
M.leprae_InhA           -----MAGLLEGKRILVSGIITDSSIAFHIAKVAQEAGAQLVLTG-FDRLRLIQRIADRL 54
E.coli_FabI             ------MGFLSGKRILVTGVASKLSIAYGIAQAMHREGAELAFTYQNDKLKGRVEEFAAQ 54
P.luminescens_FabI      ------MGFMTGKRILITGVASKLSIAYGVAKAMHDQGAELAFTYQNDKLKPRVEEFAAS 54
L.pneumophila_FabI      MGGDTIVGFLTGKKALIVGLASNRSIAYGIAKAFHNQGAELAFTYQNEKLQSRVEAMASE 60
H.pylori_FabI           ------MGFLKGKKGLIVGVANNKSIAYGIAQSCFNQGATLAFTYLNESLEKRVRPIAQE 54

M.tuberculist_InhA      PAKAPLLELDVQNEEHLASLAGRVTEAIGAGNKLDGVVHSIGFMPQTGMGINPFFDAPYA 114
M.bovis_InhA            PAKAPLLELDVQNEEHLASLAGRVTEAIGAGNKLDGVVHSIGFMPQTGMGINPFFDAPYA 114
M.marimum_InhA          PQKAPLIELDVQNEEHLASLAGRVTEVIGEGNNLDGVVHSIGFMPQSGMGINPFFDAPYE 114
M.ulcerans_InhA         PQKAPLIELDVQNEEHLASLAGRVTEVIGEGNNLDGVVHSIGFMPQSGMGINPFFDAPYE 114
M.leprae_InhA           PDKAPLIELDVQNEEHLATLAERVTAEIGEGNKLDGVVHSIGFMPQTGMGTNQFFDAPYE 114
E.coli_FabI             LGSDIVLQCDVAEDASIDTMFAELGKVWP---KFDGFVHSIGFAPGDQLDGDYVNAVTRE 111
P.luminescens_FabI      LNSTIVLPCDVAEDESIEVLFTELSKIWP---KFDGFVHSIGFAPADQLDGNYVSSVTRE 111
L.pneumophila_FabI      FNSTLVFPCDVASDEEIKAVFDNLRNHWD---KLDILVHSVAYAPADQISGDFVECANRE 117
H.pylori_FabI           LNSPYVYELDVSKEEHFKSLYNNIKQDLG---SLDFIVHSVAFAPKEALEGSLLETS-KS 110

M.tuberculist_InhA      DVSKGIHISAYSYASMAKALL-PIMNPGGSIVGMDFD-PSRAMPAYNWMTVAKSALESVN 172
M.bovis_InhA            DVSKGIHISAYSYASMAKALL-PIMNPGGSIVGMDFD-PSRAMPAYNWMTVAKSALESVN 172
M.marimum_InhA          DVSKGIHISAYSYASLAKALL-PIMNPGGSIVGMDFD-PTRAMPAYNWMTVAKSALESVN 172
M.ulcerans_InhA         DVSKGIHISAYSYASLAKALL-PIMNPGGSIVGMDFD-PTRAMPAYNWMTVAKSALESVN 172
M.leprae_InhA           DVSKGIHISTYSYASLAKALL-LIMNSGGSIVGMDFD-PTRAMPAYNWMTVAKSALESVN 172
E.coli_FabI             GFKIAHDISSYSFVAMAKACR-SMLNPGSALLTLSYLGAERAIPNYNVMGLAKASLEANV 170
P.luminescens_FabI      GFRIAHDISSYSFVAMAKTCR-EMLNPNSALLTLTYLGAERSIPNYNVMGLAKASLEANV 170
L.pneumophila_FabI      GFRIAHDISAYSLIGLSQAALPMMLDTQGSILTLSYYGAEKAVPNYNVMGVAKASLEASV 177
H.pylori_FabI           AFNTAMEISVYSLIELTNTLK-PLLNNGASVLTLSYLGSTKYMAHYNVMGLAKAALESAV 169
                                                          209 210       219 220
M.tuberculist_InhA      RFVAREAGKYGVRSNLVAAGPIRTLAMSAIVGGALGEEAGAQIQLLEEGWDQRAPIGWNM 232
M.bovis_InhA            RFVAREAGKYGVRSNLVAAGPIRTLAMSAIVGGALGEEAGAQIQLLEEGWDQRAPIGWNM 232
M.marimum_InhA          RFVAREAGKYGVRSNLVAAGPIRTLAMSAIVGGALGEEAGAQIQLLEDGWDQRAPVGWNM 232
M.ulcerans_InhA         RFVAREAGKYGVRSNLVAAGPIRTLAMSAIVGGALGEEAGAQIQLLEDGWDQRAPVGWNM 232
M.leprae_InhA           RFVAREAGKYGVRSNLVAAGPIRTLAMSAIVGGAFGEEAGAQMQLLEEGWDQRAPIGWNM 232
E.coli_FabI             RYMANAMGPEGVRVNAISAGPIRTLAASGIK----------DFRKMLAHCEAVTPIRRTV 220
P.luminescens_FabI      RYMANAMGAEGIRVNGISAGPIRTLAASGIK----------DFRKMLAHCESVNPIRRTV 220
L.pneumophila_FabI      RYLAASLGSRGLRINAISAGPIKTLAAAGIK----------DFRKIHAAYANITPLQRNV 227
H.pylori_FabI           RYLAVDLGKHNIRVNALSAGPIRTLASSGIA----------DFRMILKWNEINAPLRKNV 219

M.tuberculist_InhA      KDATPVAKTVCALLSDWLPATTGDIIYADGG-----AHTQLL----------------- 269
M.bovis_InhA            KDATPVAKTVCALLSDWLPATTGDIIYADGG-----AHTQLL----------------- 269
M.marimum_InhA          KDPTPVAKTVCAVLSEWLPATTGDIIFADGG-----AHTQLL----------------- 269
M.ulcerans_InhA         KDPTPVAKTVCAVLSEWLPATTGDIIFADGG-----AHTQLL----------------- 269
M.leprae_InhA           KDPTPVAKTVCALLSEWLPATTGSIIYADGG-----ASTQLL----------------- 269
E.coli_FabI             T-IEDVGNSAAFLCSDLSAGISGEVVHVDGG-FSIAAMNELELK--------------- 262
P.luminescens_FabI      T-TEDVGNAAAFLCSDLSGGITGEILHVDGG-FSIAAMNELELK--------------- 262
L.pneumophila_FabI      T-ADEVGNTAAFLCSDLASGITGEVLHVDAGYHAVSAMSELG----------------- 268
H.pylori_FabI           S-LEEVGNAGMYLLSSLSNGVSGEVHFVDAG-YHVMGMGAVEEKDNKATLLWDLHKEQ 275
```

Figure 3.18. Sequence alignment of InhA and FabI. Sequences were aligned using Clustalw software. Primary sequences of Enoyl-ACP reductase from bacteria and plants were compared. Basic and acidic residues in each conserved patches that are conserved in all InhA and FabI are colored red and blue respectively.

There is limited direct structural information about the interactions of ACPs with enzymes in the FAS pathway because of the paucity of crystal structure of enoyl-ACP reductase with acyl carrier protein. One reason is the low affinity between them and another one is the flexibility of acyl carrier protein in solution which brings the difficulty for the crystal construction. We used kinetics and modeling to build the structure of AcpM bound to InhA (Figure 3.19).

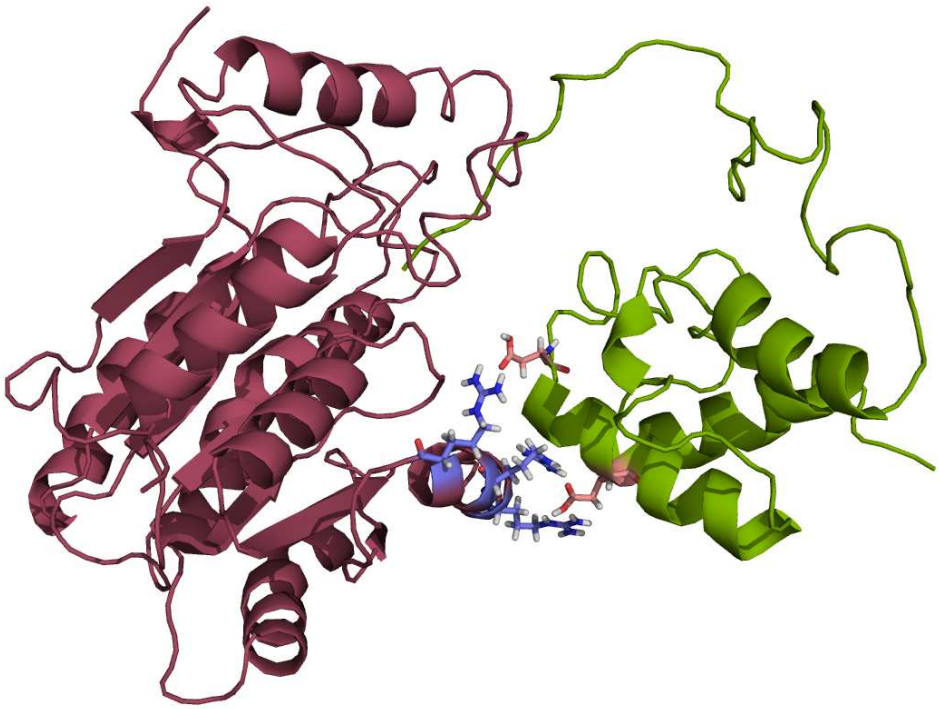

Figure 3.19. Proposed binding model of InhA-AcpM complex. InhA is shown in Raspberry. Residues R45, R49 and R53 are shown in blue. AcpM is shown in green and the residues R40 and R46 are shown in red. The interactions can help AcpM deliver the substrate to the active site of InhA through the major portal.

We proposed that InhA binds with AcpM in different way compared with ACP-FabI system. All the InhAs share the same binding priority and FabIs binds in the minor portal. One possibility is the length of the acyl chain carried by ACP can change the two-state equilibrium. The basic patch located in helix α2 of all InhA is adjacent to the major portal, where provides enough space for holding up to 90 carbons of the acyl chain carried by AcpM. Rock has mentioned the major portal of InhA will become wider when substrate binding, which give another evidence why the InhA-AcpM binding system is different with FabI-ACP.

In summary, we have purified the Apo-AcpM from the AcpM species and synthesized the natural substrate (DD-AcpM) for the enoyl-ACP reductase InhA in *M. tb*. Wild-type and mutants InhA have been measured the kinetics experiments using DD-CoA and DD-AcpM substrates. It shows that the R53, R49 and R45 amino acids located in the InhA α helix have interaction with acidic residues of AcpM and further been proved by fluorescence titration. The model of the InhA-AcpM binding interface is different with FabI-ACP module.

Chapter 4: Identification of the dehydratase component in the Fatty Acid Biosynthesis Pathway

4.1 Introduction

The *M. tb* FASII pathway has a special property of producing unusually long-chain fatty acids involved in the biosynthesis of mycolic acids. However, the enzyme that corresponds to dehydration of (3R)-hydroxyacyl-AcpM during the elongation cycles is still unknown. It remains difficult to identify the peptidic domains or proteins carrying this function within both multifunctional synthases and FASII systems because many similar functional enzymes exist (*187, 188*). In the *E. coli* system, FabZ (dehydratase) and FabA (dehydratase-isomerase) (Figure 4.1) catalyze this step, however, no such homolog are present in mycobacteria (*107, 108*).

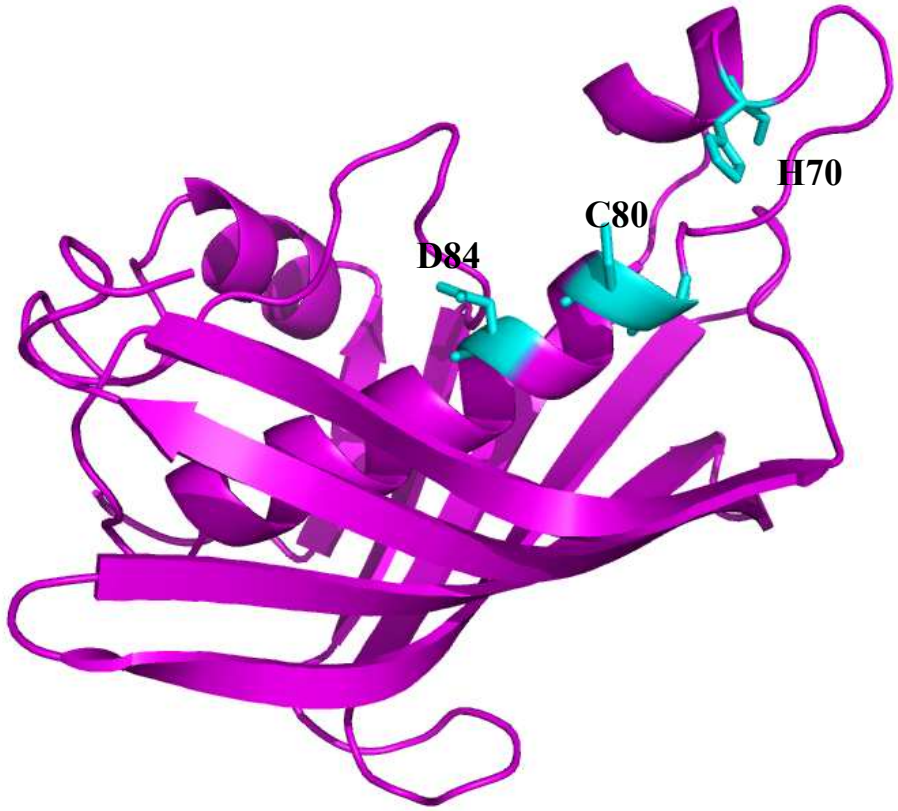

Figure 4.1. FabA structure and active site. His70 acts as a catalytic base to abstract a proton from the C2 of the substrate, and Aps84 promotes the removal of the hydroxyl group to generate the enoyl-ACP product.

FabA not only performs the dehydration step, but also has the ability to isomerize *trans*-2- to *cis*-3-decenoyl-ACP as an essential step in the formation of unsaturated fatty acids in *E. coli* (*100, 189-192*). FabA is always found in with its partner, FabB, which is a condensing enzyme that is also essential for unsaturated fatty acid biosynthesis (*193*). However, the FabA and FabB mutants still have the ability to catalyze fatty acid synthesis. This leads to the conclusion that an additional dehydratase and elongation condensing enzyme exists in *E. coli*. FabZ which is the second dehydratase found in *E. coli* was discovered in lipid A biosynthesis as a

suppressor of temperature sensitive mutants (*69*). FabZ homology are the only dehydratases which exist in most bacteria and cannot catalyze the isomerase reaction. Bioinformatic analysis divides FabA and FabZ as two subtypes even through they share highly conserved primary sequences, however, distinct differences exist in their active sites, an Asn in FabA and a Glu in FabZ. FabA functions in the metabolism of unsaturated fatty acids, while FabZ efficiently processes both saturated and unsaturated long chain acyl-ACPs (*194*).

The Rv3389c in *M. tb* has been identified as a single candidate protein which belongs to the hydratase 2 family with a distinctive asymmetric double hot dog fold (*109*). The purified recombinant *Rv3389c* protein not only catalyzed the hydration of (C_8-C_{18}) enoyl-CoA substrates, but also catalyzed the dehydration of a 3-hydroxyacyl-CoA in coupled reactions with both reductases (MabA and InhA) of the ACP-depended FASII involved in mycolic acid biosynthesis. However, *Rv3389c* decreases the activity of ACP substrate, versus CoA substrate. Derivative and *Rv3389c* knockout mutants show no change in its fatty acid biosynthesis. This suggested that *Rv3389c* is not the essential gene of the dehydration reaction.

Backbro and coworkers proposed that another gene, *Rv0216* is the dehydratase. This gene is conserved hypothetical protein from *M. tb* that is essential for bacterial survival during infection (*195*). They showed the structure exhibits the greatest similarity to bacterial and eukaryotic hydratases that catalyze the R-specific hydration

of 2-enoyl CoA. However, only part of the catalytic component is conserved in *Rv0216* and no activity was measured for the substrate crotonyl-CoA. This suggests the occurrence of additional hydratase candidates.

Besra and coworkers (*196, 197*) indicated two genes, *Rv3538* and *Rv0636* were essential for mycobacterial growth. They suggested *Rv0636* was an essential gene involved in mycolic acid biosynthesis and encodes the FASII β-hydroxyacyl-ACP dehydratase. Furthermore, Quemard and coworkers investigated *M. tb* genome to identify 11 putative (R)-specific enoyl hydratases/3-hydroxyacyl dehydratases. They explored the structure determination and modeling of three of these dehydratases to illustrate that they all belong or are related to the hydratase 2 protein family. The underlying 3D structure of FabA/FabZ enzymes are maintained in the so called hot dog fold but the catalytic site is distinct (*198*). Bioinformatics analyses and an essentiality study (*107*) lead them to propose the *Rv0635-Rv0636-Rv0637* is the candidate protein cluster for dehydration reaction.

The purpose of present work was to use the PCR to clone the *Rv0635-Rv0636-Rv0637* gene, insert into pET vector and to identify the specific enzymes corresponding to the dehydration reactions. Since we already have all the FASII enzymes, the availability of the dehydratase would allow us to reconstruct the FASII pathway *in vitro*.

4.2 Materials and Methods

4.2.1 Construction of expression plasmids for Wild-type *Rv0636*

The open reading frame coding for *Rv0636*, *Rv0636-Rv0637*, and *Rv0635-Rv0637* were amplified by PCR from total DNA of *M. tb*, strain H37Rv, using the primer pair 5'-GGAATTCCATATGATGGCGCTGCGTGAGTT (Forward) and 5'-CGGAGCCGCTTCAATCGCATCCCTAGGCGC (Reverse), 5'-GGAATTCCATATGATGGCGCTGCGTGAGTT (Forward) and 5'-CGCGGATCCTTACGCGGTCCTGATGACCTG (Reverse), 5'-GGAATTCCATATGGTGGCGTTGAGCGCAGA (Forward) and 5'-CGCGGATCCTTACGCGGTCCTGATGACCTG (Reverse) respectively. BamH1 and NdeI are the two restriction enzymes used to cut the PCR products and vectors, pET15b. The high fidelity polymerase Pfu Turbo (Stratagene) was used for ligating the DNA fragment to the pCR T7 pET15b (Invitrogen). Cloning was performed in *E. coli* TOP10 and the correctness of the isolated gene was verified by DNA sequence analysis. Plasmids were purified from XL1 Blue cells (Stratagene) using a DNA purification and gel extraction kit from Qiagen Inc. After verification of the correct sequence, the plasmid was transformed into BL21(DE3) pLysS cells (Novagen) for protein expression.

4.2.2 Overexpression and purification of *Rv0636*, *Rv0636-Rv0637*, and *Rv0635-Rv0636-Rv0637* gene

Cultures of BL21(DE3) pLysS cells carrying the *Rv0636*, *Rv0636-Rv0637*, and *Rv0635-Rv0636-Rv0637* plasmids were grown in 1 L of LB-ampicillin (200 μg/mL) medium at 37 ℃ to an OD_{600} of 1.2. The cells were induced by isopropyl β-D-thioglalctoside (150 μg/mL), and allowed to induce 4 hours at 37 ℃. After harvesting by centrifugation, the cell pellets was resuspended in 30 mL of His-bind buffer (20 mM Tris-HCl, 0.5 M NaCl, 5 mM imidazole, pH 7.9), and lysed using sonication (10 times at 20 seconds each). The cell debris was then removed by ultracentrifugation (33000 rpm for 1 hour) and the supernatant applied to a His-bind resin column (Novagen, 8 mL bed volume). The His-bind resin column was washed successively with His-bind buffer and His-wash buffer (20 mM Tris-HCl, 0.5 M NaCl, 60 mM imidazole, pH 7.9), and the protein was eluted using a gradient of 0 to 1 M imidazole in 20 mM Tris-HCl and 0.5 M NaCl (pH 7.9). Fractions containing the protein were pooled and further purified on an AKTA Superdex 200 prep grad column equilibrated in the buffer containing 50 mM NaH_2PO_4, 150 mM NaCl, pH 7.5. The protein eluted in two fractions and concentrated with Centricon-10 (Millpore). The concentration of proteins were calculated from the UV absorption at 280 nm using an absorption coefficient of 14.9, 33.8, and 51.2 $M^{-1}\cdot cm^{-1}$ for the *Rv0636*, *Rv0636-Rv0637*, and *Rv0635-Rv0636-Rv0637* enzymes respectively. 15% SDS-PAGE

and MALDI-TOF were used to identify the proteins.

4.2.3 Enzyme assays and steady state kinetics

Reactions were performed in a quartz cuvette in a total volume of 500 μL, at 25 ℃, in 50 mM NaH_2PO_4, 150 mM NaCl, pH 7.5. DD-CoA and DD-AcpM as the substrate were monitored by spectrophotometry (Varian) at 280 nm using an extinction coefficient of 3.6 $M^{-1}\cdot cm^{-1}$. Measurements of K_m and k_{cat} for DD-CoA were performed in the presence of enzyme (800 nM) variable concentration of substrate (1-60 μM). Data were fitted to the Michaelis-Menten equation by Grafit 4.0.

4.3 Results

4.3.1 Expression and purification of *Rv0636*, *Rv0635-Rv0636-Rv0637*, and *Rv0636-Rv0637* proteins

The *Rv0636* gene or *Rv0635-Rv0636-Rv0637* and *Rv0636-Rv0637* gene clusters were cloned into a T7 expression vector downstream of a His tag coding sequence. Proteins were produced in *E. coli* and purified by using a two step chromatography procedure on Ni Sepharose and Superdex 200 AKTA gel filtration columns (Figure 4.2).

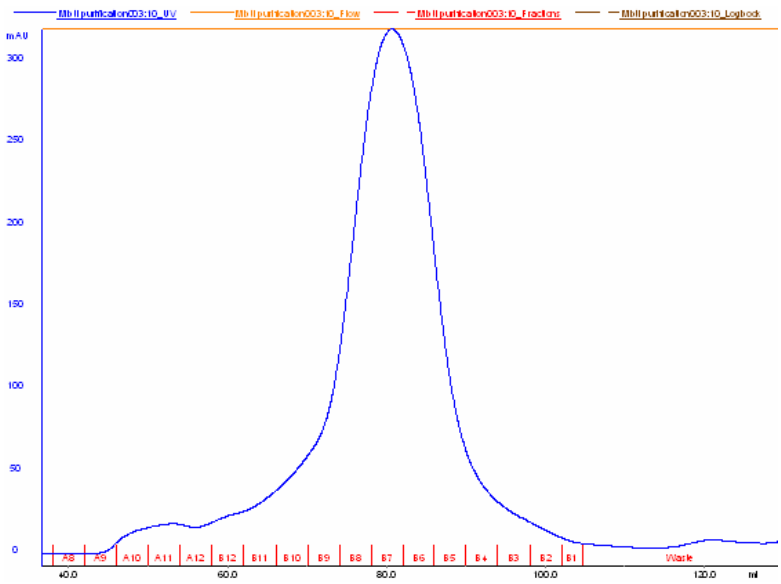

Figure 4.2. Rv0636 protein purified by AKTA gel filtration column

Most of the *Rv0636* containing a His-tag on the N-terminal was insoluble when

Rv0636 was expressed alone (*107*). The purified protein precipitated when concentrated and no activity was detected. When His-tagged *Rv0635* was copurified with untagged *Rv0636* and *Rv0637*, two bands were obtained on the 15% SDS-PAGE (Figure 4.3A). However, only one band appeared on the gel when His-tagged *Rv0636* was copurified with untagged *Rv0637* (Figure 4.3B).

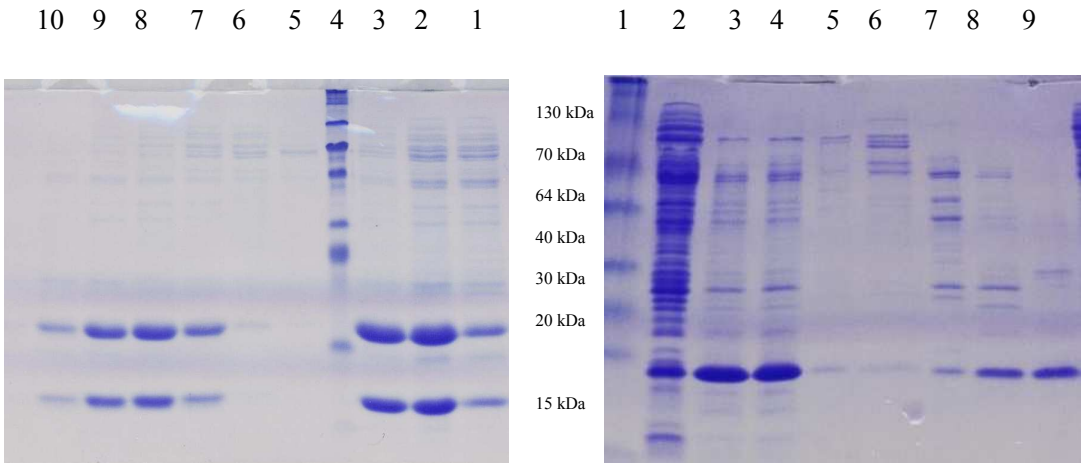

Figure 4.3. 15 % SDS-PAGE of *Rv0635-Rv0636-Rv0637* (A) and *Rv0636-Rv0637* (B) protein purification. (A) lane 1-3: Fractions of *Rv0635-Rv0636-Rv0637* protein from His tag column; Lane 4: Protein ladder; Lane 5-10: Fractions of *Rv0635-Rv0636-Rv0637* protein from Superdex 200 AKTA gel filtration columns. (B) Lane 1: Protein Ladder, Lane 2-4: Fractions of *Rv0636-Rv0637* protein from His tag column; Lane 5-9: Fractions of *Rv0636-Rv0637* protein from Superdex 200 AKTA gel filtration columns

Gel filtration chromatography displayed two protein bands. One band corresponds to *Rv0635-Rv0636-Rv0637* and the other *Rv0636-Rv0637* respectively. All the bands have been cut and run in an in-gel trypsin digestion to identify the protein. The protein tryptic digest was analyzed with a Bruker Autoflex II MALDI-TOF mass spectrometer. The protein fragment sample was mixed with

α-hydroxycinnamic acid as matrix and peptide masses were characterized in the reflection mode. The mass spectrum of *Rv0635-Rv0636-Rv0637* is displayed in Figure 4.4.

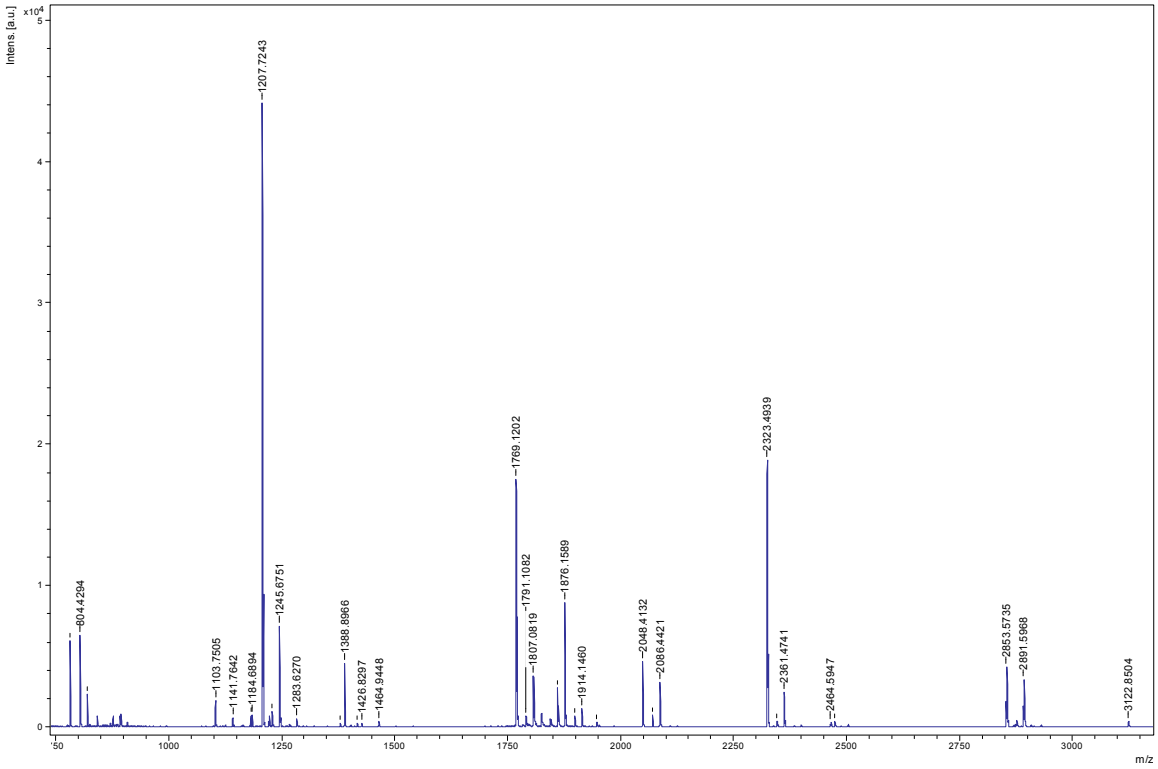

Figure 4.4. MALDI-TOF characterizes tryptic digest fragments.

Sequence of the recombinant of the top band in Figure 4.3(A) is shown below (Figure 4.5). Peptide coverage was shown in red. Sequencing results identify protein as *Rv0635* with His-tag on N-terminal.

MGSSHHHHHHSSGLVALSADIVGMHYRYPDHYEVEREKIREYAVAVQNDDAWYFEEDGAAELGYKGLLA

PLTFICVFGYKAQAAFFKHANIATAEAQIVQVDQVLKFEKPIVAGDKLYCDVYVDSVREAHGTQIIVTK

NIVTNEEGDLVQETYTTLAGRAGEDGEGFSDGAA

Figure 4.5. Sequence coverage of *Rv0635* (top band on Figure 4.2A) containing His-tag in N-terminal.

The bottom band on Figure 4.3A was determined as *Rv0636* without His-tag. The molecular weight on the gel agrees with theoretical MW (14.9 kDa). The protein bands shown on Figure 4.3B were characterized as *Rv0636* with a His-tag on the N-terminal by MALDI-TOF. The data strongly suggested that there are interactions between *Rv0635* and *Rv0636*. It was clearly shown that no *Rv0637* was detectable in *Rv0635-Rv0636-Rv0637* or *Rv0636-Rv0637* coexpression systems.

4.3.2 Enzymatic activity of *Rv0635-Rv0636-Rv0637* and *Rv0636-Rv0637*

Enzymes belonging to the (R)-sepcific enoyl hydratase/hydroxyacyl dehydratase family preferentially catalyze the dehydration reaction (*108*). The activities of *Rv0635-Rv0636-Rv0637* and *Rv0636-Rv0637* were first measured in the presence of DD-CoA and DD-AcpM or DD-ACP. *Rv0636-Rv0637* did not show any significant activity with either substrate in the experimental conditions used. A slight activity of *Rv0635-Rv0636-Rv0637* was measured only in the presence of DD-CoA (Figure 4.6).

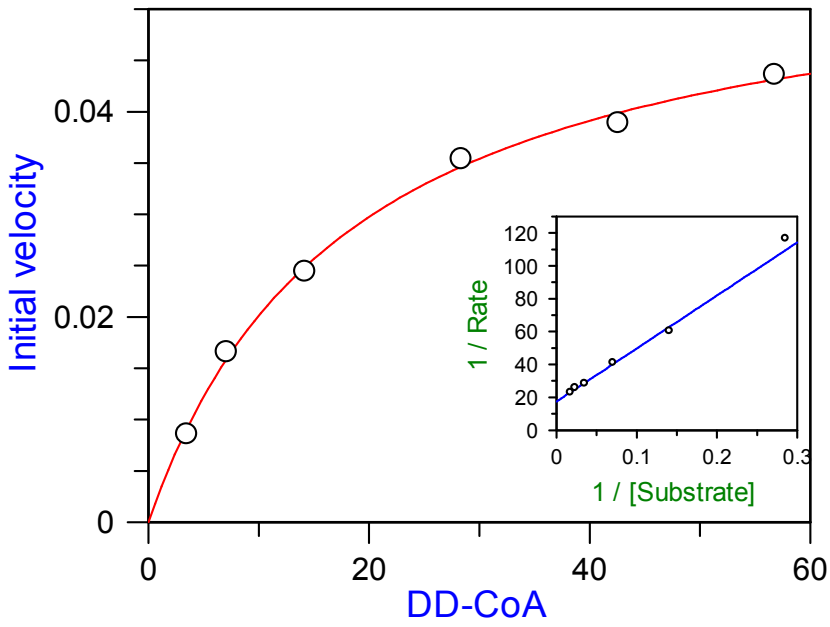

Figure 4.6. K_m determination for DD-CoA with respect to *Rv0635-Rv0636-Rv0637* gene.

Rv0635-Rv0636-Rv0637 proved to be active in the presence of DD-CoA (K_m: 18 µM and k_{cat}: 20 s^{-1}).

4.4 Discussion

No typical FabA or FabZ enzymes found in the bacterial FASII systems are present in *M. tb* or other sequenced mycobacterial genomes. Eukaryotic enoyl-CoA hydratases have led us to investigate the potential (R)-specific hydratases/dehydratases in the *M. tb* (*109, 198, 199*). *Rv0636* may share the same global topology and probably the same reaction mechanism as the FabA/FabZ family even through it exhibits very low sequence similarity and catalytic motif with the latter and its catalytic motif. Castell and coworkers also suggested that *Rv0636* of *M. tb* H37Rv is a good candidate for the unidentified β-hydroxyacyl-ACP dehydratase of FASII (*200*). In addition, *Rv0636* is highly conserved over numerous mycobacterial species, such as *M. bovis*, *M. smegmatis* and *M. leprae*. *Rv0635*, *Rv0636*, and *Rv0637* were proposed to be composed of a single hot dog fold by structural prediction. *Rv0636* is hypothesized to associate in heterodimers with either *Rv0635* or *Rv0637* in order to be functional. This is because *Rv0635* and *Rv0637* lack the hydratase 2 catalytic motif. *Rv0635* and *Rv0637* share 45% sequence identity and they are both poorly related to *Rv0636*. It is thought that *Rv0635* and *Rv0637* might have a similar role in the catalytic reaction. *Rv0635* overlaps *Rv0636* and *Rv0637* is 4 bp away from *Rv0637* (Figure 4.7) (*107*).

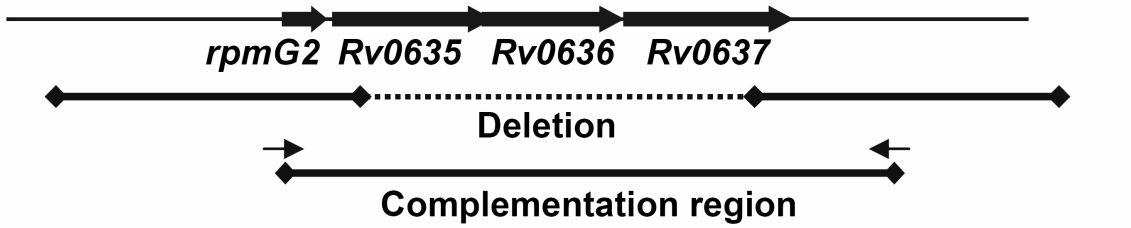

Figure 4.7. Demonstration of essentiality of *Rv0635-Rv0637*. Chromosomal organization of the region. The regions amplified to make the deletion delivery vector pTACK0636 and the complementing vector pCOLE0636 are drawn, indicating the deletion region and the complementation region, respectively. Arrows indicate the primers used to amplify the region and for PCR screening

Studies on the mitochondrial enoyl-CoA hydratase revealed that the enzyme also catalyzes the hydration of *cis*-2-enoyl-CoAs to the corresponding 3(R)-hydroxyacyl-CoA products (*201, 202*). The subsequent enzyme in the fatty acid oxidation cycle is specific for the 3(S)-hydroxyacyl-CoA. The enzyme also catalyzes the interconversion of 3(R)- and 3(S)- hydroxyacyl-CoAs in order to facilitate the metabolism of fatty acids containing *cis* double bonds. The equilibrium constant for the hydration of *trans*-2-crotonyl-CoA to 3(S)-hydroxybutyryl-CoA is 7.5. It was proposed the hydratase in *M. tb* will perform the same function. When coproduced in *E. coli*, *Rv0636* protein associates in heterodimers (confirmed by AUC) with either *Rv0635* or *Rv0637*. Only *Rv0636* showed some activity to DD-CoA when coexpressed with *Rv0635*. The *Rv0637* gene does not seem to be essential for *M. tb* growth *in vitro*. However, *Rv0635-Rv0636-Rv0637* did not perform any activity with DD-AcpM, the natural substrate. It still gives us the difficulty to investigate the dehydrates in *M. tb*.

Reference:

1. Oreilly, L. M., and Daborn, C. J. (1995) The Epidemiology of Mycobacterium-Bovis Infections in Animals and Man - a Review, *Tubercle and Lung Disease 76*, 1-46.
2. Kochi, A. (1991) The global tuberculosis situation and the new control strategy of the World Health Organization, *Tubercle 72*, 1-6.
3. Magdalena, J., Vachee, A., Supply, P., and Locht, C. (1998) Identification of a new DNA region specific for members of Mycobacterium tuberculosis complex, *Journal of Clinical Microbiology 36*, 937-943.
4. Bernstein, J., Jambor, W. P., Lott, W. A., Pansy, F., Steinberg, B. A., and Yale, H. L. (1953) Chemotherapy of Experimental Tuberculosis .7. Heterocyclic Acid Hydrazides and Derivatives, *American Review of Tuberculosis 67*, 366-375.
5. Bernstein, J., Jambor, W. P., Lott, W. A., Pansy, F., Steinberg, B. A., and Yale, H. L. (1953) Chemotherapy of Experimental Tuberculosis .6. Derivatives of Isoniazid, *American Review of Tuberculosis 67*, 354-365.
6. Bernstein, J., Lott, W. A., Steinberg, B. A., and Yale, H. L. (1952) Chemotherapy of Experimental Tuberculosis .5. Isonicotinic Acid Hydrazide (Nydrazid) and Related Compounds, *American Review of Tuberculosis 65*, 357-364.
7. Freedlander, B. L., Furst, A., and Balcom, D. (1952) Chemotherapy of

Experimental Tuberculosis with Quinoline Derivatives, *Proceedings of the Society for Experimental Biology and Medicine 81*, 66-68.

8. Kushner, S., Dalalian, H., Sanjurjo, J. L., Bach, F. L., Safir, S. R., Smith, V. K., and Williams, J. H. (1952) Experimental Chemotherapy of Tuberculosis .2. The Synthesis of Pyrazinamides and Related Compounds, *Journal of the American Chemical Society 74*, 3617-3621.

9. Siebenmann, C. O. (1953) Isoniazid in Combined Chemotherapy of Experimental Tuberculosis in Mice, *American Review of Tuberculosis 68*, 411-418.

10. Yale, H. L., Losee, K., Martins, J., Holsing, M., Perry, F. M., and Bernstein, J. (1953) Chemotherapy of Experimental Tuberculosis .8. The Synthesis of Acid Hydrazides, Their Derivatives and Related Compounds, *Journal of the American Chemical Society 75*, 1933-1942.

11. Yale, H. L., Losee, K. A., Perry, F. M., and Bernstein, J. (1954) Chemotherapy of Experimental Tuberculosis .10. Heterocyclic Acyl Derivatives of Substituted Semicarbazides, *Journal of the American Chemical Society 76*, 2208-2211.

12. Clark, J., and Wallace, A. (1967) The susceptibility of mycobacteria to rifamide and rifampicin, *Tubercle 48*, 144-148.

13. Furesz, S., Scotti, R., Pallanza, R., and Mapelli, E. (1967) Rifampicin: a new rifamycin. 3. Absorption, distribution, and elimination in man, *Arzneimittelforschung 17*, 534-537.

14. Pallanza, R., Arioli, V., Furesz, S., and Bolzoni, G. (1967) Rifampicin: a new rifamycin. II. Laboratory studies on the antituberculous activity and preliminary clinical observations, *Arzneimittelforschung 17*, 529-534.

15. Garrigo, M., Moreno, C., Aragon, L., and Coll, P. (2007) Evaluation of the BacT/Alert PZA test for susceptibility testing of Mycobacterium tuberculosis to pyrazinamide in comparison with BacTec 460TB, *International Journal of Antimicrobial Agents 29*, S576-S576.

16. Gupta, P., Roy, V., Sethi, G. R., and Mishra, T. K. (2008) Pyrazinamide blood concentrations in children suffering from tuberculosis: a comparative study at two doses, *British Journal of Clinical Pharmacology 65*, 423-427.

17. Jureen, P., Werngren, J., Toro, J. C., and Hoffner, S. (2008) Pyrazinamide resistance and pncA gene mutations in Mycobacterium tuberculosis, *Antimicrobial Agents and Chemotherapy 52*, 1852-1854.

18. Nuermberger, E., Tyagi, S., Tasneen, R., Williams, K. N., Almeida, D., Rosenthal, I., and Grosset, J. H. (2008) Powerful bactericidal and sterilizing activity of a regimen containing PA-824, moxifloxacin, and pyrazinamide in a murine model of tuberculosis, *Antimicrobial Agents and Chemotherapy 52*, 1522-1524.

19. Bobrowit, D., and Gokulana, K., (1965) Ethambutol in Retreatment of Pulmonary Tuberculosis, *Diseases of the Chest 48*, 239-244.

20. Cappiell.Vp, and Layton, W. M. (1965) A 1-Year Study of Toxicity of Ethambutol in Dogs - Results of Gross and Histopathologic Examinations,

Toxicology and Applied Pharmacology 7, 844-849.

21. Gupta, S. K., and Mathur, I. S. (1965) Stability of Ethambutol [D-2,2'-(Ethylenediimino)-Di-1-Butanol] Resistant Mycobacteria Grown in Absence of Ethambutol, *Indian Journal of Experimental Biology 3*, 176-&.

22. Tsukamur.M. (1965) Resistance Pattern of Mycobacterium Tuberculosis and Mycobacterium Bovis to Ethambutol, *Acta Tuberculosea Et Pneumologica Scandinavica 46*, 89-94.

23. Robinson, H. J., Smith, D. G., and Graessle, O. E. (1944) Chemotherapeutic properties of streptomycin, *Proceedings of the Society for Experimental Biology and Medicine 57*, 226-231.

24. Schatz, A., Bugie, E., and Waksman, S. A. (1944) Streptomycin, a substance exhibiting antibiotic activity against gram positive and gram-negative bacteria, *Proceedings of the Society for Experimental Biology and Medicine 55*, 66-69.

25. Schatz, A., and Waksman, S. A. (1944) Effect of streptomycin and other antibiotic substances upon Mycobacterium tuberculosis and related organisms, *Proceedings of the Society for Experimental Biology and Medicine 57*, 244-248.

26. Timmins, G. S., and Deretic, V. (2006) Mechanisms of action of isoniazid, *Mol Microbiol 62*, 1220-1227.

27. Youatt, J. (1969) A review of the action of isoniazid, *Am Rev Respir Dis 99*, 729-749.

28. Deretic, V., Pagan-Ramos, E., Zhang, Y., Dhandayuthapani, S., and Via, L. E.

(1996) The extreme sensitivity of Mycobacterium tuberculosis to the front-line antituberculosis drug isoniazid, *Nat Biotechnol 14*, 1557-1561.

29. Zhang, Y., Dhandayuthapani, S., and Deretic, V. (1996) Molecular basis for the exquisite sensitivity of Mycobacterium tuberculosis to isoniazid, *Proc Natl Acad Sci U S A 93*, 13212-13216.

30. Zhang, Y., Heym, B., Allen, B., Young, D., and Cole, S. (1992) The catalase-peroxidase gene and isoniazid resistance of Mycobacterium tuberculosis, *Nature 358*, 591-593.

31. Sivaraman, S., Sullivan, T. J., Johnson, F., Novichenok, P., Cui, G., Simmerling, C., and Tonge, P. J. (2004) Inhibition of the bacterial enoyl reductase FabI by triclosan: a structure-reactivity analysis of FabI inhibition by triclosan analogues, *J Med Chem 47*, 509-518.

32. Sivaraman, S., Zwahlen, J., Bell, A. F., Hedstrom, L., and Tonge, P. J. (2003) Structure-activity studies of the inhibition of FabI, the enoyl reductase from Escherichia coli, by triclosan: kinetic analysis of mutant FabIs, *Biochemistry 42*, 4406-4413.

33. Parikh, S. L., Xiao, G., and Tonge, P. J. (2000) Inhibition of InhA, the enoyl reductase from Mycobacterium tuberculosis, by triclosan and isoniazid, *Biochemistry 39*, 7645-7650.

34. Stewart, M. J., Parikh, S., Xiao, G., Tonge, P. J., and Kisker, C. (1999) Structural basis and mechanism of enoyl reductase inhibition by triclosan, *J Mol Biol 290*, 859-865.

35. Zimhony, O., Cox, J. S., Welch, J. T., Vilcheze, C., and Jacobs, W. R., Jr. (2000) Pyrazinamide inhibits the eukaryotic-like fatty acid synthetase I (FASI) of Mycobacterium tuberculosis, *Nat Med 6*, 1043-1047.

36. Boshoff, H. I., Mizrahi, V., and Barry, C. E., 3rd. (2002) Effects of pyrazinamide on fatty acid synthesis by whole mycobacterial cells and purified fatty acid synthase I, *J Bacteriol 184*, 2167-2172.

37. Zhang, Y., Wade, M. M., Scorpio, A., Zhang, H., and Sun, Z. (2003) Mode of action of pyrazinamide: disruption of Mycobacterium tuberculosis membrane transport and energetics by pyrazinoic acid, *J Antimicrob Chemother 52*, 790-795.

38. Beggs, W. H., and Andrews, F. A. (1974) Chemical characterization of ethambutol binding to Mycobacterium smegmatis, *Antimicrob Agents Chemother 5*, 234-239.

39. Takayama, K., and Kilburn, J. O. (1989) Inhibition of synthesis of arabinogalactan by ethambutol in Mycobacterium smegmatis, *Antimicrob Agents Chemother 33*, 1493-1499.

40. (1992) Transmission of multidrug-resistant tuberculosis among immunocompromised persons in a correctional system--New York, 1991, *MMWR Morb Mortal Wkly Rep 41*, 507-509.

41. Farley, T. A. (1992) AIDS and multidrug-resistant tuberculosis: an epidemic transforms an old disease, *J La State Med Soc 144*, 357-361.

42. Pearson, M. L., Jereb, J. A., Frieden, T. R., Crawford, J. T., Davis, B. J.,

Dooley, S. W., and Jarvis, W. R. (1992) Nosocomial transmission of multidrug-resistant Mycobacterium tuberculosis. A risk to patients and health care workers, *Ann Intern Med 117*, 191-196.

43. (1991) From the Centers for Disease Control. Nosocomial transmission of multidrug-resistant tuberculosis among HIV-infected persons--Florida and New York, 1988-1991, *JAMA 266*, 1483-1485.

44. (1991) Nosocomial transmission of multidrug-resistant tuberculosis among HIV-infected persons--Florida and New York, 1988-1991, *MMWR Morb Mortal Wkly Rep 40*, 585-591.

45. (1991) Transmission of multidrug-resistant tuberculosis from an HIV-positive client in a residential substance-abuse treatment facility--Michigan, *MMWR Morb Mortal Wkly Rep 40*, 129-131.

46. Marwick, C. (1992) Multidrug-resistant tuberculosis poses challenge, *JAMA 267*, 786.

47. Hirano, Y., and Ronai, Z. (2006) A new function for p53 ubiquitination, *Cell 127*, 675-677.

48. Frieden, T. R., Sterling, T., Pablos-Mendez, A., Kilburn, J. O., Cauthen, G. M., and Dooley, S. W. (1993) The emergence of drug-resistant tuberculosis in New York City, *N Engl J Med 328*, 521-526.

49. Benatar, S. R. (2006) Extensively drug resistant tuberculosis: problem will get worse in South Africa unless poverty is alleviated, *BMJ 333*, 705.

50. Dahle, U. R. (2006) Extensively drug resistant tuberculosis: beware patients

lost to follow-up, *BMJ 333*, 705.

51. Gandhi, N. R., Moll, A., Sturm, A. W., Pawinski, R., Govender, T., Lalloo, U., Zeller, K., Andrews, J., and Friedland, G. (2006) Extensively drug-resistant tuberculosis as a cause of death in patients co-infected with tuberculosis and HIV in a rural area of South Africa, *Lancet 368*, 1575-1580.

52. Masjedi, M. R., Farnia, P., Sorooch, S., Pooramiri, M. V., Mansoori, S. D., Zarifi, A. Z., Akbarvelayati, A., and Hoffner, S. (2006) Extensively drug-resistant tuberculosis: 2 years of surveillance in Iran, *Clin Infect Dis 43*, 841-847.

53. Raviglione, M. C., and Smith, I. M. (2007) XDR tuberculosis--implications for global public health, *N Engl J Med 356*, 656-659.

54. Tonge, P. J. (2000) Another brick in the wall, in *Nature Structural Biology* pp 94-96.

55. Brennan, P. J., and Nikaido, H. (1995) The envelope of mycobacteria, *Annu Rev Biochem 64*, 29-63.

56. Barry, C. E., 3rd, Lee, R. E., Mdluli, K., Sampson, A. E., Schroeder, B. G., Slayden, R. A., and Yuan, Y. (1998) Mycolic acids: structure, biosynthesis and physiological functions, *Prog Lipid Res 37*, 143-179.

57. Jarlier, V., and Nikaido, H. (1994) Mycobacterial cell wall: structure and role in natural resistance to antibiotics, *FEMS Microbiol Lett 123*, 11-18.

58. Kodali, S., Galgoci, A., Young, K., Painter, R., Silver, L. L., Herath, K. B., Singh, S. B., Cully, D., Barrett, J. F., Schmatz, D., and Wang, J. (2005)

Determination of selectivity and efficacy of fatty acid synthesis inhibitors, *J Biol Chem 280*, 1669-1677.

59. Campbell, J. W., and Cronan, J. E., Jr. (2001) Bacterial fatty acid biosynthesis: targets for antibacterial drug discovery, *Annu Rev Microbiol 55*, 305-332.

60. Mattick, J. S., Nickless, J., Mizugaki, M., Yang, C. Y., Uchiyama, S., and Wakil, S. J. (1983) The architecture of the animal fatty acid synthetase. II. Separation of the core and thioesterase functions and determination of the N-C orientation of the subunit, *J Biol Chem 258*, 15300-15304.

61. Stoops, J. K., Henry, S. J., and Wakil, S. J. (1983) The arrangement and role of some of the amino acid residues in the beta-ketoacyl synthetase site of chicken liver fatty acid synthetase, *J Biol Chem 258*, 12482-12486.

62. Wakil, S. J., Stoops, J. K., and Joshi, V. C. (1983) Fatty acid synthesis and its regulation, *Annu Rev Biochem 52*, 537-579.

63. Wong, H., Mattick, J. S., and Wakil, S. J. (1983) The architecture of the animal fatty acid synthetase. III. Isolation and characterization of beta-ketoacyl reductase, *J Biol Chem 258*, 15305-15311.

64. Tai, M. H., Chirala, S. S., and Wakil, S. J. (1993) Roles of Ser101, Asp236, and His237 in catalysis of thioesterase II and of the C-terminal region of the enzyme in its interaction with fatty acid synthase, *Proc Natl Acad Sci U S A 90*, 1852-1856.

65. Smith, S. (1994) The animal fatty acid synthase: one gene, one polypeptide, seven enzymes, *FASEB J 8*, 1248-1259.

66. Choi, K. H., Heath, R. J., and Rock, C. O. (2000) beta-ketoacyl-acyl carrier protein synthase III (FabH) is a determining factor in branched-chain fatty acid biosynthesis, *J Bacteriol 182*, 365-370.

67. Choi, K. H., Kremer, L., Besra, G. S., and Rock, C. O. (2000) Identification and substrate specificity of beta -ketoacyl (acyl carrier protein) synthase III (mtFabH) from Mycobacterium tuberculosis, *J Biol Chem 275*, 28201-28207.

68. Cronan, J. E., Jr., Li, W. B., Coleman, R., Narasimhan, M., de Mendoza, D., and Schwab, J. M. (1988) Derived amino acid sequence and identification of active site residues of Escherichia coli beta-hydroxydecanoyl thioester dehydrase, *J Biol Chem 263*, 4641-4646.

69. Mohan, S., Kelly, T. M., Eveland, S. S., Raetz, C. R., and Anderson, M. S. (1994) An Escherichia coli gene (FabZ) encoding (3R)-hydroxymyristoyl acyl carrier protein dehydrase. Relation to fabA and suppression of mutations in lipid A biosynthesis, *J Biol Chem 269*, 32896-32903.

70. Heath, R. J., and Rock, C. O. (1995) Enoyl-acyl carrier protein reductase (fabI) plays a determinant role in completing cycles of fatty acid elongation in Escherichia coli, *J Biol Chem 270*, 26538-26542.

71. Heath, R. J., and Rock, C. O. (2000) A triclosan-resistant bacterial enzyme, *Nature 406*, 145-146.

72. Heath, R. J., Su, N., Murphy, C. K., and Rock, C. O. (2000) The enoyl-[acyl-carrier-protein] reductases FabI and FabL from Bacillus subtilis, *J Biol Chem 275*, 40128-40133.

73. Kauppinen, S., Siggaard-Andersen, M., and von Wettstein-Knowles, P. (1988) beta-Ketoacyl-ACP synthase I of Escherichia coli: nucleotide sequence of the fabB gene and identification of the cerulenin binding residue, *Carlsberg Res Commun 53*, 357-370.

74. Siggaard-Andersen, M., Wissenbach, M., Chuck, J. A., Svendsen, I., Olsen, J. G., and von Wettstein-Knowles, P. (1994) The fabJ-encoded beta-ketoacyl-[acyl carrier protein] synthase IV from Escherichia coli is sensitive to cerulenin and specific for short-chain substrates, *Proc Natl Acad Sci U S A 91*, 11027-11031.

75. Rozwarski, D. A., Vilcheze, C., Sugantino, M., Bittman, R., and Sacchettini, J. C. (1999) Crystal structure of the Mycobacterium tuberculosis enoyl-ACP reductase, InhA, in complex with NAD+ and a C16 fatty acyl substrate, *J Biol Chem 274*, 15582-15589.

76. Parikh, S., Moynihan, D. P., Xiao, G., and Tonge, P. J. (1999) Roles of tyrosine 158 and lysine 165 in the catalytic mechanism of InhA, the enoyl-ACP reductase from Mycobacterium tuberculosis, *Biochemistry 38*, 13623-13634.

77. Quemard, A., Sacchettini, J. C., Dessen, A., Vilcheze, C., Bittman, R., Jacobs, W. R., Jr., and Blanchard, J. S. (1995) Enzymatic characterization of the target for isoniazid in Mycobacterium tuberculosis, *Biochemistry 34*, 8235-8241.

78. Roujeinikova, A., Sedelnikova, S., de Boer, G. J., Stuitje, A. R., Slabas, A. R., Rafferty, J. B., and Rice, D. W. (1999) Inhibitor binding studies on enoyl reductase reveal conformational changes related to substrate recognition, *J*

Biol Chem 274, 30811-30817.

79. Roujeinikova, A., Levy, C. W., Rowsell, S., Sedelnikova, S., Baker, P. J., Minshull, C. A., Mistry, A., Colls, J. G., Camble, R., Stuitje, A. R., Slabas, A. R., Rafferty, J. B., Pauptit, R. A., Viner, R., and Rice, D. W. (1999) Crystallographic analysis of triclosan bound to enoyl reductase, *J Mol Biol 294*, 527-535.

80. Baldock, C., Rafferty, J. B., Sedelnikova, S. E., Baker, P. J., Stuitje, A. R., Slabas, A. R., Hawkes, T. R., and Rice, D. W. (1996) A mechanism of drug action revealed by structural studies of enoyl reductase, *Science 274*, 2107-2110.

81. Rafferty, J. B., Simon, J. W., Baldock, C., Artymiuk, P. J., Baker, P. J., Stuitje, A. R., Slabas, A. R., and Rice, D. W. (1995) Common themes in redox chemistry emerge from the X-ray structure of oilseed rape (Brassica napus) enoyl acyl carrier protein reductase, *Structure 3*, 927-938.

82. Rozwarski, D. A., Grant, G. A., Barton, D. H., Jacobs, W. R., Jr., and Sacchettini, J. C. (1998) Modification of the NADH of the isoniazid target (InhA) from Mycobacterium tuberculosis, *Science 279*, 98-102.

83. Bell, A. F., Stratton, C. F., Zhang, X., Novichenok, P., Jaye, A. A., Nair, P. A., Parikh, S., Rawat, R., and Tonge, P. J. (2007) Evidence from Raman spectroscopy that InhA, the mycobacterial enoyl reductase, modulates the conformation of the NADH cofactor to promote catalysis, *J Am Chem Soc 129*, 6425-6431.

84. Rock, C. O., and Cronan, J. E., Jr. (1981) Acyl carrier protein from Escherichia coli, *Methods Enzymol 71 Pt C*, 341-351.

85. Rock, C. O., and Jackowski, S. (2002) Forty years of bacterial fatty acid synthesis, *Biochem Biophys Res Commun 292*, 1155-1166.

86. Tondi, D., Slomczynska, U., Costi, M. P., Watterson, D. M., Ghelli, S., and Shoichet, B. K. (1999) Structure-based discovery and in-parallel optimization of novel competitive inhibitors of thymidylate synthase, *Chem Biol 6*, 319-331.

87. Tang, L., Weissborn, A. C., and Kennedy, E. P. (1997) Domains of Escherichia coli acyl carrier protein important for membrane-derived-oligosaccharide biosynthesis, *J Bacteriol 179*, 3697-3705.

88. Brozek, K. A., and Raetz, C. R. (1990) Biosynthesis of lipid A in Escherichia coli. Acyl carrier protein-dependent incorporation of laurate and myristate, *J Biol Chem 265*, 15410-15417.

89. Sweet, C. R., Williams, A. H., Karbarz, M. J., Werts, C., Kalb, S. R., Cotter, R. J., and Raetz, C. R. (2004) Enzymatic synthesis of lipid A molecules with four amide-linked acyl chains. LpxA acyltransferases selective for an analog of UDP-N-acetylglucosamine in which an amine replaces the 3"-hydroxyl group, *J Biol Chem 279*, 25411-25419.

90. Cronan, J. E. (2003) Bacterial membrane lipids: where do we stand?, *Annu Rev Microbiol 57*, 203-224.

91. Majerus, P. W., Alberts, A. W., and Vagelos, P. R. (1964) The Acyl Carrier

Protein of Fatty Acid Synthesis: Purification, Physical Properties, and Substrate Binding Site, *Proc Natl Acad Sci U S A 51*, 1231-1238.

92. Wakil, S. J. (1989) Fatty acid synthase, a proficient multifunctional enzyme, *Biochemistry 28*, 4523-4530.

93. Vagelos, P. R., Majerus, P. W., Alberts, A. W., Larrabee, A. R., and Ailhaud, G. P. (1966) Structure and function of the acyl carrier protein, *Fed Proc 25*, 1485-1494.

94. Holak, T. A., Nilges, M., Prestegard, J. H., Gronenborn, A. M., and Clore, G. M. (1988) Three-dimensional structure of acyl carrier protein in solution determined by nuclear magnetic resonance and the combined use of dynamical simulated annealing and distance geometry, *Eur J Biochem 175*, 9-15.

95. Roujeinikova, A., Baldock, C., Simon, W. J., Gilroy, J., Baker, P. J., Stuitje, A. R., Rice, D. W., Slabas, A. R., and Rafferty, J. B. (2002) X-ray crystallographic studies on butyryl-ACP reveal flexibility of the structure around a putative acyl chain binding site, *Structure 10*, 825-835.

96. Parris, K. D., Lin, L., Tam, A., Mathew, R., Hixon, J., Stahl, M., Fritz, C. C., Seehra, J., and Somers, W. S. (2000) Crystal structures of substrate binding to Bacillus subtilis holo-(acyl carrier protein) synthase reveal a novel trimeric arrangement of molecules resulting in three active sites, *Structure 8*, 883-895.

97. Lambalot, R. H., and Walsh, C. T. (1995) Cloning, overproduction, and characterization of the Escherichia coli holo-acyl carrier protein synthase, *J Biol Chem 270*, 24658-24661.

98. Chalut, C., Botella, L., de Sousa-D'Auria, C., Houssin, C., and Guilhot, C. (2006) The nonredundant roles of two 4'-phosphopantetheinyl transferases in vital processes of Mycobacteria, *Proc Natl Acad Sci U S A 103*, 8511-8516.

99. Schaeffer, M. L., Agnihotri, G., Kallender, H., Brennan, P. J., and Lonsdale, J. T. (2001) Expression, purification, and characterization of the Mycobacterium tuberculosis acyl carrier protein, AcpM, *Biochim Biophys Acta 1532*, 67-78.

100. White, S. W., Zheng, J., Zhang, Y. M., and Rock. (2005) The structural biology of type II fatty acid biosynthesis, *Annu Rev Biochem 74*, 791-831.

101. Prescott, D. J., and Vagelos, P. R. (1972) Acyl carrier protein, *Adv Enzymol Relat Areas Mol Biol 36*, 269-311.

102. DiRusso, C. C., Metzger, A. K., and Heimert, T. L. (1993) Regulation of transcription of genes required for fatty acid transport and unsaturated fatty acid biosynthesis in Escherichia coli by FadR, *Mol Microbiol 7*, 311-322.

103. Magnuson, K., Jackowski, S., Rock, C. O., and Cronan, J. E., Jr. (1993) Regulation of fatty acid biosynthesis in Escherichia coli, *Microbiol Rev 57*, 522-542.

104. Zhang, Y. M., Rao, M. S., Heath, R. J., Price, A. C., Olson, A. J., Rock, C. O., and White, S. W. (2001) Identification and analysis of the acyl carrier protein (ACP) docking site on beta-ketoacyl-ACP synthase III, *J Biol Chem 276*, 8231-8238.

105. Peczuh, M. W., and Hamilton, A. D. (2000) Peptide and protein recognition by designed molecules, *Chem Rev 100*, 2479-2494.

106. Xu, G. Y., Tam, A., Lin, L., Hixon, J., Fritz, C. C., and Powers, R. (2001) Solution structure of B. subtilis acyl carrier protein, *Structure 9*, 277-287.

107. Sacco, E., Covarrubias, A. S., O'Hare, H. M., Carroll, P., Eynard, N., Jones, T. A., Parish, T., Daffe, M., Backbro, K., and Quemard, A. (2007) The missing piece of the type II fatty acid synthase system from Mycobacterium tuberculosis, *Proc Natl Acad Sci U S A 104*, 14628-14633.

108. Rock, C. O., and Cronan, J. E. (1996) Escherichia coli as a model for the regulation of dissociable (type II) fatty acid biosynthesis, *Biochim Biophys Acta 1302*, 1-16.

109. Sacco, E., Legendre, V., Laval, F., Zerbib, D., Montrozier, H., Eynard, N., Guilhot, C., Daffe, M., and Quemard, A. (2007) Rv3389C from Mycobacterium tuberculosis, a member of the (R)-specific hydratase/dehydratase family, *Biochim Biophys Acta 1774*, 303-311.

110. Zornetzer, G. A., White, R. D., Markley, J. L., and Fox, B. G. (2006) Preparation of isotopically labeled spinach acyl-acyl carrier protein for NMR structural studies, *Protein Expr Purif 46*, 446-455.

111. Gong, H., Murphy, A., McMaster, C. R., and Byers, D. M. (2007) Neutralization of acidic residues in helix II stabilizes the folded conformation of acyl carrier protein and variably alters its function with different enzymes, *J Biol Chem 282*, 4494-4503.

112. Zhang, Y. M., Wu, B., Zheng, J., and Rock, C. O. (2003) Key residues responsible for acyl carrier protein and beta-ketoacyl-acyl carrier protein

reductase (FabG) interaction, *J Biol Chem 278*, 52935-52943.

113. Broadwater, J. A., and Fox, B. G. (1999) Spinach holo-acyl carrier protein: overproduction and phosphopantetheinylation in Escherichia coli BL21(DE3), in vitro acylation, and enzymatic desaturation of histidine-tagged isoform I, *Protein Expr Purif 15*, 314-326.

114. Zhang, Y. M., Frank, M. W., Virga, K. G., Lee, R. E., Rock, C. O., and Jackowski, S. (2004) Acyl carrier protein is a cellular target for the antibacterial action of the pantothenamide class of pantothenate antimetabolites, *J Biol Chem 279*, 50969-50975.

115. Rock, C. O., Cronan, J. E., Jr., and Armitage, I. M. (1981) Molecular properties of acyl carrier protein derivatives, *J Biol Chem 256*, 2669-2674.

116. Hill, R. B., MacKenzie, K. R., Flanagan, J. M., Cronan, J. E., Jr., and Prestegard, J. H. (1995) Overexpression, purification, and characterization of Escherichia coli acyl carrier protein and two mutant proteins, *Protein Expr Purif 6*, 394-400.

117. Pfeifer, B. A., and Khosla, C. (2001) Biosynthesis of polyketides in heterologous hosts, *Microbiol Mol Biol Rev 65*, 106-118.

118. Flugel, R. S., Hwangbo, Y., Lambalot, R. H., Cronan, J. E., Jr., and Walsh, C. T. (2000) Holo-(acyl carrier protein) synthase and phosphopantetheinyl transfer in Escherichia coli, *J Biol Chem 275*, 959-968.

119. Majerus, P. W., and Vagelos, P. R. (1967) Fatty acid biosynthesis and the role of the acyl carrier protein, *Adv Lipid Res 5*, 1-33.

120. Zhang, Y. M., Marrakchi, H., White, S. W., and Rock, C. O. (2003) The application of computational methods to explore the diversity and structure of bacterial fatty acid synthase, *J Lipid Res 44*, 1-10.

121. Heath, R. J., White, S. W., and Rock, C. O. (2001) Lipid biosynthesis as a target for antibacterial agents, *Prog Lipid Res 40*, 467-497.

122. Rock, C. O., and Cronan, J. E., Jr. (1979) Re-evaluation of the solution structure of acyl carrier protein, *J Biol Chem 254*, 9778-9785.

123. Holak, T. A., Kearsley, S. K., Kim, Y., and Prestegard, J. H. (1988) Three-dimensional structure of acyl carrier protein determined by NMR pseudoenergy and distance geometry calculations, *Biochemistry 27*, 6135-6142.

124. Kim, Y., and Prestegard, J. H. (1989) A dynamic model for the structure of acyl carrier protein in solution, *Biochemistry 28*, 8792-8797.

125. Kim, Y., Ohlrogge, J. B., and Prestegard, J. H. (1990) Motional effects on NMR structural data. Comparison of spinach and Escherichia coli acyl carrier proteins, *Biochem Pharmacol 40*, 7-13.

126. Reed, M. A., Schweizer, M., Szafranska, A. E., Arthur, C., Nicholson, T. P., Cox, R. J., Crosby, J., Crump, M. P., and Simpson, T. J. (2003) The type I rat fatty acid synthase ACP shows structural homology and analogous biochemical properties to type II ACPs, *Org Biomol Chem 1*, 463-471.

127. Broun, P., Shanklin, J., Whittle, E., and Somerville, C. (1998) Catalytic plasticity of fatty acid modification enzymes underlying chemical diversity of

plant lipids, *Science 282*, 1315-1317.

128. Park, S. J., Kim, J. S., Son, W. S., and Lee, B. J. (2004) pH-induced conformational transition of H. pylori acyl carrier protein: insight into the unfolding of local structure, *J Biochem 135*, 337-346.

129. Wong, H. C., Liu, G., Zhang, Y. M., Rock, C. O., and Zheng, J. (2002) The solution structure of acyl carrier protein from Mycobacterium tuberculosis, *J Biol Chem 277*, 15874-15880.

130. Worsham, L. M., Earls, L., Jolly, C., Langston, K. G., Trent, M. S., and Ernst-Fonberg, M. L. (2003) Amino acid residues of Escherichia coli acyl carrier protein involved in heterologous protein interactions, *Biochemistry 42*, 167-176.

131. Lambalot, R. H., Gehring, A. M., Flugel, R. S., Zuber, P., LaCelle, M., Marahiel, M. A., Reid, R., Khosla, C., and Walsh, C. T. (1996) A new enzyme superfamily - the phosphopantetheinyl transferases, *Chem Biol 3*, 923-936.

132. Gehring, A. M., Lambalot, R. H., Vogel, K. W., Drueckhammer, D. G., and Walsh, C. T. (1997) Ability of Streptomyces spp. acyl carrier proteins and coenzyme A analogs to serve as substrates in vitro for E. coli holo-ACP synthase, *Chem Biol 4*, 17-24.

133. Shanklin, J. (2000) Overexpression and purification of the Escherichia coli inner membrane enzyme acyl-acyl carrier protein synthase in an active form, *Protein Expr Purif 18*, 355-360.

134. McMurry, L. M., Oethinger, M., and Levy, S. B. (1998) Triclosan targets lipid

synthesis, *Nature 394*, 531-532.

135. Heath, R. J., Rubin, J. R., Holland, D. R., Zhang, E., Snow, M. E., and Rock, C. O. (1999) Mechanism of triclosan inhibition of bacterial fatty acid synthesis, *J Biol Chem 274*, 11110-11114.

136. Baldock, C., Rafferty, J. B., Stuitje, A. R., Slabas, A. R., and Rice, D. W. (1998) The X-ray structure of Escherichia coli enoyl reductase with bound NAD+ at 2.1 A resolution, *J Mol Biol 284*, 1529-1546.

137. Rafi, S., Novichenok, P., Kolappan, S., Zhang, X., Stratton, C. F., Rawat, R., Kisker, C., Simmerling, C., and Tonge, P. J. (2006) Structure of acyl carrier protein bound to FabI, the FASII enoyl reductase from Escherichia coli, *J Biol Chem 281*, 39285-39293.

138. Lu, H., and Tonge, P. J. (2008) Inhibitors of FabI, an enzyme drug target in the bacterial fatty acid biosynthesis pathway, *Acc Chem Res 41*, 11-20.

139. Ellman, G. L. (1959) Tissue sulfhydryl groups, *Arch Biochem Biophys 82*, 70-77.

140. Nesbitt, N. M., Baleanu-Gogonea, C., Cicchillo, R. M., Goodson, K., Iwig, D. F., Broadwater, J. A., Haas, J. A., Fox, B. G., and Booker, S. J. (2005) Expression, purification, and physical characterization of Escherichia coli lipoyl(octanoyl)transferase, *Protein Expr Purif 39*, 269-282.

141. Haas, J. A., Frederick, M. A., and Fox, B. G. (2000) Chemical and posttranslational modification of Escherichia coli acyl carrier protein for preparation of dansyl-acyl carrier proteins, *Protein Expr Purif 20*, 274-284.

142. Tasdemir, D., Topaloglu, B., Perozzo, R., Brun, R., O'Neill, R., Carballeira, N. M., Zhang, X., Tonge, P. J., Linden, A., and Ruedi, P. (2007) Marine natural products from the Turkish sponge Agelas oroides that inhibit the enoyl reductases from Plasmodium falciparum, Mycobacterium tuberculosis and Escherichia coli, *Bioorg Med Chem 15*, 6834-6845.

143. Boyne, M. E., Sullivan, T. J., amEnde, C. W., Lu, H., Gruppo, V., Heaslip, D., Amin, A. G., Chatterjee, D., Lenaerts, A., Tonge, P. J., and Slayden, R. A. (2007) Targeting fatty acid biosynthesis for the development of novel chemotherapeutics against Mycobacterium tuberculosis: evaluation of A-ring-modified diphenyl ethers as high-affinity InhA inhibitors, *Antimicrob Agents Chemother 51*, 3562-3567.

144. Sullivan, T. J., Truglio, J. J., Boyne, M. E., Novichenok, P., Zhang, X., Stratton, C. F., Li, H. J., Kaur, T., Amin, A., Johnson, F., Slayden, R. A., Kisker, C., and Tonge, P. J. (2006) High affinity InhA inhibitors with activity against drug-resistant strains of Mycobacterium tuberculosis, *ACS Chem Biol 1*, 43-53.

145. Basso, L. A., Zheng, R., Musser, J. M., Jacobs, W. R., Jr., and Blanchard, J. S. (1998) Mechanisms of isoniazid resistance in Mycobacterium tuberculosis: enzymatic characterization of enoyl reductase mutants identified in isoniazid-resistant clinical isolates, *J Infect Dis 178*, 769-775.

146. Fillgrove, K. L., and Anderson, V. E. (2001) The mechanism of dienoyl-CoA reduction by 2,4-dienoyl-CoA reductase is stepwise: observation of a dienolate

intermediate, *Biochemistry 40*, 12412-12421.

147. Weissman, K. J., Hong, H., Popovic, B., and Meersman, F. (2006) Evidence for a protein-protein interaction motif on an acyl carrier protein domain from a modular polyketide synthase, *Chem Biol 13*, 625-636.

148. Li, Y., Li, H., Yang, F., Smith-Gill, S. J., and Mariuzza, R. A. (2003) X-ray snapshots of the maturation of an antibody response to a protein antigen, *Nat Struct Biol 10*, 482-488.

149. Ma, B., Wolfson, H. J., and Nussinov, R. (2001) Protein functional epitopes: hot spots, dynamics and combinatorial libraries, *Curr Opin Struct Biol 11*, 364-369.

150. DeLano, W. L. (2002) Unraveling hot spots in binding interfaces: progress and challenges, *Curr Opin Struct Biol 12*, 14-20.

151. Veyron-Churlet, R., Guerrini, O., Mourey, L., Daffe, M., and Zerbib, D. (2004) Protein-protein interactions within the Fatty Acid Synthase-II system of Mycobacterium tuberculosis are essential for mycobacterial viability, *Mol Microbiol 54*, 1161-1172.

152. Veyron-Churlet, R., Bigot, S., Guerrini, O., Verdoux, S., Malaga, W., Daffe, M., and Zerbib, D. (2005) The biosynthesis of mycolic acids in Mycobacterium tuberculosis relies on multiple specialized elongation complexes interconnected by specific protein-protein interactions, *J Mol Biol 353*, 847-858.

153. Kremer, L., Nampoothiri, K. M., Lesjean, S., Dover, L. G., Graham, S., Betts,

J., Brennan, P. J., Minnikin, D. E., Locht, C., and Besra, G. S. (2001) Biochemical characterization of acyl carrier protein (AcpM) and malonyl-CoA:AcpM transacylase (mtFabD), two major components of Mycobacterium tuberculosis fatty acid synthase II, *J Biol Chem 276*, 27967-27974.

154. Lim, L. S., and Sherin, K. (2008) Screening for prostate cancer in U.S. men ACPM position statement on preventive practice, *Am J Prev Med 34*, 164-170.

155. Huang, Y. S., Ge, J., Zhang, H. M., Lei, J. Q., Zhang, X. L., and Wang, H. H. (2006) Purification and characterization of the Mycobacterium tuberculosis FabD2, a novel malonyl-CoA:AcpM transacylase of fatty acid synthase, *Protein Expr Purif 45*, 393-399.

156. Geiger, O., Spaink, H. P., and Kennedy, E. P. (1991) Isolation of the Rhizobium leguminosarum NodF nodulation protein: NodF carries a 4'-phosphopantetheine prosthetic group, *J Bacteriol 173*, 2872-2878.

157. Brozek, K. A., Carlson, R. W., and Raetz, C. R. (1996) A special acyl carrier protein for transferring long hydroxylated fatty acids to lipid A in Rhizobium, *J Biol Chem 271*, 32126-32136.

158. Cole, S. T., Brosch, R., Parkhill, J., Garnier, T., Churcher, C., Harris, D., Gordon, S. V., Eiglmeier, K., Gas, S., Barry, C. E., 3rd, Tekaia, F., Badcock, K., Basham, D., Brown, D., Chillingworth, T., Connor, R., Davies, R., Devlin, K., Feltwell, T., Gentles, S., Hamlin, N., Holroyd, S., Hornsby, T., Jagels, K., Krogh, A., McLean, J., Moule, S., Murphy, L., Oliver, K., Osborne, J., Quail,

M. A., Rajandream, M. A., Rogers, J., Rutter, S., Seeger, K., Skelton, J., Squares, R., Squares, S., Sulston, J. E., Taylor, K., Whitehead, S., and Barrell, B. G. (1998) Deciphering the biology of Mycobacterium tuberculosis from the complete genome sequence, *Nature 393*, 537-544.

159. Yuan, Y., Mead, D., Schroeder, B. G., Zhu, Y., and Barry, C. E., 3rd. (1998) The biosynthesis of mycolic acids in Mycobacterium tuberculosis. Enzymatic methyl(ene) transfer to acyl carrier protein bound meromycolic acid in vitro, *J Biol Chem 273*, 21282-21290.

160. Banerjee, A., Dubnau, E., Quemard, A., Balasubramanian, V., Um, K. S., Wilson, T., Collins, D., de Lisle, G., and Jacobs, W. R., Jr. (1994) inhA, a gene encoding a target for isoniazid and ethionamide in Mycobacterium tuberculosis, *Science 263*, 227-230.

161. Kuo, M. R., Morbidoni, H. R., Alland, D., Sneddon, S. F., Gourlie, B. B., Staveski, M. M., Leonard, M., Gregory, J. S., Janjigian, A. D., Yee, C., Musser, J. M., Kreiswirth, B., Iwamoto, H., Perozzo, R., Jacobs, W. R., Jr., Sacchettini, J. C., and Fidock, D. A. (2003) Targeting tuberculosis and malaria through inhibition of Enoyl reductase: compound activity and structural data, *J Biol Chem 278*, 20851-20859.

162. Kim, Y. M., and Prestegard, J. H. (1990) Demonstration of a Conformational Equilibrium in Acyl Carrier Protein from Spinach Using Rotating Frame Nuclear-Magnetic-Resonance Spectroscopy, *Journal of the American Chemical Society 112*, 3707-3709.

163. Beltschewa-Petrowa, M. (1965) [Pharmacodynamic and therapeutic effect of the Bulgarian antitubercular preparation INHA-17], *Z Tuberk Erkr Thoraxorg 123*, 344-346.

164. Simeonov, M. N. (1964) [Study of the Absorption, Blood Concentration and Excretion in the Urine of the Bulgarian Antitubercular Preparation Inha-17.], *Probl Tuberk 42*, 39-43.

165. Ganev, G., Khadzhiev, D., Karamalakov, L., Tsekova, M., Sirakov, A., Atanasov, K., Chaikov, I., Tsolov, N., and Vasileva, I. (1961) [Treatment of parkinsonism with a new preparation INHA-17.], *Suvr Med (Sofiia) 12(4-5)*, 35-44.

166. Ganev, G., Karamalkov, L., Khadzhiev, D., Tsekova, M., Sirakov, A., Atanasov, K., Nankov, I., Tsolov, N., and Vasileva, I. (1961) [Treatment of parkinsonism with a new combined preparation INHA-17 with Bellapan (Bellazon).], *Suvr Med (Sofiia) 12(4-5)*, 45-53.

167. Debertshauser, E. (1961) [Is resistance break-through possible after INH and PAS long-term therapy in pulmonary tuberculosis by the use of INHA-PAS?], *Beitr Klin Tuberk Spezif Tuberkuloseforsch 124*, 450-455.

168. Krisch, J. (1956) [Clinical experience with INHA-PAS.], *Beitr Klin Tuberk Spezif Tuberkuloseforsch 116*, 15-20.

169. Wilde, W. (1955) [Difference in the results of bacteriological studies on animals and in vitro, as demonstrated by a new tuberculostatic (INHA-PAS).], *Arzneimittelforschung 5*, 232-237.

170. Jahn, O., and Pietsch, W. (1954) [Preliminary observations of pulmonary tuberculosis therapy with the combination drug INHA-PAS.], *Wien Klin Wochenschr 66*, 511-512.

171. Hell, M. (1954) [The compound drug INHA-PAS in the treatment of pulmonary tuberculosis.], *Med Monatsschr 8*, 762-765.

172. Frank, F., and Robel, G. (1954) [Tuberculostatic INHA-PAS in clinical examination.], *Praxis 43*, 1100-1102.

173. Tomb, J. F., White, O., Kerlavage, A. R., Clayton, R. A., Sutton, G. G., Fleischmann, R. D., Ketchum, K. A., Klenk, H. P., Gill, S., Dougherty, B. A., Nelson, K., Quackenbush, J., Zhou, L., Kirkness, E. F., Peterson, S., Loftus, B., Richardson, D., Dodson, R., Khalak, H. G., Glodek, A., McKenney, K., Fitzegerald, L. M., Lee, N., Adams, M. D., Hickey, E. K., Berg, D. E., Gocayne, J. D., Utterback, T. R., Peterson, J. D., Kelley, J. M., Cotton, M. D., Weidman, J. M., Fujii, C., Bowman, C., Watthey, L., Wallin, E., Hayes, W. S., Borodovsky, M., Karp, P. D., Smith, H. O., Fraser, C. M., and Venter, J. C. (1997) The complete genome sequence of the gastric pathogen Helicobacter pylori, *Nature 388*, 539-547.

174. Dessen, A., Quemard, A., Blanchard, J. S., Jacobs, W. R., Jr., and Sacchettini, J. C. (1995) Crystal structure and function of the isoniazid target of Mycobacterium tuberculosis, *Science 267*, 1638-1641.

175. Viola, R. E., Cook, P. F., and Cleland, W. W. (1979) Stereoselective preparation of deuterated reduced nicotinamide adenine nucleotides and

substrates by enzymatic synthesis, *Anal Biochem 96*, 334-340.

176. Orr, G. A., and Blanchard, J. S. (1984) High-performance ion-exchange separation of oxidized and reduced nicotinamide adenine dinucleotides, *Anal Biochem 142*, 232-234.

177. La Clair, J. J., Foley, T. L., Schegg, T. R., Regan, C. M., and Burkart, M. D. (2004) Manipulation of carrier proteins in antibiotic biosynthesis, *Chem Biol 11*, 195-201.

178. Mercer, A. C., La Clair, J. J., and Burkart, M. D. (2005) Fluorescent multiplex analysis of carrier protein post-translational modification, *Chembiochem 6*, 1335-1337.

179. Worthington, A. S., Rivera, H., Torpey, J. W., Alexander, M. D., and Burkart, M. D. (2006) Mechanism-Based protein cross-linking probes to investigate carrier protein-mediated biosynthesis, *ACS Chemical Biology 11*, 687-691.

180. Segel, I. H. (1975) Enzyme kinetics. Behavior and analysis of rapid equilibrium and steady-state systems, *Wiley, New York*, 355-385.

181. Wickramasinghe, S. R., Inglis, K. A., Urch, J. E., Muller, S., van Aalten, D. M., and Fairlamb, A. H. (2006) Kinetic, inhibition and structural studies on 3-oxoacyl-ACP reductase from Plasmodium falciparum, a key enzyme in fatty acid biosynthesis, *Biochem J 393*, 447-457.

182. Fischl, A. S., and Kennedy, E. P. (1990) Isolation and properties of acyl carrier protein phosphodiesterase of Escherichia coli, *J Bacteriol 172*, 5445-5449.

183. Heath, R. J., and Rock, C. O. (1995) Regulation of malonyl-CoA metabolism

by acyl-acyl carrier protein and beta-ketoacyl-acyl carrier protein synthases in Escherichia coli, *J Biol Chem 270*, 15531-15538.

184. Keating, D. H., Carey, M. R., and Cronan, J. E., Jr. (1995) The unmodified (apo) form of Escherichia coli acyl carrier protein is a potent inhibitor of cell growth, *J Biol Chem 270*, 22229-22235.

185. Lopez-Lara, I. M., and Geiger, O. (2000) Expression and purification of four different rhizobial acyl carrier proteins, *Microbiology 146 (Pt 4)*, 839-849.

186. Chothia, C., Levitt, M., and Richardson, D. (1977) Structure of proteins: packing of alpha-helices and pleated sheets, *Proc Natl Acad Sci U S A 74*, 4130-4134.

187. Joshi, A. K., and Smith, S. (1993) Construction, expression, and characterization of a mutated animal fatty acid synthase deficient in the dehydrase function, *J Biol Chem 268*, 22508-22513.

188. Kastaniotis, A. J., Autio, K. J., Sormunen, R. T., and Hiltunen, J. K. (2004) Htd2p/Yhr067p is a yeast 3-hydroxyacyl-ACP dehydratase essential for mitochondrial function and morphology, *Mol Microbiol 53*, 1407-1421.

189. Kass, L. R., and Bloch, K. (1967) On the enzymatic synthesis of unsaturated fatty acids in Escherichia coli, *Proc Natl Acad Sci U S A 58*, 1168-1173.

190. Birge, C. H., Silbert, D. F., and Vagelos, P. R. (1967) A Beta-Hydroxydecanoyl-Acp Dehydrase Specific for Saturated Fatty Acid Biosynthesis in E Coli, *Biochemical and Biophysical Research Communications 29*, 808-&.

191. Kass, L. R., Brock, D. J., and Bloch, K. (1967) Beta-hydroxydecanoyl thioester dehydrase. I. Purification and properties, *J Biol Chem 242*, 4418-4431.

192. Silbert, D. F., and Vagelos, P. R. (1967) Fatty acid mutant of E. coli lacking a beta-hydroxydecanoyl thioester dehydrase, *Proc Natl Acad Sci U S A 58*, 1579-1586.

193. Rosenfeld, I. S., D'Agnolo, G., and Vagelos, P. R. (1973) Synthesis of unsaturated fatty acids and the lesion in fab B mutants, *J Biol Chem 248*, 2452-2460.

194. Heath, R. J., and Rock, C. O. (1996) Roles of the FabA and FabZ beta-hydroxyacyl-acyl carrier protein dehydratases in Escherichia coli fatty acid biosynthesis, *J Biol Chem 271*, 27795-27801.

195. Castell, A., Johansson, P., Unge, T., Jones, T. A., and Backbro, K. (2005) Rv0216, a conserved hypothetical protein from Mycobacterium tuberculosis that is essential for bacterial survival during infection, has a double hotdog fold, *Protein Sci 14*, 1850-1862.

196. Brown, A. K., Papaemmanouil, A., Bhowruth, V., Bhatt, A., Dover, L. G., and Besra, G. S. (2007) Flavonoid inhibitors as novel antimycobacterial agents targeting Rv0636, a putative dehydratase enzyme involved in Mycobacterium tuberculosis fatty acid synthase II, *Microbiology 153*, 3314-3322.

197. Brown, A. K., Bhatt, A., Singh, A., Saparia, E., Evans, A. F., and Besra, G. S. (2007) Identification of the dehydratase component of the mycobacterial

mycolic acid-synthesizing fatty acid synthase-II complex, *Microbiology 153*, 4166-4173.

198. Hisano, T., Tsuge, T., Fukui, T., Iwata, T., Miki, K., and Doi, Y. (2003) Crystal structure of the (R)-specific enoyl-CoA hydratase from Aeromonas caviae involved in polyhydroxyalkanoate biosynthesis, *J Biol Chem 278*, 617-624.

199. Koski, M. K., Haapalainen, A. M., Hiltunen, J. K., and Glumoff, T. (2004) A two-domain structure of one subunit explains unique features of eukaryotic hydratase 2, *J Biol Chem 279*, 24666-24672.

200. Sassetti, C. M., Boyd, D. H., and Rubin, E. J. (2003) Genes required for mycobacterial growth defined by high density mutagenesis, *Mol Microbiol 48*, 77-84.

201. Wu, W. J., Feng, Y. G., He, X., Hofstein, H. A., Raleigh, D. P., and Tonge, P. J. (2000) Stereospecificity of the reaction catalyzed by enoyl-CoA hydratase, *Journal of the American Chemical Society 122*, 3987-3994.

202. Wakil, S. J. (1956) Studies on the fatty acid oxidizing system of animal tissues. IX. Stereospecificity of unsaturated acyl CoA hydrase, *Biochim Biophys Acta 19*, 497-504.